Alma Mater Studiorum – Università di Bologna

DOTTORATO DI RICERCA IN
SCIENZE BIOMEDICHE
(CURRICULUM NEUROFISIOLOGIA)

XXVI Ciclo

Settore Concorsuale di afferenza : 5/D1

Settore Scientifico disiplinare : BIO/09

EFFECT OF LOSS OF CDKL5 ON BRAIN DEVELOPMENT IN A NEW Cdkl5 KNOCKOUT MOUSE MODEL

Presentata da: Dott.ssa Claudia Fuchs

Coordinatore Dottorato

Chia.mo Prof. Lucio Ildebrando Cocco

Relatore

Dott.ssa Elisabetta Ciani

Esame finale anno 2104

„Der Mensch muss bei dem Glauben verharren, dass das Unbegreifliche begreiflich sei; er würde sonst nicht forschen.“

„Humans have to hold on to the belief that the incomprehensible is comprehensible, otherwise they would not continue to explore.“

Johann Wolfgang von Goethe

SUMMARY

MeCP2 regulation of imprinted genes

MeCP2 as splicing regulator

MeCP2's role in CNS development and neuronal maturation

MeCP2 regulates dendritic morphology

MeCP2 and synaptic transmission

CDKL5 might regulate the function of epigenetic factors and transcriptional regulators

Cdkl5 expression correlates with neuronal maturation

CDKL5 affects neuronal morphogenesis and dendritic arborization

CDKL5 contributes to correct dendritic spine structure and synapse activity

4. RESULTS pg.81

1. AIM OF THE STUDY

Rett's Syndrome (RTT) is a severe, progressive neurodevelopmental disorder that affects mainly females, occurring with an incidence of up to 1:10,000 live births (Hagberg et al. 1983). After an apparently normal development, affected children around 6-18 months old start to display signs of the disease which consist in loss of speech, reduced motor abilities, respiratory crises, stereotyped hand movements, severe cognitive impairment and autistic behavior.

Recent studies have shown that RTT is often linked to mutations in the *MECP2* gene, mapped to Xq28 and encoding for methyl-CpG-binding protein 2 (MeCP2), a methylation-dependent transcriptional repressor (Lewis et al. 1992) and splicing regulator (Young et al. 2005).

Nonetheless a significant fraction (around 30%) of children affected by RTT does not carry mutation in this gene, and recent findings highlighted the fact that **mutations in the *CDKL5* (cyclin-dependent kinase-like 5) gene** are responsible for **a new disorder** that in many aspects overlaps RTT but is also characterized by specific traits (Evans et al. 2005; Fehr et al. 2013). Mutations in the *CDKL5* gene are associated with a severe epileptic encephalopathy characterized by early-onset intractable seizures, infantile spasms, severe developmental delay, intellectual disability, and RTT-like features.

Although several distinct mutations of the *CDKL5* gene have been found associated with the disease, **the function of CDKL5 and particularly its role in the development of the nervous system remain totally cryptic yet**, as well as it remains unknown how deregulated expression or mutations of *CDKL5* determine the disease phenotype.

Several studies in rodents have shown that **Cdkl5, a serine-threonine protein kinase, is highly expressed in the developing brain** (Rusconi et al. 2008; Chen et al. 2010), **suggesting the importance of this kinase for proper brain maturation and function.**

Based on these premises **the overall aim of the study was to characterize the role of CDKL5 on brain development and to identify the molecular mechanism/s underlying its action.**

In particular our aims were:

i) to establish the role of CDKL5 on neuronal maturation, through an appropriate *in vitro* cellular system;

ii) to generate a Cdkl5 loss of function mouse model (a Cdkl5 knockout mouse model);

iii) using the new generated Cdkl5 knockout mouse, to dissect the role of Cdkl5 on brain development and to identify the molecular mechanism/s underlying its action;

This study will provide novel information on the molecular mechanism/s underlying brain alterations in the CDKL5 variant of RTT. This is a first and essential step for future studies in which the Cdkl5 knockout mouse model and the information gained in the current project can be exploited to devise new therapeutic strategies in order to improve symptoms of the CDKL5 disorder.

2. INTRODUCTION

2.1. THE RETT'S SYNDROME

2.1.1. EPIDEMIOLOGY OF RETT'S SYNDROME

Rett's Syndrome (RTT) [OMIM 312750] is a X-linked progressive neurodevelopmental disorder that affects the patient's ability to communicate and perform simple motor tasks. RTT affects mainly females, occurring with an incidence rate of 1 up to 10,000 female live births (Hagberg et al. 1983; Neul et al. 2010). Although the RTT phenotype is variable, most RTT patients have a distinctive disease course: after a period of apparently normal development (6-18 months) a regression appears with loss of social, motor and communication skills, hand stereotypies, microcephaly and mental retardation.

Several RTT variants, that deviate from the classical clinical presentation and range from milder forms with a later age of onset to more severe manifestations, have been described. The milder forms include the preserved speech variant (PSV or "Zappella variant"), characterized by the recovery of some degree of speech and the ''forme fruste" (or "worndown form"), with a milder, incomplete clinical course. Patients have a later age of onset compared to the classical form, with regression occurring between 1 to 3 years of age and the hand use is sometimes preserved with minimal stereotypic hand movements (Weaving et al. 2004). The more severe forms include the "congenital variant" that lacks the early period of normal development, and the ''early seizure variant'' (ESV or "Hanefeld" variant), with onset of seizures before the age of 6 months (Hanefeld

1985). These variants present some symptoms of RTT, but show considerable variation in type and age of onset, severity of impairment, and clinical course.

In 1999, Amir et colleagues discovered that mutations in the gene encoding methyl-CpG-binding protein 2 (MeCP2) [OMIM 300005] are associated with rare familial cases of RTT as well as more common sporadic occurrence of typical RTT (Amir et al. 1999). MeCP2 is a transcriptional repressor involved in chromatin remodeling and modulation of RNA splicing. Mutations in *MECP2* are found in 95-97% of individuals with classic RTT (Neul et al. 2008), while only 50-70% of patients with atypical variants of RTT have been diagnosed with mutations in *MECP2*, suggesting the existence of one or more RTT loci.

Mutations in the *CDKL5* gene [OMIM 300203] encoding for a serine-threonine kinase (cyclin-dependent kinase like 5) **have been identified in individuals who had been characterized as early-onset variant of RTT** (ESV o "Hanefeld" variant), supporting the existence of genetic heterogeneity in RTT. However, the increasing identification of individuals with *CDKL5* mutations has led to the observation that these individuals lack of some of the distinctive clinical features of classic RTT, such as the clear period of regression and the characteristic intense eye-gaze and very recently Fehr and colleagues proposed to consider the CDKL5 disorder as a distinctive disease (Fehr et al. 2013).

Similarly, recent reports have identified mutations in a third gene involved in a variant of RTT. In 2008 Ariani and colleagues identified *FOXG1*-truncating mutations in two patients with congenital variant of RTT (Ariani et al. 2008). *FOXG1* [OMIM 164874] encodes forkhead box protein G1, FoxG1 (formerly brain factor 1, BF-1), a brain-specific transcriptional repressor that is essential for early development of the telencephalon. Molecular analysis revealed that FoxG1 might also share common molecular mechanisms with MeCP2 during neuronal development, exhibiting partially overlapping expression domain in postnatal cortex and neuronal subnuclear localization.

The incidence of the classic form of RTT is estimated at 1 out of 10,000 females (Hagberg et al. 1983; Fehr et al. 2013). Current understanding of classical and variant forms suggests that the overall prevalence is probably higher. The annual death rate in classic RTT has been estimated about 1,2% in the UK (Kerr 1992), and a little change in the survival has been found in the last 30 years (Freilinger et al. 2010). Most of death clustered between the ages of 15 and 20 years with causes related to the disorder, such as wasted condition and poor health in general, pneuomonia and epilepsy. Poor autonomic control and autonomic manifestations are considered to play a significant role to (Julu et al. 2001).

2.1.2. THE HISTORY OF RETT'S SYNDROME

RTT was first described as a clinical entity by Andreas Rett, a pediatric neurologist in Vienna, in 1954. His publication in German medical literature in 1966 (Rett 1966), however, remained largely unnoticed. In the large textbook series on neurology by Vincken and Bruyn, Andreas Rett wrote a chapter under the misleading heading of Cerebral Atrophy and Hyperammonaemia in a series of 21 girls and women (Smeets et al. 2012). In the same time another child neurologist observed similar clinical features in Japanese girls (Smeets et al. 2012), but only in 1983 Hagberg and colleagues increased awareness of the disorder in the English medical literature. They further described the condition in 35 girls with strikingly similar clinical features of "progressive autism, loss of purposed hand movements, ataxia, and acquired microcephaly" (Hagberg et al. 1983). This article was a breakthrough in communicating details of the disease to a wide audience and in 1986 Hagberg and Witt-Engerstroem developed the first classification of clinical staging of RTT, proposing four age-related stages, that was later revised in 2001 (Witt-Engerstrom and Hagberg 1990; Hagberg et al. 2002). In addition to the worldwide recognition of RTT, the 1980s witnessed major strides in another field, namely DNA methylation. For the first time, a connection between DNA methylation and heritable changes in gene expression

was established. Scientists identified the CpG dinucleotide to be the side of almost all DNA methylation in mammalian genomes and began to define the effects of this modification on gene activity. In 1992, Dr. Adrian Bird and colleagues identified a novel mammalian protein that binds methylated CpGs, methyl-CpG binding protein 2 (MeCP2) (Lewis et al. 1992). The gene encoding MeCP2 was found to be localized to the X-chromosome (Quaderi et al. 1994) and the protein encoded was found to repress transcription *in vivo* (Nan et al. 1997). In the meantime, as the DNA methylation field was deciphering repression mechanisms mediated by methyl-CpG binding proteins, the RTT community tried to understand the pathophysiology of this puzzling condition. A major breakthrough in RTT research occurred in 1999, when researchers from Huda Zoghbi's laboratory suggested the *MECP2* gene as a candidate gene for RTT (Amir et al. 1999). The identification of mutations in *MECP2* as being causal in RTT has led to rapid increase in understanding the disease and numerous research groups are still trying to clarify the mechanism/s underlying this complex disorder.

In the last years a small proportion of clinically well-defined RTT patients (3-5%) have been found not to present mutations in the *MECP2* gene, suggesting the existence of at least one other RTT locus. Recently mutations in the gene for cyclin-dependent kinase like 5 (*CDKL5*) were identified in patients who had been diagnosed with atypical RTT, supporting the existence of genetic heterogeneity in this disease. The kinase CDKL5 was initially identified through a positional cloning study aimed at isolating disease genes mapping on the X-chromosome. Sequence analysis revealed homologies to several serine-threonine kinase genes and identified one protein signature specific for this subgroup of kinases, therefore, leading the authors to name the gene *STK9* (Serine Threonine Kinase 9) (Montini et al. 1998). The first described mutations in *CDKL5* were balanced X/autosomal translocations in two unrelated girls who, in addition to seizures and mental retardation, presented hypsarrythmia and infantile spasms (Kalscheuer et al. 2003). Even though the first patients mutated in *CDKL5* were these two girls affected by X-linked infantile spasms (ISSX), subsequent cases were reported in

female patients with a clinical phenotype mimicking RTT (Tao et al. 2004; Weaving et al. 2004). The first genetic screening for *CDKL5* mutations occurred mainly in cohorts of patients with RTT, or variants of it, which had no mutations in the *MECP2* gene. By comparing the clinical phenotypes of patients with *CDKL5* mutations already described in literature, it became clear that almost all of them presented one common characteristic: early onset seizures, starting from 10 days to 3 months after birth. Therefore in the last years the screening has been extended to cohorts of both genders affected by undefined epileptic encephalopathy, infantile spasms or West Syndrome. Consequently individuals with mutations in the *CDKL5* gene have been variably classified as having early infantile epileptic encephalopathy, X-linked dominant infantile spasm Syndrome, early-onset variant of RTT or diagnosed with other epileptic disorders such as West Syndrome. Interestingly, Intusoma et colleagues (Intusoma et al. 2011) suggested in a recent paper that screening among patients having intractable seizures with an onset before 6 months of age gives a higher score than screening among *MECP2*-negative RTT patients; this score is even increased when RTT-like features are shown as well. Only in 2013 Fehr and colleagues, using a large international data collection to describe the clinical profile of the CDKL5 disorder and comparing it with classical RTT, proposed to consider the CDKL5 disorder as an independent entity (Fehr et al. 2013). Although mutations in the *CDKL5* gene have been for a long time described in association with the early-onset variant (ESV or "Hanefeld" variant) of RTT, Fehr's paper describes, that only <25% of the analyzed cases meet the clinical criteria for this variant. They suggest that researchers and clinicians should not only concentrate on RTT features when describing the clinical picture of females and males with *CDKL5* mutations, but they should also put the focus on the characteristic features present in the CDKL5 disorder.

2.1.3. CLINICAL OVERVIEW

RTT is characterized by a specific developmental profile and the clinical diagnosis is based on a consistent constellation of clinical features and internationally accepted diagnostic criteria delineated in a staging system (Fig. 1) (Witt-Engerstrom and Hagberg 1990; Hagberg et al. 2002; Neul et al. 2010). The diagnostic criteria include a neonatal and perinatal period with normal developmental progress for the first 5-6 months of life. The birth head circumference is normal with subsequent deceleration of head growth, leading usually to microcephaly. Between 3 months and 3 years of life there is a regression and loss of acquired skills, such as purposeful hand movements, vocalization, and communication skills. The hallmark of RTT is the intense, sometimes continuous, stereotypic hand movements, which develop after the loss of purposeful hand movements. Other motor abnormalities including abnormal muscle tone and jerky truncal gait are other prominent features. Many girls with RTT have also autonomic perturbations, including hypoventilation or hyperventilation during wakefulness, breath-holding, aereophagia, forced expulsion of air and saliva, and apnea.
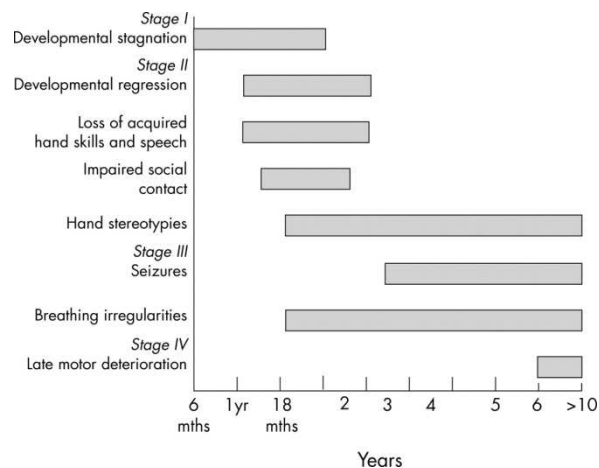
*Figure 1 **Staging system for classical RTT.** Derived from Hagberg and Witt-Engerstroem (Image taken from (Weaving et al. 2005)).*

Common features in classical Rett's Syndrome

Hand stereotypies

The hallmark and important diagnostic criteria for RTT are the intense, sometimes continuous, stereotypic hand movements, which develop after the loss of purposeful hand movements. Stereotyped hand movements are typically of small magnitude, but they may be accompanied by more proximal movements, that may also involve the trunk. Patterns consist of unimanual or bimanual wringing, mouthing, rubbing, patting, squeezing and/or clapping, or other more bizarre hand automatisms during waking hours (Fig. 2).

*Figure 2 **Stereotypic hand movements in a girl with RTT** (Image taken from (Borg et al. 2005)).*

Communication

All the patients with RTT develop intellectual disabilities and mental retardation to a variable extent. The absence of speech, the dyspraxia and the short attention span with lack of interest in play are characteristic and make the developmental testing a difficult task. Affected children show diminished interest in people and objects and their exploratory character is very poor. Their

communication is often limited to establishing visual contact by intense staring and particular care should be taken to preserve this visual sensory function. No specific ophthalmologic pathology occurs in this disorder, although strabismus and acquired cataracts after self-injurious tapping in association with behavioral agitation is very common. Some affected girls have preservation of speech and can use words and sentences in a meaningful way.

Kyphoscoliosis and Food Deformities

Mild trunk hypotonia and lack of mobility often lead to kyphoscoliosis, which develops in early school age with various degrees of severity. Progression of scoliosis is often very rapid, depending on asymmetry in muscle tone (dystonia) and degree of muscle wasting. Most commonly an S-shaped curve develops with a longer upper part (most frequently dextroconvex) and a shorter lower part (sinistroconvex) (Fig. 3). Most common food deformities in RTT are equinus and equinusvalgus/varus positions due to the reduced intersegmental mobility, related to stereotyped postures or to dystonia.
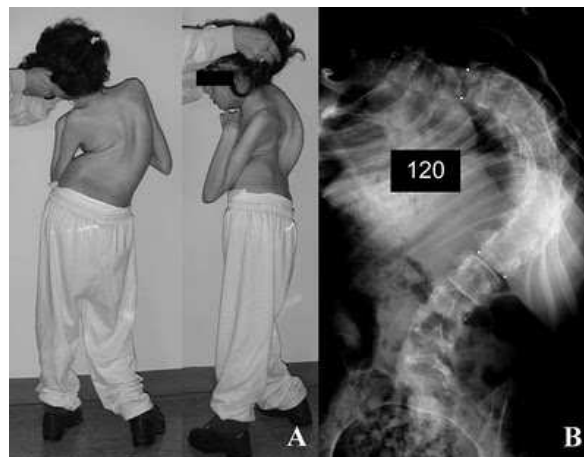
*Figure 3 **Scoliosis in a RTT patient (A) and X-ray view (B)** (Image taken from (http://syndromepictures.com/rett-syndrome-pictures/)).*

Seizures

Epilepsy is present in up to 80% of affected individuals at some times in their lives (Steffenburg et al. 2001). It usually starts after the age of 4 years and becomes less intense in adulthood. The most common types are partial complex, tonic-clonic, tonic, and myoclonic seizures and solely about 50% of seizure in classical RTT can be controlled by medication. The electroencephalogram is usually abnormal in RTT, but there is none clearly diagnostic pattern. Brain stem events, such as blinking of the eyes, facial twitching, vacant spells and hypocapneic attacks are often confused with seizures.

Autonomic Manifestations and Sleep Abnormalities

Many girls with RTT have autonomic perturbations, including irregular breathing in the waking state associated with non-epileptic vacant spells. This includes hypoventilation or hyperventilation during wakefulness, breath-holding, aereophagia, forced expulsion of air and saliva and apnea. It reflects immaturity of the brainstem and may contribute to sudden death. Sleep abnormalities are more or less a constant feature in RTT and include night laughter, prolonged wakefulness or early morning awakening. The mechanism behind this disruptive night awakening and daytime sleeping is not well-understood, but may be related to the autonomic dysfunction that has been attributed to midbrain and brainstem immaturity.

Feeding and Physical Growth

Girls with RTT love to eat and like to watch when meals are prepared and are very alert during feeding. Emergence and control of primary mouth functions such as chewing and swallowing are often delayed and can be problematic. There

is also a high incidence of gastro-esophageal reflux and decreased intestinal motility resulting in constipation. In spite of the physical growth there is a deceleration of linear growth during the first 2 years of life, while later height and/or weight for height become normal. The rate of hand and foot growth, particularly the latter, of girls with RTT is slower than that of normal children. The birth head circumference is normal with subsequent deceleration of head growth, leading usually to microcephaly. The decline in head growth may thus be very obvious in classical RTT, but it may not be present at all in atypical variants of RTT. Therefore, microcephaly is no longer an essential criterion for the diagnosis.

2.1.4. CLINICAL OVERVIEW OF THE CDKL5 VARIANT OF RTT

The clinical characteristics commonly associated with *CDKL5* mutations include early-onset seizures, severe intellectual disability and gross motor impairment. The recently published Neul criteria (Neul et al. 2010) for atypical RTT include five specific items for differentiating the early-onset variant (ESV or "Hanefeld" variant) from the classic form and the other atypical forms: seizures onset before 5 months of age, infantile spasms, refractory myoclonic epilepsy, seizures onset before regression and decreased frequency of typical RTT features (Table 1).

For several years the clinical understanding of CDKL5 disorder was limited, with most information derived from small patient groups seen at individual centers, the largest including 20 patients (Bahi-Buisson et al. 2008). Fehr et al. in 2013 used a large international data collection (InterRett database; 86 individuals with *CDKL5* mutations and 920 individuals with *MECP2* mutations) to compare the clinical profile of CDKL5 disorder with classic RTT, concluding that CDKL5 disorder should be considered as an independent clinical

entity and should not be considered part of the RTT spectrum, as < 25 % of cases didn't meet the clinical criteria for the early-onset variant of RTT (Table 2) (Fehr et al. 2013).

Consider RTT diagnosis when postnatal deceleration of head growth is observed

Required for typical or classic RTT
A period of regression followed by recovery or stabilization
1. All main and all exclusive criteria
2. Supportive criteria are not required, although often present in typical RTT

Required for atypical or variant RTT
1. A period of regression followed by recovery or stabilization
2. At least 2 of the 4 main criteria
3. 5 out of 11 supportive criteria
Main criteria
1. Partial or complete loss of acquired purposeful hand skills
2. Partial or complete loss of acquired spoken language
3. Gait abnormalities: impaired (dyspraxia) or absence of ability (apraxia)
4. Stereotypic hand movements such as hand wringing/ squeezing, clapping/tapping, mouthing and washing/ rubbing automatisms
Exclusion criteria for typical RTT
1. Brain injury secondary to trauma (peri- or postnatally), neurometabolic disease or severe infection that cause neurological problems
2. Grossly abnormal psychomotor development in the first 6 months of life
Supportive criteria for atypical RTT
1. Breathing disturbances when awake
2. Bruxism when awake
3. Impaired sleep pattern
4. Abnormal muscle tone
5. Peripheral vasomotor disturbances
6. Scoliosis/kyphosis
7. Growth retardation
8. Small cold hands and feet
9. Inappropriate laughing/screaming spells
10. Diminished sensitivity to pain
11. Intense eye communication and eye-pointing behavior

*Table 1 **RTT diagnostic criteria 2010.** (Table taken from (Neul et al. 2010)).*

Extremely likely[a]	Seizures within the first year of life (90% by 3 months)
	Global developmental delay
	Severely impaired gross motor function
Very likely[b]	Sleep disturbances
	Abnormal muscle tone
	Bruxism
	Gastrointestinal issues
Likely[c]	Subtle dysmorphic features including three or more of the following: broad/prominent forehead; large 'deep-set' eyes; full lips; tapered fingers; and anteverted nares in males
	Hand stereotypies
	Laughing and screaming spells
	Cold hands or feet
	Breathing disturbances
	Peripheral vasomotor disturbances
Unlikely[d]	Independent walking
	Microcephaly
	Major congenital malformations

[a]Observed in > 90% of cases in the current study.
[b]Observed in 80–90% of cases in the current study.
[c]Observed more variably in 40–80% of cases in the current study.
[d]Observed in < 10% of cases in the current study.

*Table 2 **Clinical features suggesting a diagnosis of CDKL5 disorder.** (Image taken from (Fehr et al. 2013)).*

Seizures and motor delay

The early-onset epilepsy is one of the hallmark features of the CDKL5 disorder and occurs in about 90% of patients by 3 months of age. In literature many seizure types and EEG changes have been described, including infantile spasms, multifocal and generalized seizures with myoclonic, tonic (tonic vibratory) and clonic features. The second key feature characteristic for the CDKL5 disorder is a severe developmental motor delay. Fehr's paper report that early development is more severely impaired in patients affected by *CDKL5* mutations, with approximately half learning to sit and 10% to walk in comparison

with 80% learning to sit and just half learning to walk affected of classic RTT (Fehr et al. 2013).

Hand function and speech

Patients with *CDKL5* mutations develop less frequently typical hand stereotypies, which are the most important diagnostic criteria of the classic variant of RTT. Fehr et al. show that functional hand use was acquired by just over the half of the cases analyzed. Patients with CDKL5 disorder were less likely to use words whereas use of some words was acquired by nearly 90% of females with classic RTT before regression (Fehr et al. 2013).

Dysmorphism

Various dysmorphic facial features have been described in individuals with *CDKL5* mutations including a prominent and/ or broad forehead, high hairline, relative mid-face hypoplasia, deep-set but "large" appearing eyes, infraorbital shadowing and strabismus. The lips appear full with often reversion of the lower lip. They also present often a wide mouth and widely spaced teeth. The fingers in young children are often tapered, some with puffy proximal and narrowed distal phalanges and some have a puffy dorsum of the hands and/ or feet. In older individuals, the fingers tend to be slender, with prominent proximal interphalangeal joints and narrow distal interphalangeal joints (Fig. 4).

Dysmorphic features have also been described in other conditions of early-onset encephalopathy, such as cases with *FOXG1* mutations and in Pitt-Hopkins Syndrome, while in classical RTT no typical facial gestalt has been described, although some clinicians have suggested a facial similarity to Angelman Syndrome. The presence of these characteristic typical facial features could provide additional assistance in the clinical identification of individuals with a *CDKL5* mutation.

Figure 4 **Characteristic facial, hand and feet features in males and females with CDKL5 disorder.** *(Image taken from (Fehr et al. 2013)).*

In the last few years individuals with mutations in the *CDKL5* gene have been variably classified and in most cases their symptoms have been attributed to the early-onset seizures variant of RTT (ESV or "Hanefed" variant), as they show some clinical overlapping phenotypes with the classic RTT. In literature CDKL5 was considered part of the RTT spectrum and only **in 2013 Fehr et colleagues suggested to consider the CDKL5 disorder as an independent clinical entity,** basing on the observation that the majority of patients with *CDKL5* mutations did not meet the diagnostic criteria proposed in 2010 by Neul et al. (Neul et al. 2010; Fehr et al. 2013).

2.1.5. CLINICAL MANAGEMENT AND THERAPEUTIC STRATEGIES

Early clinical intervention and comprehensive life-long management of RTT are essential and can significantly improve health and longevity of affected individuals. Medical management is essentially symptomatic and supportive and may be optimized by involvement of a multidisciplinary team consisting of many different medical and paramedical specialists and by an individualized approach. Management should also include psychosocial support for the families, development of an appropriate education plan and assessment of available community resources. Parent support groups are crucial in providing support for families. Pharmacologic strategies targeting specific symptoms include anti-epileptic treatments, treatment with L-carnitine, to improve patients' wellbeing and health, magnesium to reduce the episodes of hyperventilation and melatonin to improve sleep dysfunctions. Clinical management should also include rehabilitation programs adapted to the patients' individual needs, in order to improve posture and motility. Decreasing repetitive purposeless hand movements can for example be achieved by the use of various arm restraints, such as soft elbow splints, helping also in training specific hand skills such as self-feeding. Actually habilitation programs will likely remain the cornerstone of management of individuals with RTT, although a better understanding of the molecular pathophysiology of this condition is expected to lead to promising therapeutic approaches.

2.2. MeCP2

2.2.1. THE *MECP2* GENE AND ITS PRODUCTS

The *MECP2* gene is located at q28 on the human X chromosome and has been demonstrated to undergo X inactivation in human and mice (Adler et al. 1995; D'Esposito et al. 1996). It encodes the methyl-CpG-binding protein MeCP2, which belongs to a large family of DNA-binding proteins that selectively bind 5-methylcytosine residue in symmetrically positioned CpG dinucleotides. These nucleotides occur random throughout the genome; however, a recent study has shown that enrichment for A and T bases adjacent to methyl-CpG nucleotides is essential for high-affinity binding between MeCP2 and its target sites , indicating a basis for specificity (Klose et al. 2005). All proteins of this family contain a highly conserved MBD domain (methyl-CpG binding domain), which in MeCP2 extends from position 1 to 174 and it is necessary and sufficient to bind DNA. MeCP2 contains a central transcriptional repressor domain (TBD), at position 219-322, which is able to recruit co-repressor complexes that mediates repression through deacetylation of core histones, with consequent compaction of DNA into heterochromatin (Jones et al. 1998; Nan et al. 1998) and nuclear localization signal. The C-terminal domain facilitates the binding of MeCP2 to DNA(Chandler et al. 1999) and contains a WW domain that is predicted to be involved in protein-protein interactions (Fig. 5) (Buschdorf and Stratling 2004).

Two alternative spliced *MECP2* transcripts has been identified: *MECP2A* (also known as *MECP2_E2* or *MECP2β*, 498 amino acids) and *MECP2B* (*MECP2_E1* or *MECP2α*, 486 amino acids) (Kriaucionis and Bird 2004; Mnatzakanian et al. 2004). The two splicing variants differ only in their most 5' regions (Fig. 5). Although both of them are highly expressed in the brain, they differ in translation efficiency and are expressed at different relative amounts in

various tissues, with *MECP2B* being more prevalent and abundant in brain, thymus and lungs (Kriaucionis and Bird 2004), while *MECP2A* is highly expressed in other tissues, such as fibroblasts and lymphoblast cells (Mnatzakanian et al. 2004). Additional *MECP2* transcripts with 3'UTRs of different lengths are also produced by the use of alternative polyadenilation sites. Their expression levels vary between tissues and developmental stages, but the functional significance of this is unknown.
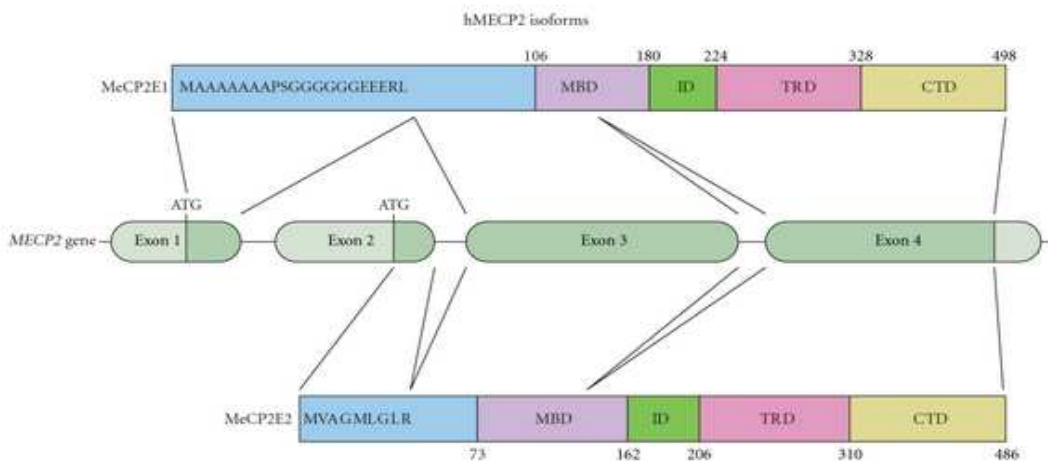
Figure 5 **MECP2 gene and protein isoforms**.

Schematic illustration of the gene structure of MECP2 and the different domains of the two protein isoforms, MeCP2E1 and MeCP2E2. The primary amino acid composition of the N-terminus of MeCP2E1 and MeCP2E2 is depicted.

(Image taken from (http://www.hindawi.com/journals/np/2012/415825/fig2))

The MeCP2 protein is present in all vertebrates, including the sea lamprey, a primitive jawless vertebrate, but no MeCP2 orthologous has been detected in invertebrate animals or plants. There are known MeCP2 orthologous in rat, mouse, monkey, *Xenopus,* and zebra fish, suggesting that MeCP2 has served important functions throughout vertebrate evolution, although these may be

different between widely divergent species. Sequences from human and mouse, for example, which diverged from a common ancestor, are 95% identical at the amino acid level. Divergences between mammalian MeCP2 and amphibian or fish MeCP2 is more extensive (33% amino acid identity between human and zebra fish), but conserved sequences as the MBD domain are present.

2.3.2. *MECP2* MUTATIONS AND THEIR INFLUENCE ON THE PHENOTYPIC OUTCOME

Over the past few years, more than 2000 pathogenic mutations have been reported in females with RTT (Amir et al. 1999; Weaving et al. 2005). This includes missense mutations, nonsense mutations, frameshift mutations, large deletions and/or duplications. 70% of the reported alteration are due to C>T substitution in CpG hotspots in *MECP2* and results in loss of function due to truncated, unstable or abnormally folded proteins. More recently, large rearrangements that involve *MECP2,* including deletions, were reported.

Attempts to establish genotype-phenotype correlations in females with RTT give conflicting results, due to the phenotypic variability consequence of different pattern of X-chromosome inactivation. However some patterns have recently begun to emerge. Female patients with mutations in *MECP2* that truncate the protein towards its C-terminal end (late-truncating mutations) have a phenotype that is less severe, and less typical of classic RTT, than patients who have missense or N-terminal (early truncating) mutations (Charman et al. 2005). In addition, the Arg270X mutation, which results in a truncated protein, is associated with increased mortality. This is consistent with greater clinical severity in cases with mutations upstream of or within the TRD domain. However, as missense and late-truncating mutations can lead to either classic or atypical RTT, it has been suggested that genetic background and/or non-random X-

chromosome inactivation in the brain influence the biological consequences of mutations in *MECP2*.

Mutations in *MECP2* in males were initially thought to be prenatally lethal; however, it has been shown that these mutations cause a variable phenotype in males, ranging from mental retardation to severe encephalopathy. *MECP2* mutations that cause classic RTT in females typically lead to neonatal encephalopathy and death in the first year of live in males with normal karyotype, while some mutations that do not cause RTT in females can cause moderate, nonspecific to profound mental retardation or psychiatric disorders in males.

2.2.3. CURRENT PERSPECTIVES ON MeCP2 FUNCTIONS

MeCP2 as a transcriptional regulator

The prevailing view of MeCP2 function at the transcriptional level is largely based on a model of methylation-dependent binding and subsequent induction of transcriptional repression. MeCP2 binds to promoter regions containing methylated CpGs upstream of the transcription start site of target genes. This binding recruits co-repressor complexes through the interaction with the TBD domain (transcriptional repressor domain) and cause local chromatin compaction and consequent transcriptional down-regulation (Fig. 6A).

MeCP2 binds to the methylated promoter of target genes and recruits chromatin-remodeling complexes that contain SIN3A (a transcriptional co-repressor), BRM (a SWI/SNF-related chromatin remodeling protein) and histone deacetylases (HDACs). This leads to chromatin condensation owing to histone deacetylation, which results in a limited accessibility of the transcriptional machinery to the promoter of the target gene (Jones et al. 1998; Nan et al. 1998). MeCP2 also interacts with other co-repressors, such as SK1 viral proto-

oncoprotein and the nuclear co-repressor NCOR, both of which are components of the HDAC complexes (Kokura et al. 2001).

In regards to MeCP2 target genes, the initial attempts to identify such targets were heavily influenced by the model that MeCP2 acts solely as transcription repressor. In order to identify putative target genes in a high-throughput, genome-wide manner, transcriptional profiling studies were performed. These early gene expression studies using either human post-mortem tissues or whole brain tissues from Mecp2-deficient animals, identified only a modest number of target genes and failed to support the role of MeCP2 only as transcriptional repressor (Colantuoni et al. 2001; Traynor et al. 2002; Tudor et al. 2002; Nuber et al. 2005; Jordan et al. 2007). The identification of both up- and down-regulated genes argues against a single role of MeCP2 in transcriptional regulation and elucidates a limited or direct role of MeCP2 also in transcriptional activation (Fig. 6B).
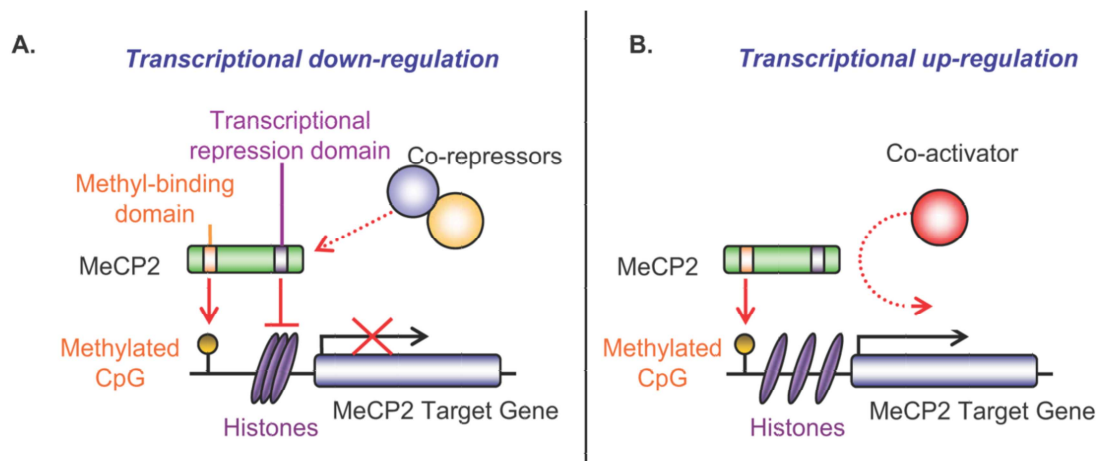
*Figure 6 **MeCP2 as a transcriptional regulator**.*

(A) MeCP2 as a transcriptional repressor. MeCP2 binds to methylated CpG upstream of the transcriptional start site of MeCP2 target genes. This recruits repressive co-factors to presumably cause local chromatin compaction and transcriptional down-regulation.

MeCP2 as a histone-like protein

Elucidating the transcriptional function of MeCP2 is further complicated by the recent evidence that MeCP2 is also a potent chromatin-condensing protein, which mediates the assembly of novel chromatin secondary structures independently of its binding to methylated DNA (Georgel 2007). This role of MeCP2 as histone-like protein was further confirmed by Skene et al. (Skene et al. 2010). An important observation of this study is that neurons only have half the amount of histone H1 compared with non-neurons; in the absence of MeCP2, histone H1 increases in neurons up to the level of non-neuronal cells. This is accompanied by a global increase in acetylation state. These findings indicate a complex interplay between gene expression regulation in neurons that may involve compensatory mechanisms between MeCP2 and histone H1. Nevertheless more work is needed to determine the relationship between gene expression changes and MeCP2's role as histone-like protein.

MeCP2 regulation of imprinted genes

An involvement of MeCP2 in the regulation of imprinted genes was first indicated by studies that showed subtly altered expression of *UBE3A* (ubiquitin protein ligase E3A), *GABRB3* (γ-aminobutyric-acid receptor β3) and *Dlx5* (distal-less homebox 5) in patients with RTT and in Mecp2-deficient mice (Horike et al. 2005; Makedonski et al. 2005; Samaco et al. 2005).

UBE3A, which encodes the ubiquitin ligase E3A, is located in an imprinted region, that has a causal role in Prader-Willi Syndrome (PWS) and Angelman Syndrome (AS). The imprinted expression of genes in this region involves a complex regulation that requires *cis*-acting elements, known as imprinting control regions (ICRs). The ICRs coordinate the expression of several neighboring genes and direct expression of genes within this region from the allele that is derived from one parent only, based on allele-specific epigenetic modifications of chromatin. The imprinting control region for the PWS-AS locus consists of two parts, with the AS ICR located more centromeric. Regulation of *UBE3A* expression also involves both a region that is located upstream of the nearby small nuclear ribonucleoprotein polypeptide N (*SNRPN*)-*SNRPN* upstream reading frame (*SNURF*) locus, known as the PWS-AS imprinting center, and the recently identified small nucleolar RNAs that overlap with *UBE3A* and are transcribed in the opposite direction. This transcript is also thought to inhibit the expression of *UBE3A* from the paternal allele through an antisense mechanism. *UBE3A* mRNA and protein levels are slightly reduced in MeCP2-deficient human and mice brains and *UBE3A* expression has been shown to be regulated by MeCP2. This downregulation of expression correlates with a biallelic production of *UBE3A* antisense RNA and changes in the chromatin structure, with increased acetylation and methylation of H3K4 (histone 3 lysine 4), and reduced methylation of H2K9 at the PWS-AS imprinting center. This indicate that MeCP2 might regulate the interpretation of imprinted DNA-methylation marks in this region, in combination with other chromatin-binding proteins.

MeCP2 can also regulate gene expression and maternal imprinting through the formation of a silent chromatin-loop. Horike et al. used chromatin immunoprecipitation to identify Mecp2-binding sites in mouse brains and revealed several sequences located within an imprinted gene cluster on chromosome 6, including Dlx5 and Dlx6 (Horike et al. 2005). The expression of these two genes is two times higher in the brains of Mecp2-null mice and interestingly the Dlx5-imprinted pattern is disrupted in these brains. Mecp2 has

shown to interact with sequences near the imprinted Dlx5 and Dlx6 genes, mediating the formation of a 11-kb chromatin loop at the Dlx5-Dlx6 locus that is enriched in methylated H39K. This leads to an integration of Dlx5 and Dlx6 into a loop of silent, methylated chromatin, and represses their expression. In Mecp2-deficient brains this loop is absent and the expression of Dlx5 and Dlx6 is no longer repressed, which results in the over-expression of these two genes.

MeCP2 as splicing regulator

Another mechanism by which alterations in MeCP2 function might contribute to the characteristic features of RTT is through disruption of alternative splicing in the brain (Young et al. 2005). MeCP2 has been shown to interact with the YB1 protein (Y-box-binding protein 1, also known as p50 and EF1A), a principal component of messenger ribonucleoprotein particles that controls multiple steps of mRNA processing, including the selection of alternative splicing sites. The role of the MeCP2-YB1 complex was investigated by examining its function in the regulation of alternative splicing of candidate genes, such as NMDA receptor unit 1 (NR1) *in vivo*. The expression of NR1 is regulated by an alternative splicing event that is independent on neuronal activity and generates two functional variants. The comparison of wild-type and Mecp2-null mice showed significant differences in the amount of the two variants of NR1.

2.2.4. MECP2 TARGETS

Brain-derived neurotrophic factor (BDNF)

Two research groups (Chen et al. 2003; Martinowich et al. 2003) found that MeCP2 specifically binds to methylated CpG sites near the promoter III region of BDNF in rats and promoter IV region of BDNF in mice, respectively, thereby repressing BDNF transcription in resting neuronal cells. When the neurons where exposed to potassium chloride, which induce membrane depolarization, calcium influx and BDNF release, MeCP2 dissociated from the BDNF promoter. This displacement has been suggested to result from reduced CpG methylation in the relevant region of the activated promoter (Martinowich et al. 2003). An alternative mechanism has been proposed by Chen and his group, which showed a time-dependent increase in MeCP2 phosphorylation when neurons where stimulated with potassium chloride, which might influence the affinity of MeCP2 for the methylated promoter site (Chen et al. 2003). SIN3A, a MeCP2 co-repressor, is also displaced from the repressor complex after membrane depolarization induced by potassium chloride, and loss of MeCP2 is accompanied by changes in histone modification, which results in a transcriptionally permissive chromatin state.

Although the specific functions of BDNF have not been completely elucidated, its important role in regulating synaptic plasticity and its effects as neurotrophic factor are well defined. A deficit in MeCP2 function and its downstream effects on BDNF expression might therefore account for the neurobiological and cellular defects observed in RTT. In support of this, transgenic mice that overexpress BDNF develop symptoms that are similar to those in Mecp2-deficient mice (Croll et al. 1999).

Hairy 2

A recent study has identified another gene involved in neuronal differentiation as a target of MeCP2. In *Xenopus*, MeCP2 inhibits the expression of *xHairy2a*, which itself is a target of the Notch/Delta signaling pathway. With reduction of MeCP2 activity, *xHairy2* expression is increased, and this leads to inhibition of primary neurogenesis (Stancheva et al. 2003). It will be interesting to study whether MeCP2 plays a role in other Notch regulated aspects of neuronal maturation.

UBE3A (ubiquitin protein ligase E3A)

UBE3A encodes for an ubiquitin ligase, an enzyme that is involved in the polyubiquitylation of target proteins in order to mark them for degradation. Mutations in the maternal allele of this gene (the paternal allele is normally inactivated in the brain due to paternal imprinting) are responsible for some cases of Angelman Syndrome, a genetic disorder characterized by hyperactivity, ataxia, problems with speech and language. If the paternally material from the same region is mutated instead, the brother syndrome, the Prader-Willi Syndrome, characterized by similar features such as mental retardation, learning disabilities and behavioral problems, is the result. MeCP2 regulates the imprinted gene *UBE3A* in a temporally and spatially defined manner and the deregulation of *UBE3A* expression that results from MeCP2 loss of function might contribute to the clinical manifestations of RTT, such as mental retardation, seizures, muscular hypotonia and acquired microcephaly, that overlap also with the other two disorders.

DLX5 (distal-less homebox 5)

DLX5 regulates the production of enzymes that synthetize γ-amino butyric acid (GABA) and is overexpressed in Mecp2-deficient brains as a consequence of loss of imprinting. This might alter GABA-dependent neuron activity and contribute to the clinical manifestations of RTT.

Glucocorticoid-regulated genes (Fkpb5 and Sgk1)

Nuber et al. found that Mecp2-null mice differentially express several genes that are induced during the stress response by glucocorticoids. Increased levels of mRNAs for serum glucocorticoid-inducible kinase 1 (Sgk 1) and FK506-binding protein 51 (Fkbp5) were observed before and after onset of neurological symptoms, but plasma glucocorticoid was not significantly elevated in Mecp2-null mice. Mecp2 is bound to the *Fkbp5* and *Sgk* genes in brain and may function as a modulator of glucocorticoid-inducible gene expression. Given the known deleterious effect of glucocorticoid exposure on brain development, this data raises the possibility that disruption of MeCP2-dependent regulation of stress-responsive genes contributes to the symptoms of RTT (Nuber et al. 2005).

2.2.5. Mecp2 MOUSE MODELS

To uncover the molecular mechanisms underlying MeCP2 dysfunction in the past few years several mouse models were generated.

Mecp2 conditional male knockout mice (Mecp2$^{-/Y}$), lacking either exon 3 or both exon 3 and 4 (Chen et al. 2001; Guy et al. 2001), display severe neurological symptoms, including uncoordinated gate, hypoactivity, tremor, hind limb clasping and irregular breathing. Similarly to RTT patients they undergo a period of normal development, followed by severe neurological dysfunction, leading to death at 8-10 weeks of age. Behavioral testing of these conditional Mecp2 knockout models revealed phenotypes similar to RTT patients, including deficits in motor learning, increase in anxiety-like behavior, impairments in social interaction and altered learning and memory-related behaviors. Female Mecp2$^{+/-}$ mice show similar behavioral abnormalities, but with a later stage of onset. The brains of Mecp2-null mice are smaller in weight and size than brains of wild type littermates, but have no detectable structural abnormalities, except smaller, more densely packed neurons were found in hippocampus, cortex and cerebellum (Chen et al. 2001). In addition, the olfactory neurons of Mecp2-null mice demonstrate abnormalities of axonal targeting in the olfactory bulb, suggesting a function for MeCP2 in terminal neuronal differentiation (Matarazzo and Ronnett 2004). To elucidate the role of Mecp2-loss in the brain, a conditional KO approach, using a nestrin-Cre transgene, was used to specifically delete Mecp2 expression in the brain during early embryonic development. These mice show phenotypes similar to those observed in Mecp2-null mice, demonstrating that MeCP2 dysfunction in the brain is sufficient to cause the disease (Guy et al. 2001). Similar but less severe neurological phenotypes are observed when Mecp2 is only deleted in postmitotic neurons of broad forebrain regions using a calcium-calmodulin-dependent kinase II (CaMKII)-Cre transgene, confirming an important role of MeCP2 in mature neurons (Chen et al. 2001; Gemelli et al. 2006). To further confirm the idea that MeCP2 is not essential for early brain development but has a

crucial role in mature neurons, Mecp2 was expressed under the control of the endogenous tau promoter in Mecp2-null mice and a total recovery of the neurological symptoms were observed (Luikenhuis et al. 2004).

Shahbazian et al. created another mouse model, introducing a truncating disease-causing mutation in the murine Mecp2 gene (at amino acid 308) effectively deleting only the C-terminus end of Mecp2's coding sequence (Shahbazian et al. 2002a). The $Mecp2^{308/Y}$ mice appear normal until 6 weeks of age, when they start to display impairments in motor learning, forepaw stereotypes, hypoactivity, tremor, seizures anxiety-related behaviors and deficits in social interactions. This model as well as female heterozygous mice for the truncation display milder and more variable traits.

Transgenic mouse models with two-fold overexpression of human MeCP2 under the control of its endogenous promoter ($MECP2^{Tg}$) recapitulate many of the same behavioral phenotypes seen in Mecp2 KO mice, with the onset around 10 weeks of age. Initially these mice display increased synaptic plasticity, with consequent enhancement in motor and contextual learning abilities, followed by social impairment, hypoactivity and motor deficits around 20 weeks of age. Mouse lines that overexpress MeCP2 have also been created by using a large insert genomic clone from a P1-derived artificial chromosome contacting MeCP2 locus (Collins et al. 2004), demonstrating that higher levels of MeCP2 expression are associated with more severe phenotypes. Overexpression of MECP2 in adult neurons under control of the tau promoter also results in a progressive neurological symptomatology (Luikenhuis et al. 2004). These studies suggest that MeCP2 levels must be tightly regulated even postnatally and that the slightest perturbation results in deleterious neurological consequences.

The characterization of these different mouse models clearly indicate that homeostatic regulation of MeCP2 is necessary for normal CNS functioning. Both the loss and the overexpression of MeCP2 result in neurological phenotypes

similar to those seen in patients with RTT, revealing a need for precise control over the amount of MeCP2 expression.

2.2.6. THE ROLE OF MeCP2 IN THE BRAIN

MeCP2 is an essential epigenetic regulator in human brain development. *MECP2* mutations and dysfunctions, responsible for the classic form of RTT, have also been associated with a broad array of other neurodevelopmental disorders in males and females, including X-linked mental retardation (XLMR), severe neonatal encephalopathy, Angelman Syndrome (AS), and autism, demonstrating that disruption of MeCP2 can have wide-ranging effects on neurodevelopment and plays an important role during correct brain development (Hammer et al. 2002).

MeCP2's role in CNS development and neuronal maturation

Patients with RTT display a normal period of development prior to symptom onset and then undergo a period of regression, suggesting that MeCP2 may play a more functional role in early postnatal development rather than during embryonic periods. Additional confirmation has come from studying the timing of MeCP2 expression in both human and rodents. In the rodent CNS, MeCP2 expression is first detected in the brainstem and spinal cord around day E12, while *MECP2* mRNA is detected in subcortical regions at the beginning stages of embryonic neurogenesis (Shahbazian et al. 2002b; Jung et al. 2003). In thalamus, caudate putamen, cerebellum, hypothalamus and hippocampus MeCP2 expression starts at days E14-16, similarly to the cerebral cortex, where expression is first limited to the deeper cortical layers before spreading out to more superficial layers around day E18. Over the course of cellular differentiation, amounts of MeCP2

protein increase from early postnatal development into highly adulthood, in accordance with high MeCP2 expression in the mature brain (Shahbazian et al. 2002b). In olfactory neurons, MeCP2 expression is also correlated with neuronal maturation (Cohen et al. 2003), during a period between neurogenesis and synaptogenesis. In humans this period occurs in the early embryonic week 12-20, and the loss of MeCP2 in RTT patients within this time window may be responsible for the observed decrease in neuronal and overall brain size. Autopsy studies show a 12%-34% reduction in brain weight and volume in patients with classic RTT, the effect most pronounced in the prefrontal, posterior frontal, and anterior temporal regions (Armstrong 2005). There is a decrease in the size of cortical minicolumns (Casanova et al. 2003), which is in accordance with the observation that there is a reduced dendritic branching of layers III and V of pyramidal neurons in frontal, temporal and motor regions, and of layer II and IV of the subiculum (Armstrong et al. 1995). At the same time, neurons of hippocampal CA1 and occipital regions are relatively preserved and although neuronal size is reduced in the cortex, thalamus, basal ganglia, amygdala and hippocampus, there is an increase in neuronal cell packing in the hippocampus (Kaufmann and Moser 2000). The loss of MeCP2 expression within the critical period for neuronal maturation and synaptogenesis, cumulating in an abnormal development of the CNS, may be responsible for the characteristic neuronal RTT phenotype.

MeCP2 regulates dendritic morphology

The reduction in brain size and neuron size seen in Mecp2-null mice and RTT patients is accompanied by a reduction in axonal and dendritic processes and decreased levels of the dendritic cytoskeletal protein MAP2 (microtubule associated protein 2). In addition neurons in RTT patients show a decrease of dendritic spine density (Armstrong 2002; Chapleau et al. 2009). In female RTT patients, CA1 pyramidal neurons exhibit decreased spine density (Chapleau et al.

2009) and MeCP2- deficient neurons have fewer dendritic spines and reduced arborization in the hippocampus and in the olfactory system (Zhou et al. 2006; Smrt et al. 2007; Palmer et al. 2008). Similar abnormalities in dendritic spines have been seen in human subjects with mental retardation and in animal models of Down syndrome (Kurt et al. 2000; Belichenko et al. 2004; Belichenko et al. 2007) and these dendritic abnormalities may contribute to the cognitive impairment in RTT patients (Fig.7).
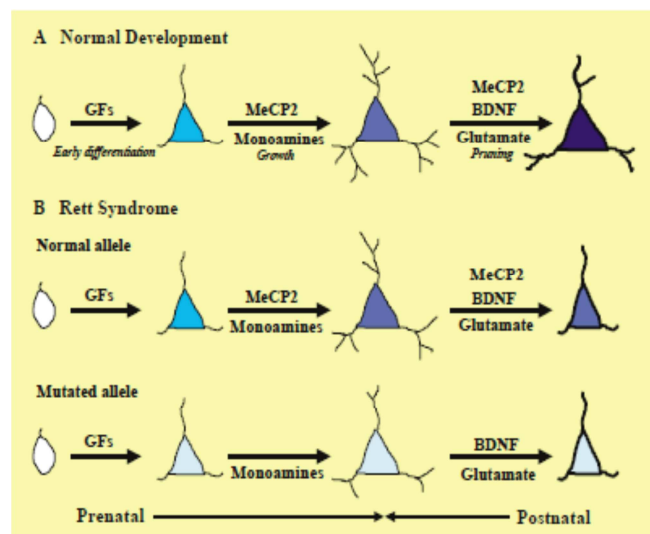
Figure 7 **Model of neuronal pathology in RTT based on dendritic development in prefrontal cortex.**

During normal development, onset of MeCP2 expression coincides with early neuronal differentiation. Direct targets of MeCP2, such as BDNF, in conjunction with other synaptic signals have a particularly strong effect on the process of dendritic pruning. Marked reduction in MeCP2 function and deficient afferent input, in neurons carrying a MeCP2 mutated allele, impair appropriate dendritic expansion. The abnormality extends and worsens during dendritic puring because of the abnormally high levels of MeCP2 targets and additional neurotransmitter disturbance. The ultimate neuronal phenotype is characterized by a smaller cell with markedly decreased MeCP2 expression and dendritic arborization.

(Image taken from (Kaufmann et al. 2005)).

MeCP2 and synaptic transmission

Long-term synaptic plasticity is widely accepted as the cellular basis for learning and memory, which can be observed as long-term potentiation (LTP) or long-term depression (LTD) of synaptic responses. LTP has been shown to be adversely affected in cortical and hippocampal slides of Mecp2-nullmice (Asaka et al. 2006¸Moretti, 2006 #86). A number of studies also show that MeCP2 KO hippocampal and cortical cultures display a significant decrease in spontaneous excitatory synaptic transmission, while inhibitory activity is increased (Dani et al. 2005; Nelson et al. 2006; Chao et al. 2007). These changes in neurotransmission suggest an overall shift in the ration of excitation and inhibition and indicate that MeCP2 is essential in modulating synaptic function and plasticity.

2.3. CDKL5

2.3.1. THE *CDKL5* GENE AND ITS PRODUCTS

The kinase CDKL5 was initially identified through a positional cloning study aimed at isolating genes mapping to Xp22 (Montini et al. 1998). The eukaryotic protein kinases represent a large superfamily of homologous proteins, related by the presence of a highly conserved kinase domain of 250-300 amino acids. There are two many subdivisions within the superfamily of eukaryotic protein kinases: the serine-threonine protein kinases and the protein tyrosine kinases. Sequence analysis revealed homologies to several serine-threonine kinase genes, and further characterization of the predicted protein product identified two protein kinase signature, one of which is specific for serine-threonine kinases. Consequently Montini et colleagues first named the identified gene *STK9* (Serine Threonine Kinase 9). Serine-threonine kinases very frequently have been involved in the pathogenesis of genetic disorders and a number of human genetic disorders have been mapped to the Xp22 region. Montini et al. suggest the Nance-Horan syndrome (NH), a X-linked recessive disorder characterized by cataract and dental anomalies, as a candidate disorder for *STK9* mutations. In the next five years, mutations in this gene were found in epileptic patients and in 2003 Vera Kalscheuer suggested *STK9* to be a chromosomal locus associated with X-linked infantile spasms (ISSX) (Kalscheuer et al. 2003). The X-linked infantile spasm is characterized by early-onset generalized seizures, hypsarrhytmia and mental retardation and majority of cases are due to mutations in the aristaless-related homebox gene (*ARX*), which maps to the Xp21.3-p22.1 interval. Kalscheuer and colleagues in this paper show the disruption of *STK9* in two unrelated patients with identical phenotype and suggest that the lack of functional STK9 protein may

be the second cause of this X-linked disorder. Given the strong similarity to some cell division protein kinases, the *STK9* gene subsequently got renamed *CDKL5* (cyclin-dependent kinase like 5).

The human *CDKL5* gene occupies approximately 240 kb of the Xp22 region and is composed of 24 exons of which the first three exons (exon 1, 1a and 1b) are untranslated, whereas the coding sequence are contained within the exons 2-21 (Fig. 8A). Following the identification of the human *CDKL5* gene in 1998 by Montini et al., a number of different isoforms and splicing variants have been identified. Two different splice variants with different 5'UTRs have been identified: isoform I, containing exon 1, is transcribed in a wide range of tissues, whereas isoform II, including exon 1a and 1b, is limited to testis and fetal brain (Kalscheuer et al. 2003; Williamson et al. 2011). Alternative splicing events lead to three distinct human protein isoforms (Fig. 8B, C). The original CDKL5 transcript generates a protein of 1030 amino acids and 115 kDa of molecular weight (CDKL5$_{115}$) and is mainly expressed in the testis. Two other more recently identified transcripts, characterized by an altered C-terminal region, are likely to be relevant for CDKL5 brain functions (Fichou et al. 2011; Williamson et al. 2011). Firstly, an alternatively spliced isoform has been described in both human and mouse, which has an additional in-frame exon of 123 bp, exon 16b, between exons 16 and 17, producing a predicted protein of 120kDa in humans and a 110 kDa protein in mice (Fichou et al. 2011; Rademacher et al. 2011). Interestingly this variant is highly conserved in species through evolution, suggesting a potential functional role, but does not display any homology with other referenced sequences. Fichou et al. also demonstrate that the amount of exon 16b-containing (CDKL5$_{115+ex.16b}$) transcript varied depending on the brain region analyzed and that this transcript is brain specific. The second isoform identified also in 2011 by Williamson et al. is a 107 kb isoform with an alternative C-terminus that terminates in intron 18 (CDKL5$_{107}$) and is the predominant isoform in human and mouse brains, suggesting that this isoform is likely to be of primary pathogenic importance in the CDKL5 disorder. Although this is the major CDKL5 splice

variant, there are species-specific CDKL5 splice variants. Very recently, another previously unidentified CDKL5 splice variant producing a protein product with a variant C-terminus has been described in rat neurons and glial cells (Chen et al. 2010). These isoforms have specific tissue distributions and end in rat exon 19, which is unique to the rat genome.
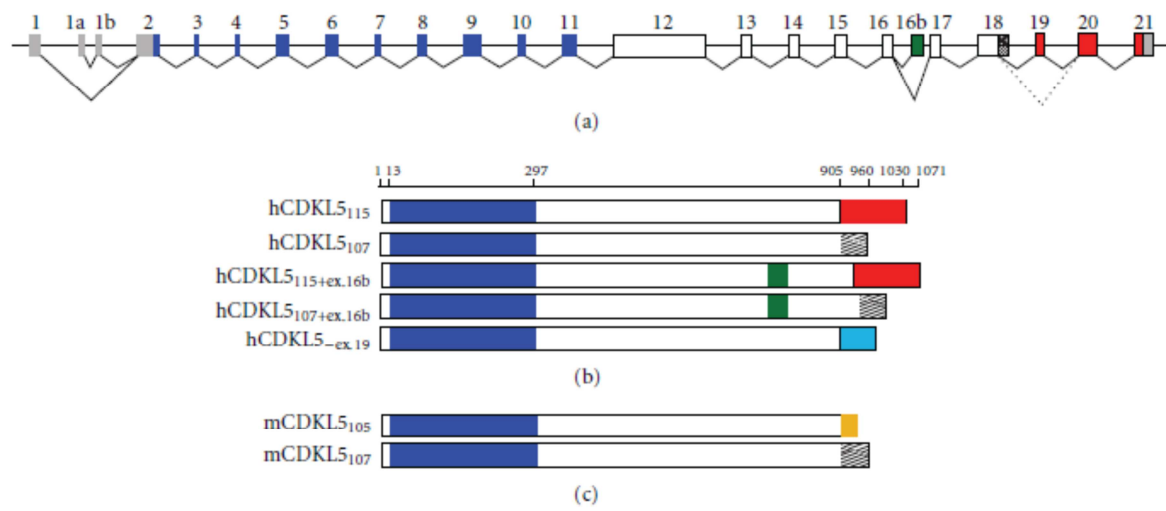
*Figure 8 **The genomic structure of CDKL5 and its splice variants.***

(A) The human CDKL5 gene with untranslated sequences in grey and exons encoding the catalytic domain in blue. Exons encoding the common C-terminal region appear in white, whereas isoform-specific sequences are shown in red, green, and as hatched.

(B) hCDKL5 protein isoforms differing in the C-terminal region. $CDKL5_{115}$ contains the primate specific exons 19-21. In $CDKL5_{107}$, intron 18 is retained. The inclusion of exon 16b would generate $CDKL5_{115+ex.16b}$ and/or $CDKL5_{107+ex.16b}$. $hCDKL5_{-ex19}$ is a hypothetical splice variant in which exon 19 is excluded generating alternative C-terminus (light blue).

(C) The murine CDKL5 isoforms. $mCDKL5_{105}$ harbors a distinct C-terminal region encoded by a mouse specific exon 19 (orange). As in humans, the retention of intron 18 generates the common $CDKL5_{107}$ isoform.

(Image taken from (Kilstrup-Nielsen et al. 2012)).

The CDKL5 protein belongs to the CMGC family of serine-threonine kinases, which include cyclin-dependent kinases (CDKs), mitogen-activated protein kinases (MAP kinases), glycogen synthase kinases (GSK), and CDK-like kinases, and is characterized by a N-terminal catalytic domain (amino acids 13-297), homologous to that of other CDKL-family members, such as p56KKIAMRE (CDKL1), p42KKIALRE (CDKL2) and NKIAMRE (CDKL3). This N-terminal catalytic domain contains the ATP-binding region (amino acids 13-43), the serine-threonine kinase active site (amino-acids 131-143) and a Thr-Xaa-Tyr motif (TEY) at amino acids 169-171, whose dual phosphorylation is normally involved in activating kinases of the MAP kinase family. In analogy to all the other members of the family of serine-threonine kinases, 12 conserved subdomains can be identified in this 284-amino acid kinase domain (Fig. 9).

Interestingly, most of the pathogenic missense mutations identified so far hit the catalytic domain, suggesting that the enzymatic activity of CDKL5 is essential for normal neurodevelopment.
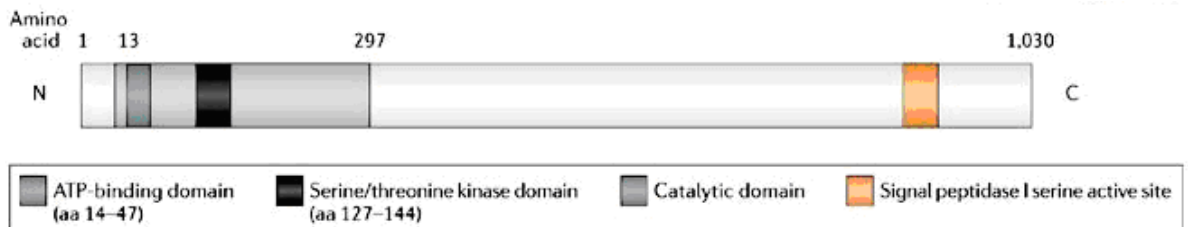
*Figure 9 **Schematic representation of the CDKL5 protein.** (Image taken from (Bienvenu and Chelly 2006)).*

CDKL5 is unique in his family of kinases as it presents an unusual long C-terminal tail of more than 600 amino acids, highly conserved between different CDKL5 orthologous. This region contains putative signals for nuclear import (NLS) and export (NES) and seems to be involved in the cellular localization of the protein (Rusconi et al. 2008) and either the catalytic activity (Bertani et al. 2006).

2.3.2. *CDKL5* MUTATIONS AND THEIR INFLUENCE ON THE PHENOTYPIC OUTCOME

Since 2003, when Kalscheuer et al. identified the first mutations in *CDKL5* in two unrelated girls who, in addition to seizures and mental retardation, had hypsarrythmia and infantile spasms (Kalscheuer et al. 2003), patients with different phenotypic outcome of the disorder, harboring a wide range of pathogenic mutations, have been described in literature. More than 80 different point sequence variations have been described so far, including missense and nonsense mutations, small and large deletions, frameshift and splicing mutations. Even considering the small number of patients described, some "hot-spots" and genotype-phenotype correlations can be proposed.

It has been suggested that missense mutations are mainly localized in the N-terminal catalytic domain, underlining the important role of the CDKL5 kinase activity during brain function and/or development. These mutations are associated with a more severe phenotype, characterized by early onset of intractable infantile spasms followed by late onset multifocal myoclonic epilepsy, while patients with stop-codon mutations in the long C-terminus of *CDKL5* present a milder phenotype (Bahi-Buisson et al. 2008).

As previously described CDKL5 contains an ATP-binding motif and a conserved kinase catalytic domain in its N-terminus. The missense mutation p.Ala40Val in the ATP-binding domain has been described in 5 independent patients with common prominent autistic features. Compared to girls with other *CDKL5* mutations these patients had better hand use and tend to present a better ability to walk, suggesting that mutations in the ATP-binding domain may result in a less severe phenotype (Bahi-Buisson et al. 2012). Even though the less number of cases described, some hot spots, as the ARG178-codon, located in the kinase catalytic domain, have been identified. Different missense mutations (p.Arg178Pro, pArg178Trp, pArg178Gln) have been identified at this codon, and it seems that the exchange of a positively charged amino acid such as arginine for an uncharged one (Pro, Trp and Gln), would likely influence substrate-binding specificity (Bahi-Buisson et al. 2012). Missense mutations in this catalytic kinase domain can be considered as loss-of function mutations as they impair the kinase activity of CDKL5 and generally result in a more several phenotypic outcome of the disease. Truncating mutations can be found anywhere in the gene, leading to CDKL5 derivatives of various length. Several truncating mutations, including the mutations p.Arg59X and p.Arg134X and the splice mutation c145+2T>C have been identified in the catalytic kinase domain, while different pathogenic mutations have also been found in the rather uncharacterized C-terminus of *CDKL5*. Some reports suggest that mutations in the C-terminus originate a milder clinical picture than those caused by mutations in the catalytic domain. Interestingly, the c.23635_2636delCT mutation, which leads to a protein truncation in position 908, is associated with a more severe phenotype, without affecting the catalytic domain (Bahi-Buisson et al. 2012).
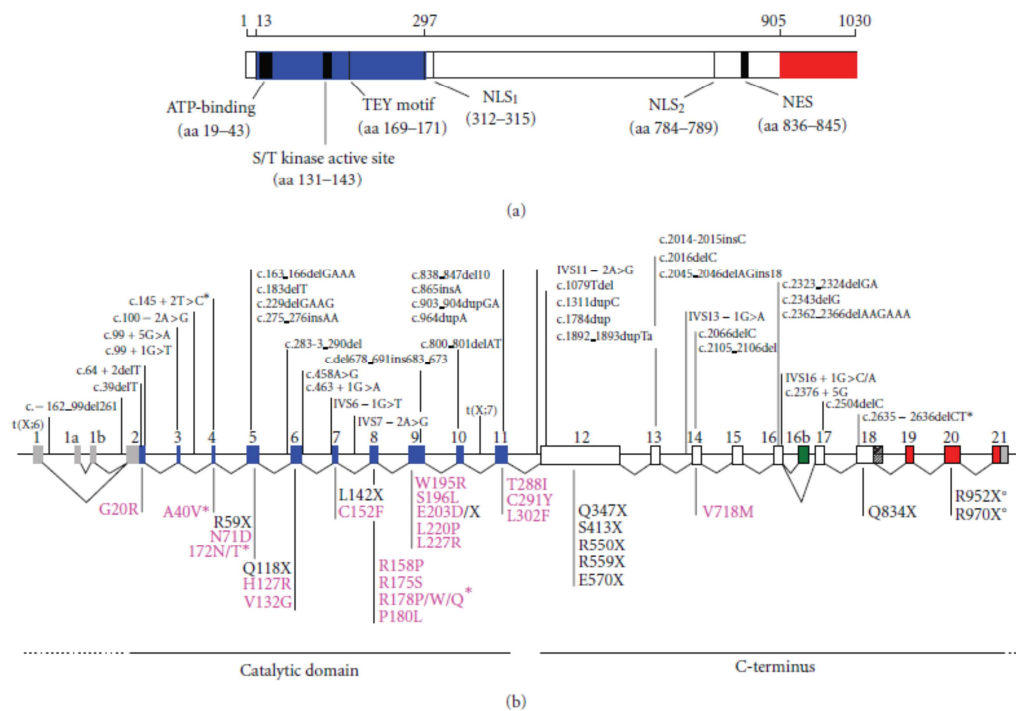
*Figure 10 **Pathogenic CDKL5 mutations.***

(A) Schematic representation of CDKL5₁₁₅ with the functional domains and signatures indicated. NLS: nuclear localization signal; NES: nuclear export signal.

(B) All mutations in CDKL5 reported to date are indicated corresponding to their location within the gene. Mutations shown above the CDKL5 gene are deletion and frame shift mutations as well as splice variants indicated with cDNA nomenclature. Missense and nonsense mutations (fuchsia and black, resp.) are represented with amino acid nomenclature below the CDKL5 gene.

(Image taken from (Kilstrup-Nielsen et al. 2012)).

2.3.3. CURRENT PERSPECTIVES ON CDKL5 FUNCTIONS

CDKL5 might regulate the function of epigenetic factors and transcriptional regulators

The first demonstrating the phosphorylation activity of CDKL5 were Mari et al. in 2005. Considering the similar phenotypes caused by mutations in *MECP2* and *CDKL5*, they investigated the expression patterns of both proteins in embryonic and postnatal mouse brains. MeCP2 and Cdkl5 show a spatial and temporal overlapping expression during neuronal maturation and synaptogenesis in the brain, in favor of a possible involvement of the two proteins in the same development pathway (Mari et al. 2005). They also investigate whether MeCP2 and CDKL5 directly interact in *vitro* and in *vivo*. By classical pull-down assays Mari et colleagues demonstrated that MeCP2 and CDKL5 are directly interacting in *vitro* and that a portion on MeCP2, containing the last residues of the TRD and the C-terminal region, is responsible for this association. An analog interaction was demonstrated also in *vivo* by co-immunoprecipitation experiments. Given the direct interaction between MeCP2 and CDKL5 and the overlapped expression in different brain regions, they further investigated whether CDKL5, based on the sequence homologies with other kinases, is able to autophosphorylate and to phopsphorylate MeCP2.

Their results demonstrate that CDKL5 is indeed a kinase, which is able to autophosphorylate itself and to mediate also MeCP2 phosphorylation, suggesting that these proteins belong to the same molecular pathway. There are some controversial results from another research group, which was able to demonstrate the autophosphorylate capacity of CDKL5 to, but not to confirm that CDKL5 is a direct target of MeCP2, neither ARX, the gene responsible for the X-linked infantile spasms (Lin et al. 2005).

Furthermore, a recent report has suggested a new link between CDKL5 and MeCP2. Both proteins have been shown, indeed, to bind to DNA Methyltransferase 1 (DNMT1), an enzyme that recognizes and methylates hemimethylated CpG dinucleotides after DNA replication to maintain a correct methylation pattern (Kameshita et al. 2008). More recently Carouge and colleagues addressed the question of the transcriptional control of Cdkl5 by Mecp2 as a potential link between the two genes, taking advantage of MeCP2 induction by cocaine in rat brain structures (Carouge et al. 2010). Their data reveal that over-expression of Mecp2 in transfected cells results in the repression of Cdkl5 expression and that *in vivo* Mecp2 directly interacts with Cdkl5 gene in a methylation-dependent manner. Taken together these results are consistent with Cdkl5 being a Mecp2-repressed target gene and provide new insights into the mechanism by which mutations in the two genes result in overlapping neurological symptoms (Carouge et al. 2010).

An interesting feature of CDKL5 that distinguishes it from MeCP2 is its subcellular localization. While MeCP2 is only a nuclear protein, CDKL5 seems to shuttle between the nucleus and the cytoplasm. The subcellular localization of CDKL5 within the cell seems to be important also for its function. In the nucleus CDKL5 co-localizes and is associated with a number of splicing factors that are stored in structures called nuclear speckles, in both cell lines and tissues. In these structures CDKL5 seems to manage the nuclear trafficking of splicing factors and thus indirectly of the splicing machinery (Ricciardi et al. 2009). It is already known that phosphorylation of the RS domain of Serine-rich (SR) splicing factors is necessary to release these factors from speckles and direct them to sites where pre-mRNA processing takes place. Considering that several protein kinases have been described to be able to phosphorylate the RS domain of SR proteins, Ricciardi and colleagues have hypothesized that also CDKL5 could have a role in nuclear speckles organization. Interestingly it has been demonstrated that CDKL5 acts on nuclear speckle disassembly determining a redistribution of at least some speckle proteins (Ricciardi et al. 2009). These results suggest that CDKL5 may

play a role in controlling gene expression through phosphorylation of DNMT1 and alteration of CpG methylation, which may affect the transcription of numerous genes. In addition, altering the distribution of the splicing factor machinery within the nucleus may result in alternative splicing of different RNA's leading to a subset of proteins with subtly altered functions. Rosas Vargas et al. looked at the effect of two missense mutations (p.Ala40Val and p.Leu220Pro) causing severe infantile encephalopathy on cellular distribution. These mutations are both within the catalytic domain of *CDKL5* and therefore likely to affect phosphorylation. In both cases the proteins were unable to cross into the nucleus suggesting that the phosphorylation state of CDKL5 may regulate its ability to enter the nucleus (Rosas-Vargas et al. 2008).

Cdkl5 expression correlates with neuronal maturation

Expression studies in human and mouse tissues have shown that CDKL5/Cdkl5 mRNA is present in a wide range of tissues, with highest levels of expression in the brain, underlining its importance for the nervous system functions. Comparing the expression levels of Mecp2 and Cdkl5 in mouse brains, Rusconi and colleagues demonstrated that Mecp2 expression is induced during embryogenesis and its levels remain rather constant during postnatal stage until adulthood, while Cdkl5 expression is very low during embryonic stages and is highly induced during the first two postnatal weeks, and after this period it declines (Fig. 11H) (Rusconi et al. 2008). Moreover Cdkl5 levels also vary in the different brain regions in adulthood, with highest levels in the cortex, hippocampus, and striatum. Interestingly very high expression levels are detected in the most superficial cortical layer, particularly involved in the connection of the two hemispheres through the corpus callosum, suggesting a possible role of CDKL5 in this brain region. In the hippocampus Cdkl5 mRNA is present at high levels in all the CA fields, while it presents lower expression in the dentate gyrus (DG), in accordance with the fact that DG neuronal maturation occurs mainly in

adulthood. Surprisingly compared to the other brain regions low levels of Cdkl5 were found in the cerebellum (Fig. 11) (Rusconi et al. 2008).
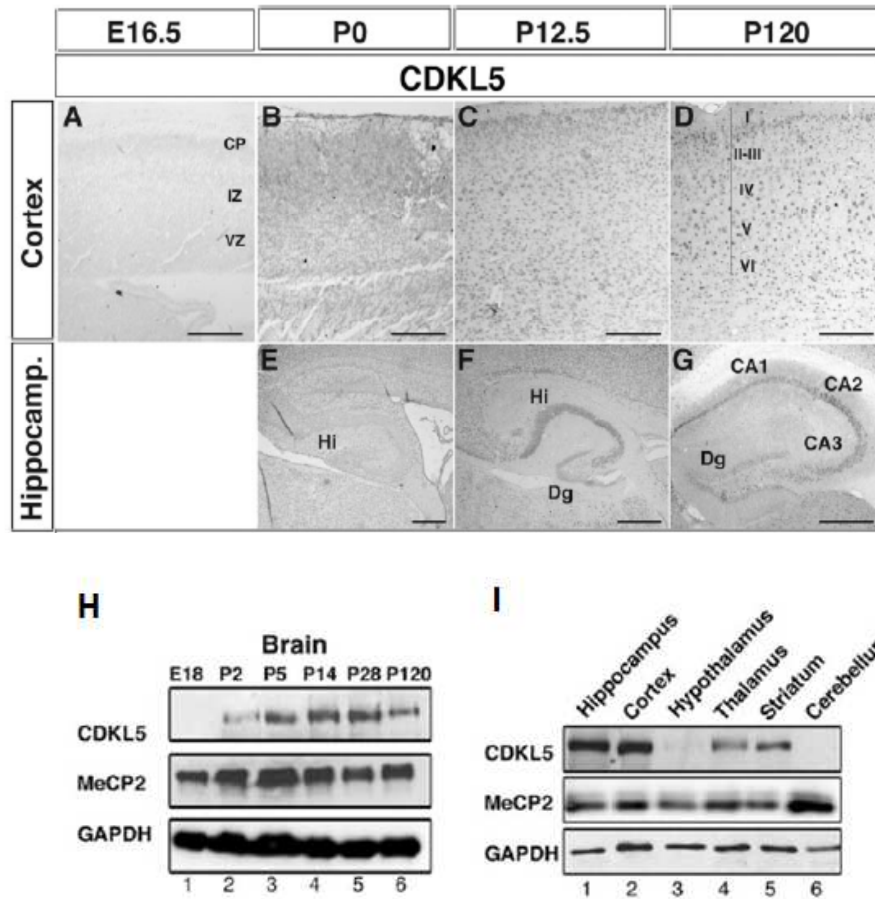
*Figure 11 **Cdkl5 expression is highly induced at early postnatal stages of brain development.***

(A-G) Immunohistochemistry experiments showing Cdkl5 expression in the cortex (A-D) and hippocampus (E-G) of mouse brains at different embryonic or postnatal stages.

(H) Western blot showing Cdkl5 and Mecp2 levels in the total brain at different embryonic and postnatal stages.

(I) Western blot showing Cdkl5 and Mecp2 levels in different brain area of adult mice (P120)

(Image taken from (Rusconi et al. 2008)).

As mentioned, CDKL5 seems to shuttle between the nucleus and the cytoplasm. In the mouse brain, Cdkl5 is initially predominantly cytoplasmatic and progressively accumulates in the nucleus, starting from roughly P14 when approximately 40% of total Cdkl5 can be detected in this cellular compartment. However, Cdkl5 gets significantly translocated to the nucleus only in certain brain areas; in the cerebellum for example more than 80% of Cdkl5 remains cytoplasmatic, while in the cortex it is almost equally distributed between the two compartments (Rusconi et al. 2008). The nuclear fraction increases during early postnatal stages consistently with neuronal maturation and remains as such until adult stages, suggesting that CDKL5 functions might be modulated through mechanisms regulating its shuttling between nucleus and cytoplasm. In accordance with this, Rusconi et al. also demonstrated that the C-terminal region of CDKL5 is important for its subcellular dynamic localization (Rusconi et al. 2008).

At the cellular level, CDKL5 is easily detectable in virtually all NeuN-positive neurons while it is expressed at very low levels in the glia (Rusconi et al. 2008), in accordance with an important role of CDKL5 in neuronal maturation and function. In cultured non-neuronal cells exogenous CDKL5 shuttles constitutively between the nucleus and the cytoplasm through an active nuclear export-dependent mechanism, which involves the C-terminus of CDKL5 and the CMR1 nuclear export receptor. Interestingly Rusconi and colleagues observed that a similar mechanism is not present in rat hippocampal neurons and this result integrated with the knowledge that Cdkl5 is mainly cytoplasmic in young brains and moves into the nucleus upon neuronal maturation suggests that, in neurons, CDKL5 is not dynamically cycling between the nucleus and cytoplasm. Cdkl5 intracelluar trafficking occurs in rat hippocampal neurons after specific stimulation with glutamate through an active nuclear export system. This phenomenon needs further investigation, but it might be hypothesized that CDKL5 plays different roles also depending on the specific neuronal subpopulation (Rusconi et al. 2011). In addition, it has been found that sustained

glutamate stimulation promoted CDKL5 proteasomal degradation and that degradation of CDKL5 itself seems to be involved in regulating its function. Both events are mediated by the specific activation of extrasynaptic pool of *N*-methyl-D-aspartate receptors. Proteasomal degradation was also induced by withdrawal of neurotrophic factors and hydrogen peroxide treatment, two different paradigms of cell death. Altogether, these results by Rusconi et al. indicate that both subcellular localization and expression of CDKL5 are modulated by the activation of extrasynaptic *N*-methyl-D-aspartate receptors and suggest a regulation of CDKL5 by cell death pathways (Rusconi et al. 2011). Why neurons degrade CDKL5 upon cell death induction and how this degradation is regulated are still unanswered questions.

CDKL5 affects neuronal morphogenesis and dendritic arborization

As already mentioned, CDKL5 expression correlates both *in vitro* and *in vivo* with neuronal maturation, reaching the highest levels of expression when neurons acquire a mature phenotype and suggesting an involvement of the kinase in neuronal differentiation and arborization. Chen et al. recently demonstrated that Cdkl5 affects neuronal morphogenesis and dendritic arborization through a cytoplasmic mechanism. In cortical rat neurons down regulation of Cdkl5 by RNA interference inhibits neurite outgrowth and dendritic arborization, while overexpression had opposite effects (Chen et al. 2010). They also found out that in fibroblasts and neurons CDKL5 co-localizes with F-actin in the growth cone and forms a protein complex with Rac1, a critical regulator of actin remodeling and neuronal morphogenesis. Rac1 belong to the Rho GTPas family of proteins that promote the formation and/or maturation of spines by remodeling the actin cytoskeleton of neuronal spines (Chen et al. 2010). Functional experiments suggest that CDKL5 influences neuronal morphogenesis by acting upstream of Rac1. Chen et al. also demonstrated that brain-derived neurotrophic factor

(BDNF) transiently phosphorylates CDKL5 and CDKL5 is necessary for the capability of BDNF to activate Rac1 (Chen et al. 2010). These results confirm a critical role of CDKL5 in neuronal morphogenesis and suggest that deregulation of the BDNF-Rac1 signaling pathway may contribute to the neuronal phenotype of the CDKL5 disorder.
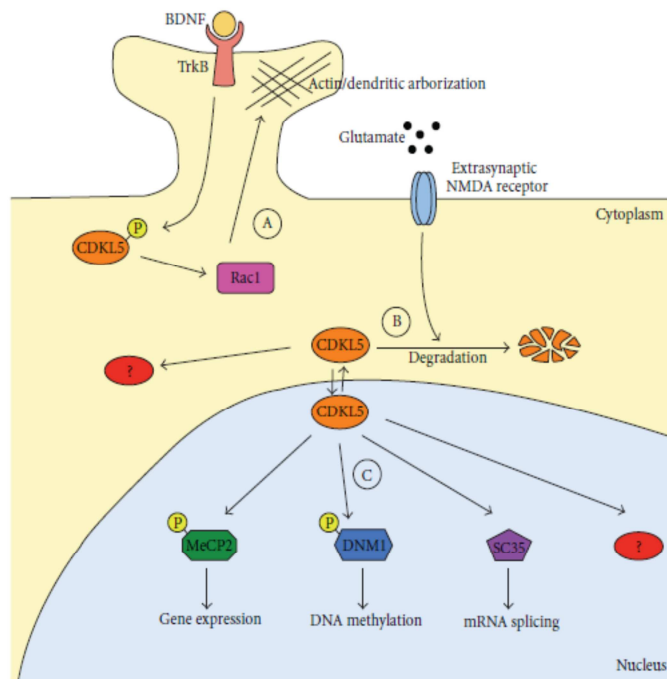
Figure 12 **A model depicting the different functions of CDKL5 in the cytoplasmic and nuclear compartments.**

(A) In the cytoplasm CDKL5 is involved in the regulation of actin cytoskeleton and dendritic arborization. This function is mediated by the interaction of CDKL5 with Rac1. Importantly, a link between BDNF and Rac1 activation has been suggested. (Chen et al.; 2011).

(B) In the cytoplasmic compartment, the levels of CDKL5 are regulated by degradation. Furthermore several phosphorylation targets remain to be identified.

(C) In the nucleus, CDKL5 has been proposed capable of interacting and phosphorylating MeCP2 and DNMT1, thereby influencing gene expression and DNA methylation. Furthermore, the protein has been shown to colocalize with RNA speckles involved in RNA splicing. Several targets have not been identified so far.

(Image taken from (Kilstrup-Nielsen et al. 2012)).

CDKL5 contributes to correct dendritic spine structure and synapse activity

The important role of CDKL5 in neuronal morphogenesis was further confirmed by Ricciardi and colleagues, which demonstrated that CDKL5 contributes to correct spine structure and synapse activity. Ricciardi et al. demonstrated that CDKL5 localizes almost exclusively at the post synaptic density (PSD) of excitatory synapses both *in vivo* and *in vitro*. CDKL5 silencing in rat hippocampal neurons leads to severe deficits in spine density and morphology and similar alterations have been found in neurons established from patient fibroblast-derived pluripotent stem cells (iPSCs), indicating that CDKL5 is required for ensuring a correct number of well-shaped spines. In line with the compromised development of spines, CDKL5-downregulated neurons exhibit a significant decrease in spontaneous miniature excitatory postsynaptic currents (mEPSCs), while there was no significant effect on inhibitory synapse density or any significant changes in miniature inhibitory postsynaptic currents (Ricciardi et al. 2012). These data suggest that CDKL5 is a key-limiting factor in regulating glutamatergic synapse formation and that changes in excitatory synaptic strength might be responsible, at least in part, for the neurodevelopmental symptoms associated with this disorder.

Ricciardi and colleagues also demonstrated that CDKL5 interacts and phosphorylates the netrin-G1 ligand (NGL-1, also known as LRRC4C), a synaptic cell adhesion molecule (CAMs) that plays a crucial role in synapse homeostasis. NGLs have a conserved C-terminal PDZ-binding domain, which specifically binds to PSD95, a protein that plays a significant role in learning and memory, and NGL-1 spine-inducing capability is promoted by targeting PSD95 to new forming dendritic protrusions. CDKL5 phosphorylates NGL-1 on a unique serine (Ser631), which is very close to the PZD-binding domain and this phosphorylation event ensures a stable association between NGL-1 and PSD95 (Ricciardi et al. 2012). These data indicate that CDKL5 is critical for the

maintenance of synaptic contacts, mainly by regulating the NGL-1 phosphorylated state and, thereby, its ability to bind PSD95 and stabilizes this association.

More recently another research group confirmed the critical role of CDKL5 in regulating spine development and synapse activity, demonstrating that CDKL5 binds directly to PSD95 in a palmitoylation-dependent way (Zhu et al. 2013). The multidomain protein postsynaptic density (PSD) 95 is a major scaffold in the postsynaptic density and has an essential role in synapse development and maturation. Its N-terminal domain is posttranslationally modified by palmitoylation, a reversible attachment of 16-carbon palmitate to a cysteine residue, and this palmitate cycling on PSD95 controls its polarized targeting to synapses, which is essential for its synaptic function. Zhu and colleagues demonstrated that CDKL5 binds to palmitolyated PSD95 and that this binding promotes the targeting of CDKL5 to excitatory synapses. They propose two possible ways by which palmitolyated PSD95 regulates synaptic targeting of CDKL5. First, CDKL5 may bind to palmitolyated PSD95 at the Golgi apparatus and the complex moves to the postsynaptic side. Second and more likely important in neurons, free CDKL5 is captured by newly palmitolyated PSD95 at the dendrites and then trafficked to synapses, and becomes enriching at the subsynaptic side. Taken tighter these results demonstrate a critical role of the palmitoylation-dependent CDKL5-PSD95 interaction in localizing CDKL5 to synapses for normal spine development.

These data imply that two pathways are important in mediating the cytoplasmic function of CDKL5: first of all CDKL5 is required for BDNF-induced activation of Rac1, which participates in stabilizing the actin cytoskeleton; on the other hand CDKL5, PSD95 and NGL-1, form a protein complex that functions coordinately to regulate synapse development. These data show that different CDKL5-signaling cascades are involved in synaptic plasticity and learning, acting on spines, dendritic branching and actin cytoskeleton and

elucidate, in part, how the lack of CDKL5 may contribute to the typical neuronal phenotype of the CDKL5 disorder, characterized by intellectual disability, early-onset epilepsy and autistic features.

Another recently identified cytoplasmatic target of CDKL5 is amphiphysin 1 (AMPH1), a brain specific protein involved in neuronal transmission and synaptic vesicle recycling through clathrin-mediated endocytosis (Sekiguchi et al. 2013). Sekiguchi and colleagues explored the endogenous substrates of Cdkl5 in mouse brains extracts using a newly developed method and found Amph1 as specific substrate of Cdkl5. They demonstrated that Cdkl5 phosphorylates Amph1 exclusively at Ser 293 and that this phosphorylation is disrupted by Cdkl5 catalytic domain mutations. Interestingly Cdk5 also phosphorylates Amph1 but at different positions (Ser-272, 276 and 285) to that of Cdkl5 (Sekiguchi et al. 2013). It still remains unclear what effect phosphorylation of AMPH1 by CDKL5 has on its function in neuronal development, but interestingly Amph1 deficient mouse shows major learning difficulties and irreversible seizures, suggesting that Amph1 is a critical molecular component of the pathogenic pathway of the CDKL5 disorder.

2.4. NEUROGENESIS IN THE POSTNATAL BRAIN

CDKL5 expression correlates, both *in vitro* and *in vivo,* with neuronal maturation, reaching the highest levels of expression during postnatal development, when neurons acquire a mature phenotype, suggesting an involvement of this kinase in neuronal differentiation and arborization (Rusconi et al. 2008; Chen et al. 2010; Rusconi et al. 2011). Considering its temporal expression pattern, CDKL5 might have an important role also in postnatal and adult neurogenesis. Impairment of adult neurogenesis has been observed in a variety of models relevant to neuropsychiatric diseases, such as major depression, schizophrenia and Alzheimer's disease, and neurodevelopmental disorders, including Fragile X and Down syndrome (DS).

Noteworthy, neurogenesis persists in the postnatal and adult brain in two distinct brain regions, the subventricular zone (SVZ) and the hippocampal dentate gyrus (DG).

2.4.1. POSTNATAL NEUROGENESIS IN THE SVZ

In the central nervous system of mammals, most neurons are generated in two specific regions that form the germinal ventricular system: the ventricular zone (VZ) and the subventricular zone (SVZ). The cells from the VZ descend directly from the neural plate, and give rise to post-mitotic neuroblasts that migrate up in a radial direction to the surface of the pia mater. At E16 in the mouse brain, these cells leave the cell cycle (Haydar et al. 2000) and during early postnatal development the VZ disappears completely, while the number of cells in the SVZ reaches a peak in the first postnatal week in rodents (approximately the 35th gestational weeks in humans). After this period there is a gradual decrease in size, but a region of small mitotically active SVZ persists also into adulthood.

During development the SVZ is divided into four regions: MGE (medial ganglionic eminence), LGE (lateral ganglionic eminence), CGE (caudal ganglionic eminence) and SVZn (foetal neocortical SVZ). Each region presents different progenitors, which generate neurons and glia that populate different areas of the developing brain. The VZ, SVZn, MGE, LGE and CGE give rise to neurons that populate the neocortex, striatum, thalamus, hippocampus and other subcortical structures. The MGE and LGE disappear in the postnatal period.

In the perinatal period, the SVZ can be subdivided into two key anatomical regions: the anterior SVZ (SVZa) and the SVZ back side (SVZdl) regions. The first one is the main source of the cells of the RMS (rostral migratory stream), while the SVZdl gives rise to the neuroglia of the telencephalon. The migration of cells from the SVZa region through the RMS to the olfactory bulb occurs in forms of cell chains and, once reached the bulb, individual cells disperse radically (Alvarez-Buylla 1997). SVZdl cells migrate into the white matter and then rotate 90 degrees to reach the neocortex. In mice at the second day after birth (P2) 80% of the progeny cells derived from SVZdl cells migrate into the neocortex, 10% in the white matter and the remaining percentage of marked cells colonize the surrounding regions (Brazel et al. 2003). The SVZdl region is the main source of macroglia. In the grey matter, the cells which leave the SVZ in the early perinatal period, differentiate in astrocytes, while in the white matter this differentiation is not allowed. SVZdl cells which migrate into a more advanced stage of development differentiate primarily in myelinated and non-myelinated oligodendrocytes,, and NG2+ cells. Oligodendrocytes have been observed in the neocortex (where the precursors are mitotically active), in the striatum and in the subcortical white matter.

The ultrastructure and organization of the adult SVZ has been recently studied in detail and there have been identified four cell types (excluding resident microglia). These cells were classified as types A, B1, B2 and C. The cells of type

A are small, intensely marked and correspond to neuroblasts destined to the olfactory bulb, while the cell types B1 and B2 show the characteristics of astrocytes. B1 cells are immature astrocytes, whereas B2 cells are probably neural stem cells. C cells, the fourth cell type, appear larger and isolated in clusters. They are very mitotically active and are transient multipotent cells (Fig. 13).

Electron microscopy combined with staining with 3H-thymidine have shown that the migrating cells in the RMS belong to type A. Immature progenitor cells in the SVZ in adulthood continue to migrate through the RMS in the olfactory bulb, where cells mature into post-mitotic neurons in the granular layer and around the glomeruli (Lois et al. 1996). It has been estimated that in the adult mouse brain there are approximately 1200 neural stem cells.
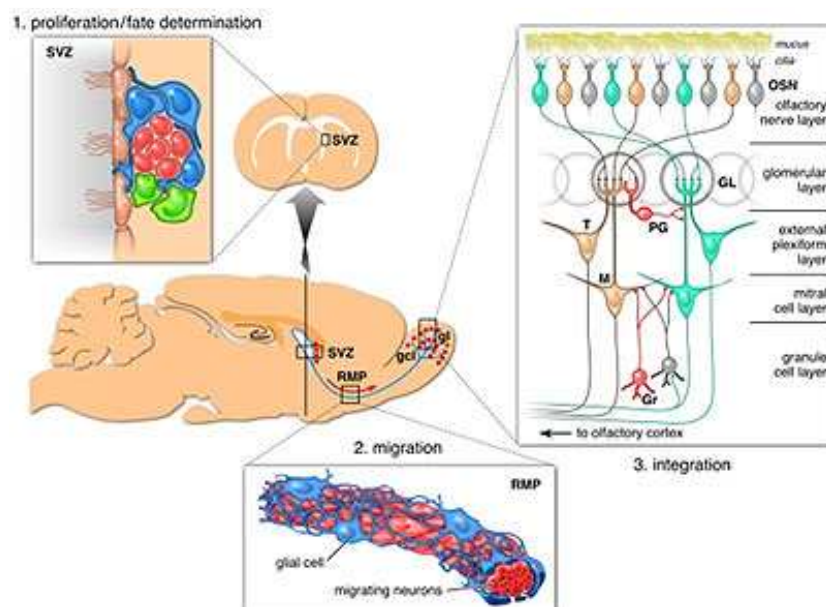
Figure 13 **Model of neurogenesis in the subventricular zone (SVZ) /olfactory bulb system.**

1. Proliferation and fate determination: Stem cells in the SVZ of the lateral ventricle (blue) give rise to transit amplifying cells (green) that differentiate into immature neurons (red). Adjacent ependymal cells (light brown) of the

lateral ventricle are essential for the neuronal fate determination by providing inhibitors of glial differentiation.

2. Migration: Immature neurons (red) migrate along each other in chains through the rostral migratory pathway (RMP). The migrating neurons are ensheathed by astrocytes (blue).

3. Integration: Immature neurons differentiate local interneurons (red) in the granule cell layer and the periglomerular layer. Olfactory sensory neurons (OSN); tufted neurons (T); mitral neurons (M); granule neurons (Gr); periglomerular neurons (PG).

(Image taken from (Lie et al. 2004))

Many studies show that the SVZ responds to damage in the adult brain by producing new progenitor cells that migrate to sites where there had been a neurodegeneration or a brain injury. In response to diseases such as epilepsy or Huntington's syndrome it is observed an increase of stem cells, cytokine levels and migration proteins in the SVZ (Curtis et al. 2007).

2.4.2 POSTNATAL NEUROGENESIS IN THE DG

The hippocampus is integral to learning and memory function and evidences suggest that adult hippocampal neurogenesis is involved in acquisition of declarative memory in the short and long term and other hippocampal functions (Zhao et al. 2008). If the hippocampus is damaged facts and events cannot be stored over a long-term memory. Given its fundamental importance in learning and memory, the hippocampus has always been the subject of intense anatomical psychological and psychophysical studies. The main structures of the hippocampal formation are the entorhinal cortex (EC), the dentate gyrus (DG), CA3 and CA1 regions and the subiculum.

The hippocampal dentate gyrus (DG) is formed over a long time period that begins during gestation and continues in the postnatal period. It contains a

neurogenic niche, the subgranular zone (SGZ), which is inhabited by a heterogonous population of cells and cellular elements, which play an important role in neurogenesis. Type 1 neural stem cells (NSCs) are radial glia-like progenitors and express the markers nestin and Sox2/BLBp. It is hypothesized that these cells divide asymmetrically to self-renew and give rise to daughter cells, termed actively dividing progenitors (type 2, type 3 cells). Type 2 cells are differentiated into two different subtypes: type 2a or type 2b cells. Type 2a progenitor cells are nestin-positive, and their morphology suggest that they are capable of tangential migration (Kuhn et al. 1996). On the other hand type-2b cells are also considered actively dividing progenitor cells but, unlike type-2a cells, they have limited self-renewal capabilities and are lineage determined. In addition to nestin, type 2b cells also express doublecortin (DCX), similar to type 3 cells which only express DCX. After progressing through these stages, precursors exit the cell cycle and enter a post-mitotic stage, where they are termed immature granule cells and actively establish network connections. The final stage of differentiation is the post-mitotic, mature granule cell (DGCs) that expresses the neuronal marker NeuN. These cells are considered to be terminally differentiated granule cells and project their axons (known as mossy fibers) to CA3 pyramidal cells and their dendrites to the molecular layer (Fig. 14).

Adult-born neurons make up about 6% of the granule cell layer in adult rats (Cameron and McKay 2001) and newly generated granule cells are continuously integrated into the hippocampal circuit as bromodeoxyuridine (BrdU) labeling studies indicate (van Praag et al. 2002).
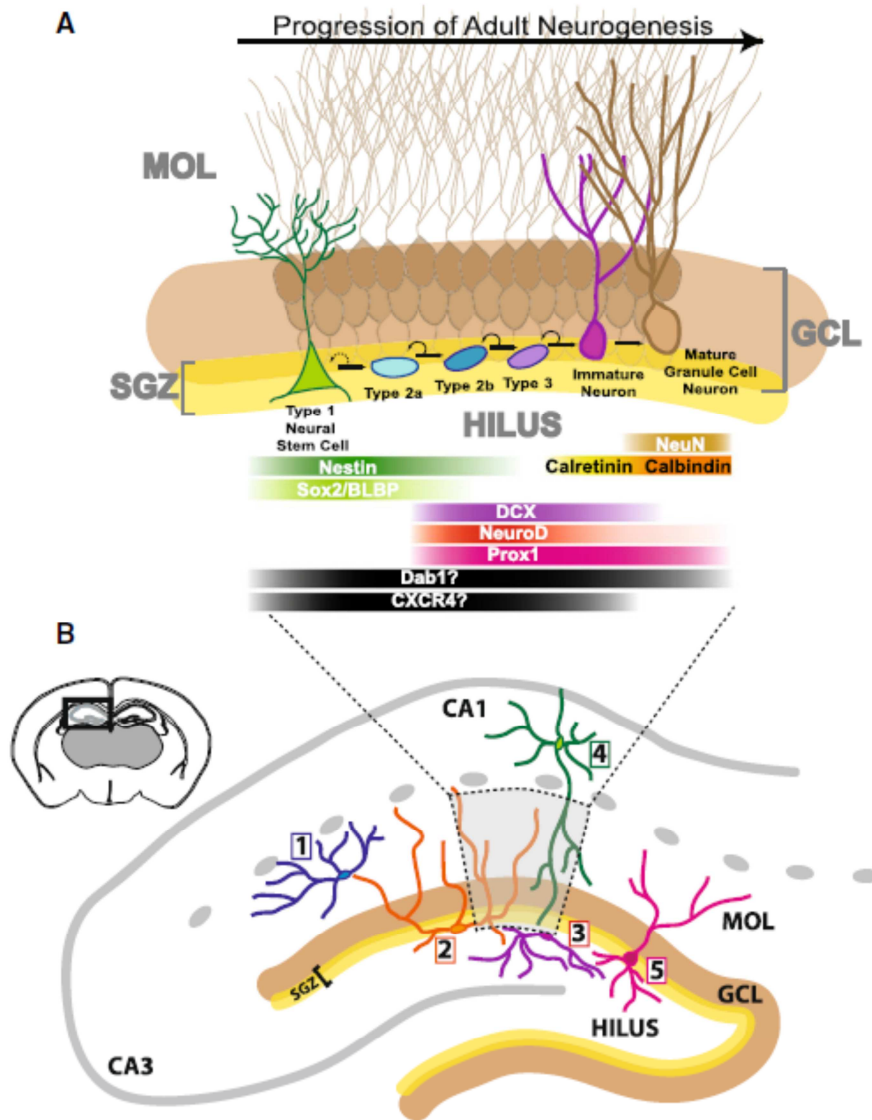
*Figure 14 **An overview of hippocampal neurogenesis**. (Image taken from (Masiulis et al. 2011)).*

Increasing evidence supports a role for adult-born neurons in learning and memory. Stimulation of adult hippocampal neurogenesis with behavioral interventions such as exercise or environmental enrichment is associated with better performance on certain hippocampal learning tasks (van Praag et al. 1999; Kempermann et al. 2004). More direct evidence that neurogenesis supports

hippocampal-dependent learning and memory derives from experiments in which depletion of adult-generated neurons impairs specific learning tasks such as associative learning and fear conditioning (Shors et al. 2001).

3. MATERIALS AND METHODS

3.1. HUMAN NEUROBLASTOMA CELL LINES

3.1.1. Cell cultures

Human neuroblastoma cell lines SH-SY5Y and SKNBE, obtained from ATCC (Manassas, VA, USA), were maintained in Dulbecco Modified Eagle Medium (DMEM) supplemented with 10% heat-inactivated fetal bovine serum (FBS), 2 mM glutamine and antibiotics (penicillin, 100 U/ml; streptomycin, 100 µg/ml), in a humidified atmosphere of 5% of CO2 in air at 37 °C. Cell medium was replaced every 3 days and the cells were sub-cultured once they reached 90% confluence.

3.1.2. Plasmids

Human CDKL5 cDNA was kindly provided by Marsha Rich Rosner (University of Chicago) (Lin et al. 2005). CDKL5 cDNA was PCR amplified and cloned into pCMV14 plasmid (Sigma) in frame with a 3xFLAG C-terminal epitope. CDKL5-3xFLAG sequence was subcloned into the bicistronic pIRES2-EGFP plasmid (Clontech) to obtain a GFP and CDKL5-3xFLAG co-expression vector (pGFP/CDKL5-FLAG).

3.1.3. Immunocytochemistry

For cell proliferation analyses SH-SY5Y cells were plated onto poly-D-lysine coated slides in 6-well plates at density of 3×10^5 cells per well and transfected

with 3 μg of CDKL5-FLAG expression plasmid using lipofectamin (Roche). Twenty-four hours after transfection cells were fixed in a 4% paraformaldehyde 4% sucrose solution at 37 °C for 30 minutes. For immunofluorescence studies the following antibodies were used. Primary antibodies: anti-Ki-67 rabbit monoclonal (1:100, Thermo Scientific), anti-BrdU rat monoclonal (1:100, AbD Serotec), anti-cleaved caspase-3 (asp175) rabbit polyclonal (1:100, Cell Signaling Technology), anti-β-tubulin III rabbit polyclonal (TubJ, 1:500, Sigma) and anti-FLAG M2 mouse monoclonal (1:1000; Sigma). Secondary antibodies: FITC-conjugated anti-rat antibody (1:200, Jackson Immuno Research Laboratories), FITC-conjugated anti-rabbit antibody (1:200, Jackson Immuno Research Laboratories), FITC conjugated anti-mouse antibody (1:200, Jackson Immuno Research Laboratories) and Cy3-conjugated anti-rabbit antibody (1:200, Jackson Immuno Research Laboratories). Double immunofluorescence images, taken from random microscopic fields (10–12 for each coverslip), were superimposed and used to determine the labeling index (LI), defined as percentage of cells co-labeled with: anti-BrdU and anti-FLAG or anti-cleaved caspase-3 and anti-FLAG or anti-Ki-67 and anti-FLAG antibodies. In each experimental condition we randomly analyzed a total of 600 cells. Fluorescence images were taken on an Eclipse TE 2000-S microscope (Nikon, Tokyo, Japan) equipped with a digital camera Sight DS-2MBW (Nikon).

3.1.4. Western blotting

For the total cell extracts preparation, cells were lysed in RIPA lysis buffer (Tris–HCl 50 mM, NaCl 150 mM, Triton X-100 1%, sodium deoxycholate 0.5%, SDS 0.1%, protease and phosphatase inhibitors cocktails 1%; Sigma). Cell extracts were immediately processed by Western blot or kept frozen (−80 °C) until assayed. Sample protein concentration was estimated by the Lowry method (Lowry et al. 1951). Equivalent amounts (50 μg) of protein were subjected to electrophoresis on a 10% SDS-polyacrylamide gel. The following antibodies were

used: anti-CDKL5 (1:500; Sigma) and anti-GADPH (1:5000; Sigma). Densitometric analysis of digitized images was performed with Scion Image software (Scion Corporation, Frederick, MD, USA) and intensity for each band was normalized to the intensity of the corresponding GAPDH band.

3.1.5. Analysis of neurite outgrowth

For differentiation analyses neuroblastoma cells were plated onto poly-D-lysine coated slides in a 24-well plated at density of 2×10^4 cells per well. After 24 hours of cell plating, differentiation was induced by retinoic acid (RA; 10 μM) for the indicated time. This treatment was replaced each 2 days to replenish RA in culture media. Phase contrast photographs of the cultures were taken at various time intervals with an Eclipse TE 2000-S microscope (Nikon, Tokyo, Japan) equipped with an AxioCam MRm (Zeiss, Oberkochen, Germany) digital camera. Ten different areas were randomly selected and neurite outgrowth was measured using the image analysis system Image Pro Plus (Media Cybernetics, Silver Spring, MD 20910, USA). Only cells with neurites longer than one cell body diameter were considered as neurite-bearing cells. All experiments were performed at least 3 times. In each experiment we analyzed a total of around 450 cells. The total length of neurites was divided for the total number of cells counted in the areas.

3.1.6. Flow cytometric analysis

SH-SY5Y cells were harvested 24 hours after transfection with pGFP or pGFP/CDKL5-FLAG plasmids, collected by trypsinization, pelleted and resuspended in phosphate buffered saline (PBS) to a final concentration of 1×10^6 cells/ml. Transfected cells were then analyzed on a flow cytometer (FACSCalibur, Becton Dickinson, San Jose, CA, USA) and sorted by GFP fluorescence

(detection filter set at 525 nm). Cell aggregates were gated out, and 10,000 events were analyzed. Untransfected SH-SY5Y cells were used to establish a threshold for green fluorescence (up to 102 arbitrary fluorescence units in a typical case), and which was taken as a threshold for positivity (see Fig. 17C results). For differentiation analysis an aliquot of GFP sorted cells was plated in 6-well at the density of 3×10^5 cells per well in the presence or absence of RA (10 μM). For cell cycle analysis cells were fixed in 70% ethanol in PBS at −20 °C for at least 1 hour, washed several times with cold PBS, treated with RNaseA (50 μg/ml) for 30 minutes at 37 °C and incubated with propidium iodide (30 μg/ml). GFP-positive and -negative populations were analyzed separately for DNA content (filter set at 675 nm) and assigned to specific cell-cycle phases by applying the Cell Quest Software (Becton Dickinson, San Jose, CA, USA).

3.1.7. Small interfering RNA assay

The siRNA oligonucleotides used for silencing CDKL5 were purchased from QIAGEN and were: Hs-CDKL5-5 cat. No:SI02223116 (sense; Si1) and Hs-CDKL5-10 cat. No:SI004437244 (sense; Si2). Control cells were transfected with a scramble siRNA duplex; AllStars Negative Control siRNA (siSCR QIAGEN), which does not present homology with any other human mRNAs. SH-SY5Y cells were transfected with HiPerFect Transfection Reagent (QIAGEN) with 50 nM siRNA (final concentration). For differentiation experiments retinoic acid was added to the cells 6 hours post transfection and the cells harvested after further 42 hours. For proliferation experiments 10 μM BrdU was added to the cells 46 hours post transfection and the cells harvested after further 2 hours.

3.1.8. Quantitative real time PCR and standard reverse transcription-PCR

RNA samples from cell cultures were prepared using Tri-Reagent (Sigma) and treated with DNase (DNA-freeTM; Ambion). Reverse transcription was performed using a SuperScript reverse transcription-PCR kit (Invitrogen). Real time quantitative PCR (RT-qPCR) was performed using a SYBR Premix Ex Taq kit (Takara, Shiga, Japan) and the iQ5 thermocycler (Bio-Rad). The efficiency of the used primers was evaluated by calculating the linear regression of Ct data points obtained with a series of different primer dilutions and inferring the efficiency from the slope of the line. We used the primers that gave efficiency close to 100%. Primers used for RT-qPCR are as follows: human CDKL5 (Cyclin-dependent kinase-like 5) (NM_003159.2) forward, 5'CGGTGGATGTGA TGGCAGAAGAC-3', and reverse 5'GGACTGGAGATTGGACGATGAAGG-3'; human GUSB (Glucuronidase beta) (NM_000181.3) forward, 5'-AGCGTGG AGCAAGACAGTGG-3', and reverse 5'-ATACAGATAGGCAGGGCGTTCG-3'. Quantifications were always normalized using endogenous control GUSB.

3.2. Cdkl5 KNOCKOUT MICE

3.2.1. Generation of Cdkl5 knockout mice

A 10 kb genomic fragment containing exon 4 of Cdkl5 (ENSMUSE00000346596) was subcloned into a pDTA targeting plasmid by recombineering-mediated transfer from a 178-kb genomic fragment containing the C57BL/6J mouse Cdkl5 locus (RP23-213O8, ChoriBACPAC, Oklahoma, CA). A loxP site was inserted 806 bp upstream of the exon by recombineering-mediated insertion of a loxP- flanked pEM7::kanamycin gene and subsequent Cre recombination. An FRT-flanked pEM7/PGK::neomycin selection cassette was inserted 347 bp downstream of exon 4. The plasmid was linearized with NruI before electroporation into ES cells (129/Sv x C57BL/6N, clone A8, kindly

provided by A. Wutz, Wellcome Trust Centre for Stem Cell Research, Stem Cell Institute, University of Cambridge). G418-resistent clones were identified and screened by long-range PCR. Hybridization with a specific probe for the 5' and 3' arms was used to confirm PCR results. Two independent positive ES cell clones were injected into C57BL/6N host embryos using a piezo-drill assisted 8-cell stage injection procedure developed at the European Molecular Biology Laboratory (EMBL, Monterotondo, Italy). Four out of five offspring (all >95% ES cell derived) provided germline transmission. Positive offspring were crossed to C57BL/6J congenic FLP-deleter mice (Farley et al. 2000) to remove the neomycin selection cassette and further crossed to C57BL/6J congenic Cre-deleter mice (Tang et al. 2002) to generate the Cdkl5 null allele (see Fig. 18A results).

3.2.2. Mouse strains and husbandry

Mice for testing were produced by crossing heterozygous female (-/+) *Cdkl5* knockout with hemizygous male (-/Y) Cdkl5 knockout mice or with wild-type male mice (+/Y). Littermate controls were used for all experiments. Animals were karyotyped by PCR on genomic DNA using the following primers: 108F: 5'-ACGATAGAAATAGAGGATCAACCC-3', 109R: 5' CCCAAGTATACCCCTT TCCA-3'; 125R: 5'-CTGTGACTAGGGGCTAGAGA-3'. The day of birth was designed as postnatal day (P) zero and animals with 24 hours of age were considered as one-day-old animals (P1). After weaning, mice were housed three to five per cage on a 12 h light/dark cycle in a temperature controlled environment with food and water provided *ad libitum*. Experiments were performed in accordance with the Italian and European Community law for the use of experimental animals and were approved by Bologna University Bioethical Committee. In this study all efforts were made to minimize animal suffering and to keep the number of animals used to a minimum.

3.2.3. Semi-quantitative PCR

Brains from wild-type and Cdkl5 knockout mice aged 2 months were collected, washed in PBS-DEPC and one hemisphere was homogenized using an automate dounce. Total RNA was extracted using RNeasy Mini Kit (Qiagen, Hilden, Germany) and converted into first-strand cDNA (SuperScript II Reverse Transcriptase, Invitrogen, Paisley, UK) using oligo-dT according to the manufacturer's protocol. For semiquantitative PCR, DNA was amplified using primers against Cdkl5 exons using 1xnPCR Buffer (Promega, Madison, WI), 0.5 units of Dream Taq (Promega) and 200 mM each dNTPs (Fermentas, Vilnius, Lithuania).

3.2.4. EEG analysis

Male mice aged 2/4 months were anesthetized with ketamine/xylazine supplemented with isofluorane as needed, kept on a heating pad to maintain body temperature at $35\pm1°C$, and immobilized in a stereotaxic frame. An incision above the skull was cut and burr holes drilled into the skull. Four stainless steel screws were used as electrodes placed bilaterally above hippocampus (2.0 mm posterior, 1.5 mm lateral to bregma) and frontal cortex (1.8 mm anterior, 1.5 mm lateral to bregma). Ground and reference screws were anchored on the posterior and middle portions of the skull, respectively. A wireless Neurologger 2A recording device (400 HZ sampling rate) acquired and stored data in real-time for later downloading (Brankack et al. 2010). After surgery animals were housed individually and allowed at least one week to recover. Mice were tested in a novel cage for a thirty minutes baseline period followed by a 2 hour recording after treatment with kainic acid (10 mg/kg and 25 mg/kg, i.p.). Each animal received both doses separated by at least one day. Data were downsampled to 200 Hz and filtered between 1-25 Hz (Chebyshev I filter, 3rd order). To quantify seizure episodes, a Fourier transform (4 s window, 3.5 s overlap, 2 hours period) was

applied to the EEG. Seizure events in the 1-8 Hz frequency range were used to quantify amplitude The baseline period was used as a cutoff criterion (mean power + 8x SD) to define seizure events.

3.2.5. Behavior testing

Behavior testing was performed in mice aged 2/4 months. A portion of the behavioral data derived from knockout mice containing the neomycin selection cassette. No difference in behavior was noted between this allele and the neo-negative allele and the results were combined.

Clasping - Mice were suspended by their tail for 2 minutes and hind-limb clasping was assessed from video recordings. Clasping was defined as present if it occurred for more than 5 seconds in an animal.

Home-cage activity - Locomotion was measured using activity-monitoring cages similar in size, shape, and material to the home cage (TSE Systems, Bad Homburg, Germany). A mouse was placed in the chamber at least 3 hours before recording started. Relative activity was monitored continuously for 4 days and binned into 12 hour epochs.

Open field - Mice were placed in the center of a 50 x 50 cm open arena equipped with video tracking and infrared rearing detection systems (VideoMot2, TSE Systems). Cumulative distance travelled was collected in 5 minute intervals for 30 minutes.

Y-maze spontaneous alternation – Y-Maze Spontaneous Alternation was used for measuring the willingness of rodents to explore new environments and hippocampus-dependent spatial reference memory. Each mouse was placed at the distal part of one arm facing the center of the maze. Each of three arm is 34cm x 5

cm x 10 cm height, angled 120° from the others and made of grey opaque plastic. After the introduction to the maze, the animal is allowed to freely explore the three arms for 8 minutes. Over the course of the multiple arm entries, the subject should show a tendency to enter a less recently visit arm. Arm entries were defined by the presence of all four-paws in an arm. Each 8 minute trial was recorded and scored via ANY-maze videotracking software (Stoelting). The maze was washed with 50% ethanol between trials. The percentage of spontaneous alternations is defined as: (total alternations / total arm entries-2) x 100. One alternation is defined as consecutive entries in three different arms.

3.2.6. BrdU injection

On P40, some animals received for five consecutive days an intraperitoneal injection (150 μg/g body weight) of BrdU (5-bromo-2-deoxyuridine; Sigma) in 0.9% NaCl solution. Animals were sacrificed either 24 hours after the last BrdU injection (on P45), to examine cell proliferation, or after one month (on P75), to examine the fate of the BrdU-labeled cells.

3.2.7. Histological procedures

Some animals were deeply anesthetized with ether and transcardially perfused with ice cold phosphate-buffered saline (PBS), followed by a 4% solution of paraformaldehyde in 100 mM PBS, pH 7.4. Brains were stored in the fixative for 24 hours, cut along the midline and kept in 20% sucrose in phosphate buffer for an additional twenty-four hours. Hemispheres were frozen and stored at -80°C. The right hemisphere was cut with a freezing microtome in 30-μm-thick coronal sections that were serially collected in antifreeze solution containing sodium azide. Some animals were decapitated and the brain was removed, cut along the midline and fixed by immersion in Glyo-Fixx (Thermo Electron Corp.,

Waltham, MA, USA) for 48 hours. Samples were dehydrated through a series of ascending ethanol concentrations, embedded in paraffin, and cut with a microtome in ultra-thin sections (4 µm) and mounted on poly-lysine slides.

Sections from the dentate gyrus (DG) and subventricular zone (SVZ) were used for immunohistochemistry. The SVZ of this study corresponds to the rostral horn of the lateral ventricle and starts at the rostral pole of the lateral ventricle, stretching for 900-1200 µm in the caudal direction. Its rostral and caudal borders correspond approximately to +1.18 mm and +0.02 mm planes, respectively, of Franklin and Paxinos atlas of the mouse brain.

3.2.8. Immunohistochemistry/double-fluorescence immunohistochemistry

One out of six 30-µm-thick coronal sections from the DG and the SVZ of animals were processed for immunohistochemistry as previously described (Contestabile et al. 2007; Bianchi et al. 2010). Immunohistochemistry was carried out on free-floating sections for the frozen brains. For Cdkl5 detection sections were incubated overnight at 4°C with rabbit anti-Cdkl5 antibody (1:250, Sigma-Aldrich) and for 2 hours with a Cy3 conjugated anti-rabbit IgG (1:200; Jackson Immunoresearch). For BrdU immunohistochemistry sections were denatured in 2 N HCl for 30 minutes at 37°C and incubated overnight at 4°C with a primary antibody anti-BrdU (mouse monoclonal 1:100, Roche Applied Science, Mannheim, Germany). Detection was performed with a Cy3-conjugated anti-mouse secondary antibody (1:200; Jackson Immunoresearch). For Ki-67 immunohistochemistry sections were incubated overnight at 4°C with rabbit monoclonal anti-Ki67 antibody (1: 200; Thermo Scientific Neumarkers, Fremont, CA. USA) and for 2 hours with a Cy3 conjugated anti-rabbit IgG (1:200; Jackson Immunoresearch). For cleaved caspase-3 immunohistochemistry, sections were incubated overnight at 4°C with a rabbit cleaved caspase-3 antibody (1:100; Cell

Signaling Technology) and for 2 hours with an HRP-conjugated anti-rabbit secondary antibody (dilution 1:200; Jackson Immunoresearch). Detection was performed using the TSA Cyanine 3 Plus Evaluation Kit (Perkin Elmer). For Synaptophysin immunohistochemistry, sections from the DG were incubated for 48 hours at 4°C with mouse monoclonal anti-SYN (SY38) antibody (1:1000, Millipore Bioscience Research Reagents) and for two hours with a Cy3 conjugated anti-mouse IgG secondary antibody (1:200; Jackson Immunoresearch). For DCX immunohistochemistry sections from the DG were incubated overnight at 4°C with a goat polyclonal anti-DCX antibody (1:100; Santa Cruz Biotechnology). Sections were then incubated for 2 hours at room temperature with a biotinylated anti-goat IgG secondary antibody (1:200; Vector Laboratories) and thereafter incubated for 1 hour with VECTASTAIN® ABC kit (Vector Laboratories). Detection was performed using DAB kit (Vector Laboratories). For double-fluorescence immunostaining, sections were incubated overnight at 4°C with a primary antibody, rat monoclonal anti-BrdU antibody (1:100; AbD Serotec, Kidlington, Oxford, UK) and one of the following primary antibodies: i) mouse monoclonal anti NeuN (1:250; Chemicon, Billerica, MA, USA) and ii) mouse monoclonal anti-glial fibrillary acidic protein (GFAP) (1:400; Sigma). Sections were then incubated with a Cy3 conjugated anti-rat IgG (1:100; Jackson Immunoresearch) secondary fluorescent antibody, for BrdU immunoistochemistry and FITC conjugated anti-mouse IgG (1:100; Sigma-Aldrich) for NeuN or GFAP immunoistochemistry. Fluorescent images were taken with an Eclipse TE 2000-S microscope (Nikon, Tokyo, Japan) equipped with an AxioCam MRm (Zeiss, Oberkochen, Germany) digital camera or with a Leica TCS confocal microscope (Leica Microsystems, Wetzlar, Germany).

Ultra-thin consecutive sections were deparaffinized, incubated with a goat anti-DCX antibody (1:100; Santa Cruz Biotechnology) or with a rabbit cleaved caspase-3 antibody (1:200; Cell Signaling Technology). Detection was performed with a HRP-conjugated anti-goat or anti-rabbit secondary antibody (dilution

1:200; Jackson Immunoresearch, West Grove, PE, USA) and DAB kit (Vector Laboratories, Burlingame, CA, USA).

3.2.9. Measurements

Cell counting - The total number of positive cells (BrdU, Ki-67, NeuN/BrdU, GFAP/BrdU, cleaved caspase-3, DCX) was estimated by multiplying the number counted in the series of sampled sections by the inverse of the section sampling fraction (section sampling fraction = 1/6).

Stereology of the DG - In the series of Hoechst-stained sections, the volume of the granule cell layer was estimated as previously described (Contestabile et al. 2007; Bianchi et al. 2010) by multiplying the sum of the cross sectional areas by the spacing T between sampled sections. Granule cell numerical density was determined using the optical fractionators (Bianchi et al. 2010). Counting frames with a side length of 30 μm and a height of 8 μm spaced in a 150 μm square grid (fractionator) were systematically used. The total number of granule cells was estimated as the product of the volume of the granule cell layer and the numerical density.

Measurement of the dendritic tree - Dendritic trees of DCX-positive granule cells of the DG were traced with a dedicated software, custom-designed for dendritic reconstruction (Immagini Computer, Milan, Italy), interfaced with Image Pro Plus (Media Cybernetics, Silver Spring, MD 20910, USA). The dendritic tree was traced live, at a final magnification of 500x, by focusing into the depth of the section. The operator starts with branches emerging from the cell soma and after having drawn the first parent branch goes on with all daughter branches of the next order in a centrifugal direction. At the end of tracing the program reconstructs the number and length of individual branches, the mean length of branches of each order and total dendritic length.

Connectivity in the molecular layer of the DG – To evaluate the connectivity in the molecular layer of the DG, intensity of SYN immunoreactivity (IR) was determined by optical densitometry of immunohistochemically stained sections. Fluorescence images were captured using a Nikon Eclipse E600 microscope equipped with a Nikon Digital Camera DXM1200 (ATI system). Densitometric analysis of SYN in the inner (I), middle (M) and outer (O) third of the molecular layer was carried out using Nis-Elements Software 3.21.03 (Nikon). For each image, the intensity threshold was estimated by analyzing the distribution of pixel intensities in the image areas that did not contain IR. This value was then subtracted to calculate IR of each sampled area.

3.2.10. Western blotting

For the preparation of total brain extracts mice aged 2 months were decapitated and brain rapidly collected on ice. One hemisphere was homogenized in lysis buffer (50 mM HEPES pH 7.0, 250 mM NaCl, 0.5% NP-40, 5 mM EDTA, 1 mM DTT, protease/phosphatase inhibitor mix composed of 0.5 mM Na_3VO_4, 0.5 mM PMSF, protease inhibitor mixture (Roche Applied Sciences, Monza, Italy), using an automated dounce. For the preparation of hippocampal extracts from P19 mice, tissues were homogenized in RIPA buffer (Tris-HCl, 50 m M, NaCl 150 mM. Triton X-100 1%, SDS, 0,1%, sodium deoxycholate 0,5%, PMSF 1mM, protease and phosphatase inhibitors cock-tails, 1%). Extracts were immediately processed by Western blot or kept frozen (-80°C) until assayed. Sample protein concentration was estimated by the Lowry method (Lowry et al. 1951). Equivalent amounts (50 µg) of protein were subjected to electrophoresis on a 10% SDS-polyacrylamide gel and incubated with the following antibodies: anti-CDKL5 (1:500), anti-GAPDH (1:5000), anti-tubulin (1:5000) (Sigma) anti-phosphorylated Erk1/2 (1:1000), anti Erk1/2 (1:1000), anti-phospho-AKT-Ser473

(1:1000), anti-phospho-AKT-Thr308 (1:1000), anti-AKT (1:1000), anti-phospho-GSK3-β-Ser9 (1:1000), anti-GSK3-β (1:1000), anti-phospho-CRMP2 Thr514 (1:1000), anti-CRMP2 (1:1000) (Cell Signaling Technology); anti β-catenin (1:1000; BD Transduction Laboratories); anti-phospho-CREB-Ser133 (1:1000) and anti-CREB (1:1000) (Upstate Biotechnology) overnight at 4 C, incubated with secondary antibodies (one hour at room temperature) and developed using ECL detection (GE Healthcare, Chalfont St. Giles, UK). Densitometric analysis of digitized images was performed with Scion Image software (Scion Corporation, Frederick, MD, USA) and intensity for each band was normalized to the intensity of the respective total protein levels, tubulin or GAPDH band.

3.3. NPC cultures

3.3.1. NPC cultures and treatments

Cells were isolated from the subventricular zone (SVZ) of newborn (P1-P2) homozygous (-/-), heterozygous (-/+) and wild-type (+/+) female Cdkl5 knockout mice. To obtain neurospheres, cells were cultured in suspension in DMEM/F12 (1:1) containing B27 supplements (2%), FGF-2 (20 ng/mL), EGF (20 ng/mL), heparin (5 μg/mL), penicillin (100 units/mL), and antibiotics, as previously reported (Trazzi et al. 2011). Primary neurospheres were dissociated at day 7-8 using Accutase (PAA, Pasching, Austria) to derive secondary neurospheres. The sub-culturing protocol consisted of neurosphere passaging every 7 days with whole culture media change (with freshly added FGF-2 and EGF). All experiments were done using neurospheres obtained after 1-3 passages from the initially prepared cultures. Cell cultures were kept in a 5% CO_2 humidified atmosphere at 37°C. 2mM Lithium chloride (Sigma) was administrated on alternate days.

3.3.2. Viral Particles Transduction

NPCs were infected, at day 1 post-plating, with CDKL5 Adenovirus Particles (Vector BioLabs) or GFP Adenovirus Particles (Vector BioLabs) at 100 multiplicities of infection (MOI).

3.3.3. BrdU immunocytochemistry

For proliferation analysis dissociated neurospheres were cultured for 3 days, treated with 10 µM BrdU for additional 16 hours and harvested on microscope slides by cytospin centrifugation (215 x g, 5 min, Shandon, Thermo, Dreieich, Germany). Specimens, processed as previously described (Contestabile et al. 2009), were incubated with a mouse anti-5-bromo-2-deoxyuridine (BrdU) monoclonal antibody (1:100; Roche Applied Science) and a Cy3-conjugated anti-mouse secondary antibody (1:200; Sigma). Samples were counterstained with Hoechst-33258.

3.3.4. In vitro differentiation, immunocytochemistry and analysis of neurite length.

Neurospheres were dissociated into a single cell suspension and plated onto poly-L-ornithyine-coated 24-well chamber slides at a density of 3×10^4 cells per well. Cells were cultured for 2 days in DMEM/F12 medium containing EGF (20 ng/mL), FGF (20 ng/mL) and 2% fetal bovine serum (FBS) and then transferred to differentiation medium (EGF and FGF free plus 1% FBS) for 6 or 12 days. Every 2 days half of the medium was replaced with fresh differentiation medium. For immunofluorescent staining, differentiated NPC cultures were paraformaldehyde-fixed and stained with antibodies against: GFAP (1:400;

Sigma) and β-tubulin III (1:100; Sigma) as primary antibodies, and with mouse FITC-conjugated (1:200; Sigma) and rabbit Cy3-conjugated (1:200; Jackson Laboratories), as secondary antibodies. Samples were counterstained with Hoechst-33258. Ten random fields from each coverslip were photographed and counted. The number of positive cells for each marker was referred to the total number of Hoechst-stained nuclei. Evaluation of neurite length was performed by using the image analysis system Image Pro Plus (Media Cybernetics, Silver Spring, MD 20910, USA). The average neurite length per cell was calculated by dividing the total neurite length by the number of cells counted in the areas.

3.3.5. Western blotting

Total proteins from neurosphere cultures of *Cdkl*5 knockout and wild-type mice were homogenized in ice-cold RIPA buffer (50 mM Tris-HCl pH 7.4, 150 mM NaCl, 1% Triton-X100, 0.5% sodium deoxycholate,0.1 % SDS) supplemented with 1mM PMSF and 1% proteases and phosphatases inhibitor cocktail (Sigma). Protein concentration was determined by the Lowry method (Lowry et al. 1951). Equivalent amounts (50 µg) of protein were subjected to electrophoresis on a 4-12% Mini-PROTEAN® TGX™ Gel (Bio-Rad) and transferred to a Hybond ECL nitrocellulose membrane (Amersham Life Science). The following primary antibodies were used: anti-CDKL5 (1:500), anti-GAPDH (1:5000) (Sigma), anti-phospho-AKT-Ser473 (1:1000), anti-AKT (1:1000), anti-phospho-GSK3-β-Ser9 (1:1000) and anti-GSK3-β (1:1000) (Cell Signaling Technology). Densitometric analysis of digitized images was performed with Scion Image software (Scion Corporation, Frederick, MD, USA) and intensity for each band was normalized to the intensity of the respective total protein levels or GAPDH band.

3.4. Statistical analysis

Results are presented as the mean $\pm$ standard error (SE) of the mean. Statistical significance was assessed by two-way analysis of variance (ANOVA), followed by Duncan's post hoc test or by the two-tailed Student's t-test A probability level of $P<0.05$ was considered to be statistically significant.

4. RESULTS

Despite the clear involvement of *CDKL5* mutations in intellectual disability, the function/s of CDKL5 and particularly its role in the development of the nervous system are still poorly understood. Several studies in rodents have shown that Cdkl5 is highly expressed in the developing brain (Rusconi et al. 2008; Chen et al. 2010), suggesting an important role of CDKL5 in neuronal maturation.

In order to elucidate the role of CDKL5 on neuronal maturation we used, as an *in vitro* neuronal model, human neuroblastoma cell lines. Human neuroblastoma cell lines show several biochemical and functional features of neurons and are considered a good *in vitro* model of neurons, as they can be induced to differentiate upon treatment with retinoic acid (RA) (Melino et al. 1997; Singh and Kaur 2007). For these reasons neuroblastoma cells have been here employed to study the CDKL5 function *in vitro*.

In parallel we created a Cdkl5 knockout (KO) mouse model in collaboration with the European Molecular Biology Laboratory (EMBL), Monterotondo, Italy. In the current study we performed a first behavioral characterization on the Cdkl5 KO mouse. In rodents, the hippocampal dentate gyrus produces its neurons mainly postnatally (Altman and Bayer 1990). This makes the hippocampus an ideal structure in order to examine the role of Cdkl5 on fundamental neurodevelopmental processes such as neurogenesis and dendritic development. In the current study we used a Cdkl5 KO mouse model in order to dissect the role of CDKL5 on hippocampal development and to establish the mechanism/s underlying its actions.

4.1. CDKL5 enhances neuronal differentiation in the SH-SY5Y neuroblastoma cell line

We first sought to establish whether human neuroblastoma cell lines exhibit a positive correlation between CDKL5 expression and neuronal differentiation similar to those observed *in vivo* during brain development (Rusconi et al. 2008; Chen et al. 2010).

We evaluated morphological differentiation and CDKL5 expression in two neuroblastoma cell lines, SH-SY5Y and SKNBE, following RA treatment. Within 3 days of treatment with RA, SH-SY5Y cells present long branched processes measuring up to 5–6 fold the length of the cell body (Fig. 15A,B). Consistent with previous studies (Ciani et al. 2004), SKNBE cells were still undifferentiated after 3 days of treatment and RA-mediated differentiation started only after 7 days from RA exposure (Fig. 15A,B). Although basal *CDKL5* expression was notably higher in untreated SH-SY5Y than in untreated SKNBE cells (Fig. 15C), differentiating SH-SY5Y cells exhibited strong up-regulation of *CDKL5* expression (Fig. 15C), whereas SKNBE cells did not show any change in *CDKL5* expression within the same RA-treatment period (Fig. 15C).

The up-regulation of CDKL5 expression in differentiating RA-treated SH-SY5Y cells was further confirmed at the protein level (Fig. 15D). We found that CDKL5 expression increased significantly in this cell line after 3 (+40%) and 7 (+100%) days of RA exposure (Fig. 15D).
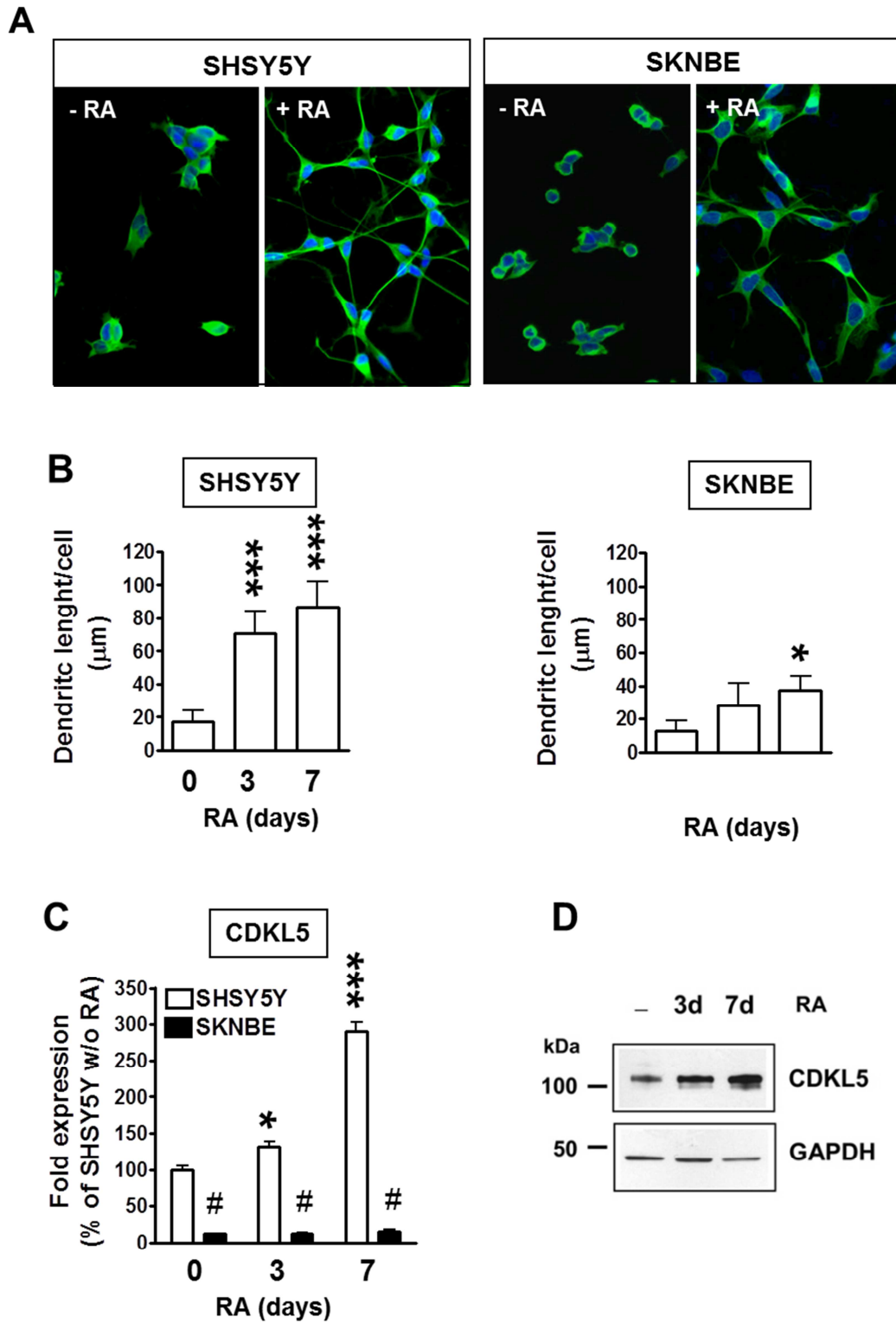
Figure 15 **CDKL5 expression during differentiation in neuroblastoma cell lines.**

(A) Immunofluorescence images showing the morphology of SH-SY5Y (left panel) and SKNBE (right panel) cells after 7 days of treatment with (+RA) or without (−RA) retinoic acid. Cells were stained for β-tubulin III (green) and nuclei were counterstained with Hoechst dye (blue). Scale bar: 30 μm.

*(B) Quantification of neurite outgrowth of SH-SY5Y (left histogram) and SKNBE (right histogram) cells that were either untreated or treated with RA (10 μM) for 3 and 7 days. Neurite outgrowth was expressed as mean neurite length (μm) per cell. Data are expressed as mean±SE of 4 independent experiments. A minimum of 400 cells were evaluated in each experiment for each condition. *P<0.05; ***P<0.001, treated vs. untreated condition (Duncan's test after ANOVA).*

*(C) Quantification by RT-qPCR of CDKL5 expression in SH-SY5Y and SKNBE cells that were either untreated or treated with RA (10 μM) for 3 or 7 days. Data, given as percentage of untreated SH-SY5Y cells, are expressed as mean±SE. The asterisks indicate a significant difference between treated vs. untreated condition, *P<0.05, ***P<0.001 (Duncan's test after ANOVA)*

(D) CDKL5 protein expression in SH-SY5Y cells either untreated or treated with RA (10 μM) for 3 and 7 days was analyzed by western blot with a CDKL5 specific antibody.

The positive correlation between CDKL5 expression and SH-SY5Y differentiation indicates that SH-SY5Y neuroblastoma cells may represent a suitable model to study the role of CDKL5 in neuronal differentiation.

To further investigate the role of CDKL5 in neuronal differentiation, we over-expressed CDKL5 in SH-SY5Y cells by transient transfection of a pGFP/CDKL5-FLAG expression vector. We compared neuritic outgrowth in GFP- and GFP-CDKL5-positive cells isolated by cell sorting 24 hours after transfection and then grown for 1–2 days either in the absence or presence of RA. We found that CDKL5 was able to induce a beginning differentiation also in the absence of RA treatment. While cells expressing GFP alone (controls) occasionally emitted very short processes (Fig. 16B, left panel), cells over-expressing CDKL5 had longer processes with a length increase by +100% after 2

days in culture (Fig. 16A,B, left panel), indicating that CDKL5 is able to promote differentiation also in the absence of pro-differenziative stimuli such as RA treatment. To investigate the effects of CDKL5 over-expression also on RA-induced differentiation, GFP- and GFP-CDKL5-tranfected cells were cultured for 1–2 days in the presence of RA (Fig. 16A,B). After 1 day of RA treatment, CDKL5 expressing cells exhibited a greater neurite length compared to control cells (+30%, Fig. 16A,B), but this difference was no longer detectable after 2 days of RA treatment (Fig. 16A,B).

These data clearly show that CDKL5 can promote neuronal differentiation also in the absence of pro-differentiative stimuli and enhances RA-induced differentiation in SH-SY5Y neuroblastoma cells.

To further confirm this finding, we tested whether a reduction in CDKL5 expression interfered with RA-induced differentiation. To this purpose, SH-SY5Y cells were transfected with two different siRNAs against CDKL5 (si1, si2) to inhibit CDKL5 expression and treated with RA. After 48 hours of treatment, the reduced expression of CDKL5 induced by the siRNAs against CDKL5 (−45% and −60%, Fig. 16C), confirmed by western blot analysis, was paralleled by a significant reduction (−46% and −58%, Fig. 16C) in neurite outgrowth. Transfection with a scrambled siRNA (siScr), as negative control, had no effect on CDKL5 expression and RA induced cell differentiation (Fig. 16C,D), to further confirm the role of CDKL5 on differentiation of SH-SY5Y cells.
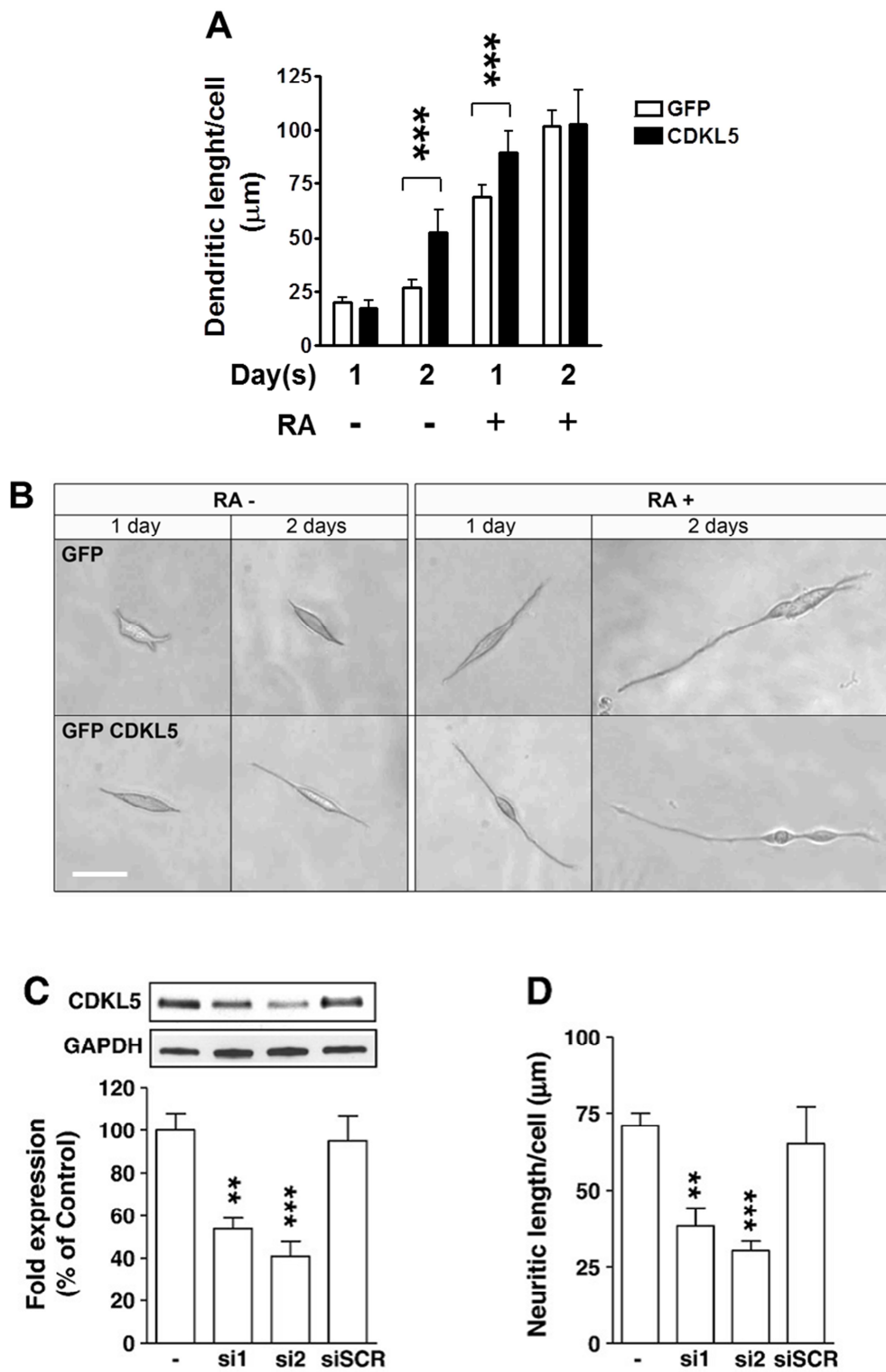
Figure 16 **CDKL5 induces differentiation in the SH-SY5Y neuroblastoma cell line.**

(A) Quantification of neurite outgrowth of SH-SY5Y cells transfected with either GFP-CDKL5 or GFP. Twenty-four hours from transfection, cells were FACS sorted for GFP fluorescence and cultured for 1–2 days with or without retinoic acid (RA; 10 μM). Neurite elongation was expressed as mean neurite length (μm) per cell. Data are expressed as mean±SE of 3–4 independent experiments. A minimum of 400 cells were evaluated in each experiment for each condition. The asterisks indicate a significant difference between cells expressing GFP-CDKL5 vs. cells expressing GFP alone. ***P<0.001; two-tailed t-test.

(B) Representative phase-contrast images of cells expressing GFP-CDKL5 or GFP and cultured for 1 or 2 days in absence (RA-) or in presence of 10 μM RA (RA+). Scale bar: 15 μm.

(C) SH-SY5Y cells were transfected with two different siRNAs against CDKL5 (si1 and si2; 50 nM) or with scramble siRNA (siScr; 50 nM). Quantification by western blots of CDKL5 expression was performed 48 hours after transfection. Data are expressed as mean±SE of 3 independent experiments. **P<0.01; ***P<0.001; two-tailed t-test.

(D) Quantification of neurite outgrowth of SH-SY5Y cells transfected with si1, si2 or siSCR (50 nM). Six hours after siRNA transfection cells were treated with RA (10 μM) and analyzed 42 hours later for neurite outgrowth. Data are expressed as mean±SE of 3 independent experiments. **P<0.01; ***P<0.001; two-tailed t-test.

4.2. CDKL5 negatively regulates cell proliferation in the SH-SY5Y neuroblastoma cell line by blocking cell cycle progression

CDKL5 expression peaks during late embryonic stage and the first postnatal period (Chen et al. 2010), when most of the neuronal progenitors stop proliferating and enter the differentiated state, suggesting that it may negatively control neuron proliferation.

To address this point, SH-SY5Y cells transiently expressing the CDKL5-FLAG fusion protein were evaluated for proliferation rate by a bromodeoxyuridine (BrdU) incorporation assay, in which the thymidine analogue

is incorporated into DNA during the S-phase of the cell cycle. The effect of CDKL5 over-expression on cell proliferation was determined by evaluating the number of proliferating cells (BrdU positive cells) that expressed CDKL5 (CDKL5-FLAG positive cells). Interestingly, we never found cells that, in addition to express CDKL5, were also BrdU positive, supporting our hypothesis that CDKL5 may inhibit cell proliferation (Fig. 17A). Similar results were obtained with a second proliferation marker, Ki-67, which is expressed in dividing cells through late-G_1+S+G_2+M but not G_0 and early G_1 phases of cell cycle. As expected no CDKL5-positive cells were also positive for Ki-67 (data not shown).

This data indicate that CDKL5 over-expression specifically blocks cell proliferation of neuroblastoma cells.

To further confirm the anti-proliferative role of CDKL5 in neuroblastoma cells, we silenced the endogenous expression of CDKL5 using two siRNAs directed against CDKL5 (si1, si2) and evaluated the effect on proliferation by BrdU-immunostaining. A reduced expression of CDKL5 after siRNAs transfection was accompanied by a significant increase in cell proliferation (+31% si1, +39% si2, Fig. 17B), while treatment with a scrambled siRNA (siScr), as negative control, had no effect on cell proliferation (data not shown). These data support the idea that CDKL5 can inhibit cell proliferation.

The hypothesis that CDKL5 can inhibit proliferation leads us to speculate that CDKL5 may affect the cell cycle dynamics. To clarify this point, we compared the cell cycle profile of GFP vs. GFP-CDKL5 transfected SH-SY5Y cells. FACS sorted GFP and GFP-CDKL5 positive cells (Fig. 17C) were treated with propidium iodide to stain DNA and analyzed by flow cytometry. We found that the fraction of cells in G_0/G_1 was significantly increased in CDKL5 over-expressing cells as compared to control cells and, as a consequence, the fraction of

S phase cells was decreased. In CDKL5 over-expressing cells, the percentage of G_0/G_1 became approximately 70%, suggesting that CDKL5 blocks cells in G_0/G_1 phase (Fig. 17D). We found no differences in the percentage of cells in the sub-G_1, which is considered to indicate the proportion of apoptotic cells over total, indicating that CDKL5 does not induce apoptosis in neuroblastoma cells. To further confirm that CDKL5 over-expression does not induce apoptotic cell death in this cell line, we performed an immunostaining for intracellular cleaved-caspase-3 and found no differences between CDKL5 positive and negative cells (Fig. 17E).

These data clearly show that CDKL5 over-expression does not induce apoptotic cell death in human neuroblastoma cells and that **the inhibition of cell proliferation is due to an arrest in the G_0/G_1 phase of the cell cycle.**
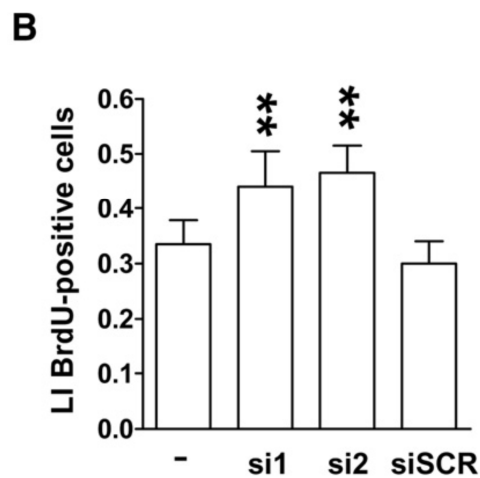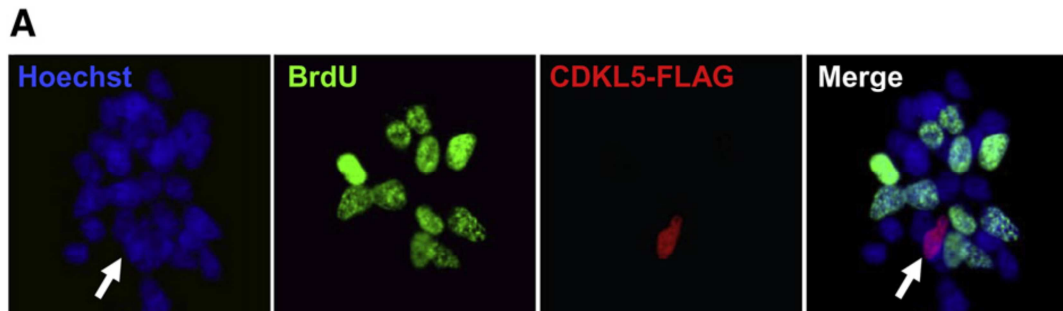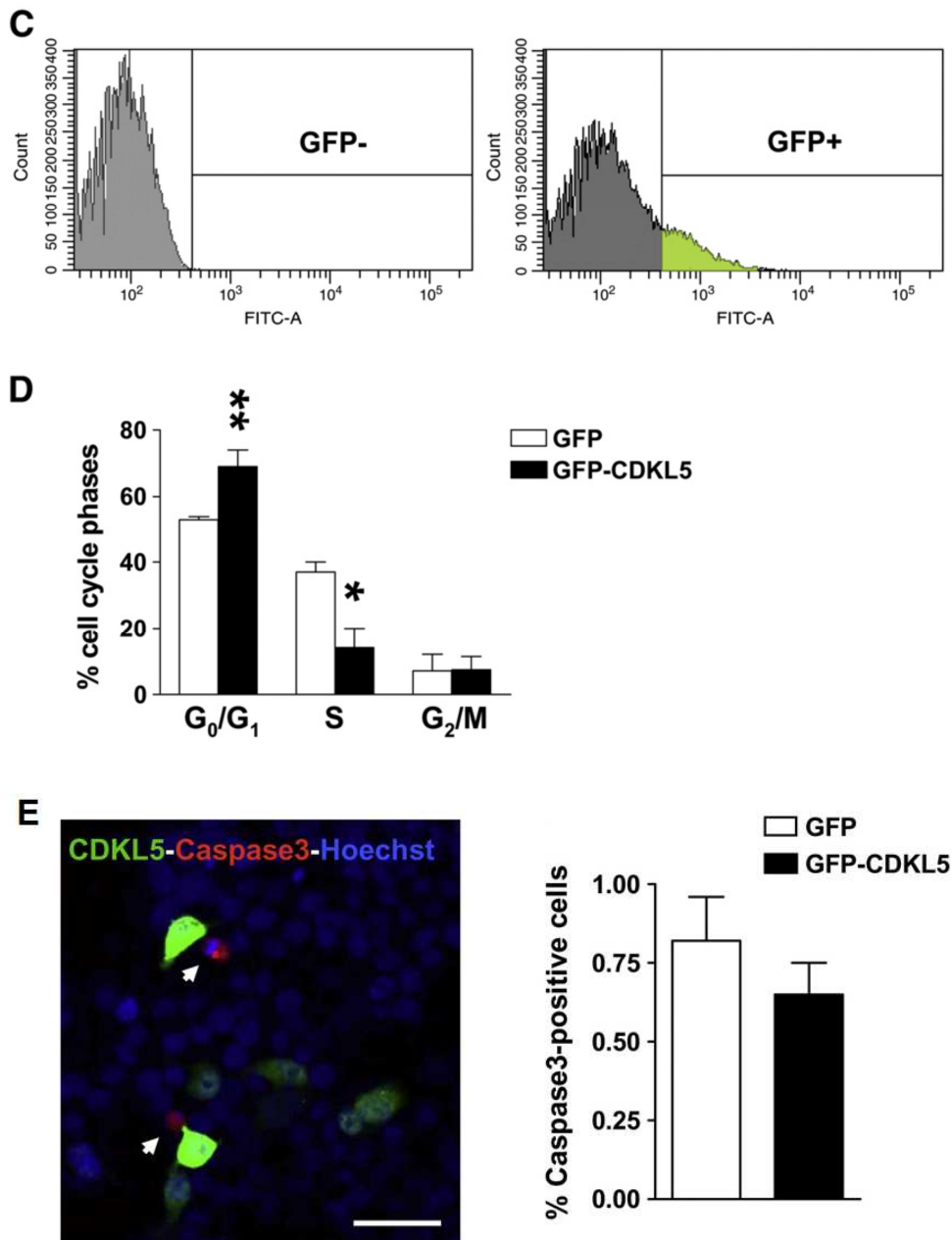
Figure 17 CDKL5 negatively regulates proliferation in SH-SY5Y neuroblastoma cell lines by blocking cell cycle progression.

(A) Immunofluorescence images of SH-SY5Y neuroblastoma cells transfected with CDKL5-FLAG. Twenty-four hours after transfection, SH-SY5Y cells were treated with BrdU (10 μM) for 2 hours and thereafter cells were processed for double immunocytochemistry. Cells were immunostained for FLAG (red signal) and BrdU (green signal) and cell nuclei were counterstained with Hoechst dye (blue signal). The arrows in Hoechst and

merge images indicate the nuclei of cells expressing exogenous CDKL5. Three independent experiments were performed and a minimum of 600 cells were evaluated in each experiment for each condition. Scale bar: 20 μm.

(B) Labeling index (LI), defined as percentage of BrdU positive cells over total cell number, was determined for SH-SY5Y transfected with two different siRNAs against CDKL5 (si1 and si2; 50 nM) or with scramble siRNA (siSCR; 50 nM). Forty-six hours after transfection cells were exposed to BrdU (10 μM) for the last 2 hours. Data, given as percentage of control condition, are expressed as mean±SE of 3 independent experiments. **P<0.01; two-tailed t-test.

(C) Twenty-four hours after transfection with GFP-CDKL5 or GFP alone, SH-SY5Y cells were FACS sorted for GFP expression. The threshold for positivity for GFP was established as the levels corresponding to untransfected cells (histogram on the left). The green area in the histogram on the right shows fluorescence intensity of sorted GFP-CDKL5 positive cells.

(D) Distribution of cell populations in the $G_0/_1$, S, or G_2/M phases of the cell cycle, identified by flow cytometry analysis. Data, given as percentage of either GFP-CDKL5 or GFP cells in each phase of the cell cycle, are expressed as mean±SE of 3 independent experiments, *P<0.05, **P<0.01, two-tailed t-test.

(E) Immunofluorescence image of cleaved caspase-3 immunostainig of SH-SY5Y neuroblastoma cells transfected with GFP-CDKL5. Twenty-four hours after transfection, SH-SY5Y cells were immunostained for cleaved caspase-3 (red signal), CDKL5 (green signal) and cell nuclei were counterstained with Hoechst dye (blue signal). Scale bar: 25 μm.
Percentage of cleaved caspase-3-positive cells over total number of GFP-CDKL5-positive cells and GFP-positive cells (histogram on the right). Data are expressed as mean±SE of 3 independent experiments. A minimum of 450 cells were evaluated in each experiment for each condition.

These results demonstrate that CDKL5 affects both neurite growth and cell proliferation, suggesting that CDKL5 may modulate not only dendritic maturation but also cell proliferation in the developing brain.

4.3. Creation and validation of Cdkl5 conditional knockout mice

A constitutive knockout allele of Cdkl5 was produced by germline deletion of exon 4 of a Cdkl5 conditional knockout allele produced by standard gene targeting in embryonic stem cells (Fig. 18A). Since Cdkl5 is localized on X chromosome, the genotypes deriving from deletion of the Cdkl5 gene are: homozygous females (-/-), heterozygous female (+/-) and hemizygous males (-/Y). Semi-quantitative PCR on total brain RNA from female wild-type (+/+), heterozygous (+/-) and homozygous (-/-) Cdkl5 knockout (KO) mice with primers spanning exons confirmed the absence of exon 4, but normal levels of exon 2,3 and 5 in Cdkl5 KO female mice (Fig. 18B). To confirm the absence of the full-length Cdkl5 protein we performed western blot analysis on whole brain extracts using a specific antibody against CDKL5. As shown in Fig. 18C hemizygous male (-/Y) and homozygous female (-/-) Cdkl5 KO mice do not express the protein, while heterozygous females (-/X) show intermediate levels of Cdkl5 expression. The absence of the Cdkl5 protein in mutant mice was further confirmed by immunofluorescence analysis of CA1 hippocampus brain sections (Fig. 18D).
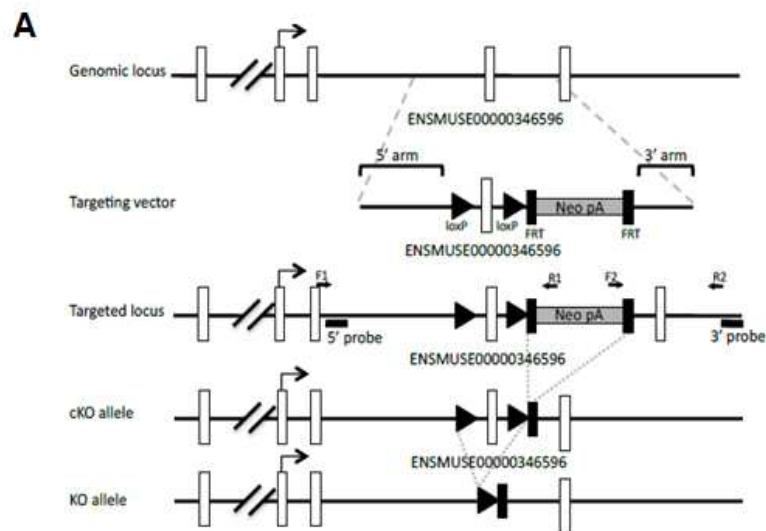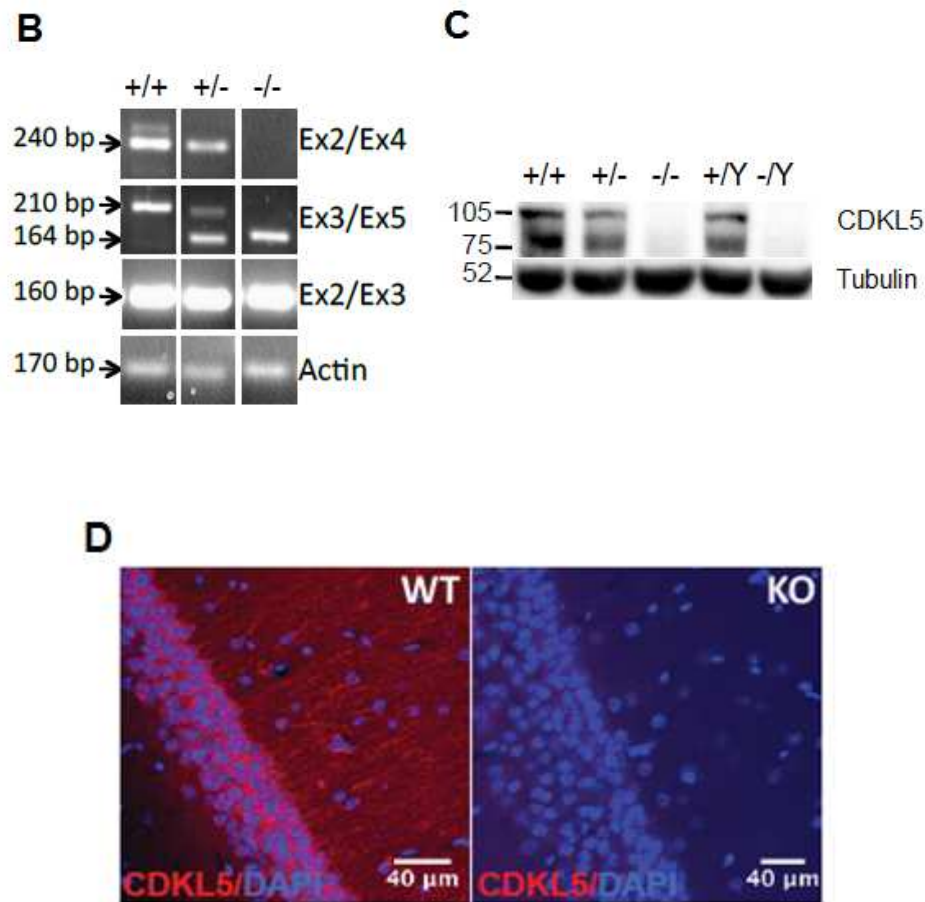
*Figure 18 **Generation and validation of Cdkl5 conditional knockout mice.***

(A) Genomic organization of the Cdkl5 locus showing critical exon 4 (ENSMUSE00000346596), the targeting construct, successfully targeted Cdkl5 locus (genotyping primers indicated by arrows), FRT-deleted conditional Cdkl5 knockout allele, and Cre-deleted constitutive Cdkl5 knockout allele used in the present study.

(B) Semi-quantitative PCR on total brain RNA from female wild-type (+/+), heterozygous (+/-) and homozygous (-/-) Cdkl5 KO mice with primers spanning exons confirmed an absence of exon 4, but normal levels of exon 2,3 and 5 in Cdkl5 mutant female mice.

(C) Western blot analysis of whole brain protein extracts of wild-type (+/+), heterozygous (+/-), and homozygous (-/-) female Cdkl5 KO mice and wild-type (+/Y) and hemizygous (-/Y) male Cdkl5 KO mice using a polyclonal anti-Cdkl5 antibody confirm the absence of Cdkl5 in homozygous female (-/-) and hemizygous male (-/Y) mutant mice, while heterozygous females (+/-) show intermediate levels of Cdkl5 expression.

(D) Examples of CA1 hippocampus brain sections from adult male wild-type (WT) and Cdkl5 knockout (KO) mice processed for fluorescent immunostaining for CDKL5 (red signal). Cell nuclei were counterstained with Hoechst dye (DAPI- blue signal). Scale bar: 40 µm.

4.4. Behavioral impairments in Cdkl5 knockout mice

A first characterization of the Cdkl5 mutant mice show that heterozygous (+/-) and homozygous females (-/-), as well as hemizygous male (-/Y) Cdkl5 KO mice had no differences in viability, body weight (Fig. 19A), and absolute as well as relative brain weight compared to wild-type littermates (data not shown; Fig. 19B).

In order to identify behavioral features that mimic the clinical features described in CDKL5 disorder, including seizures, motor abnormalities and impaired hippocampal-dependent learning and memory, we performed a general behavioral screen (Rogers et al. 1999) on Cdkl5 mutant mice.

We first evaluated clasping of hind-limbs and observed that a significant fraction of heterozygous (+/-) and homozygous female (-/-) as well as hemizygous male (-/Y) Cdkl5 KO mice revealed abnormal clasping of hind-limbs compared to wild-type littermates (Fig. 19C,D).

Continuous monitoring of home cage activity showed a significant decrease in locomotion in both homozygous female (-/-) and hemizygous male (-/Y) Cdkl5 KO mice and intermediate levels in heterozygous (+/-) Cdkl5 KO females (Fig 19E,F). Hypolocomotion was not seen when mice were placed in a novel open arena (data not shown), suggesting that the deficit did not reflect a reduced capacity for locomotion.
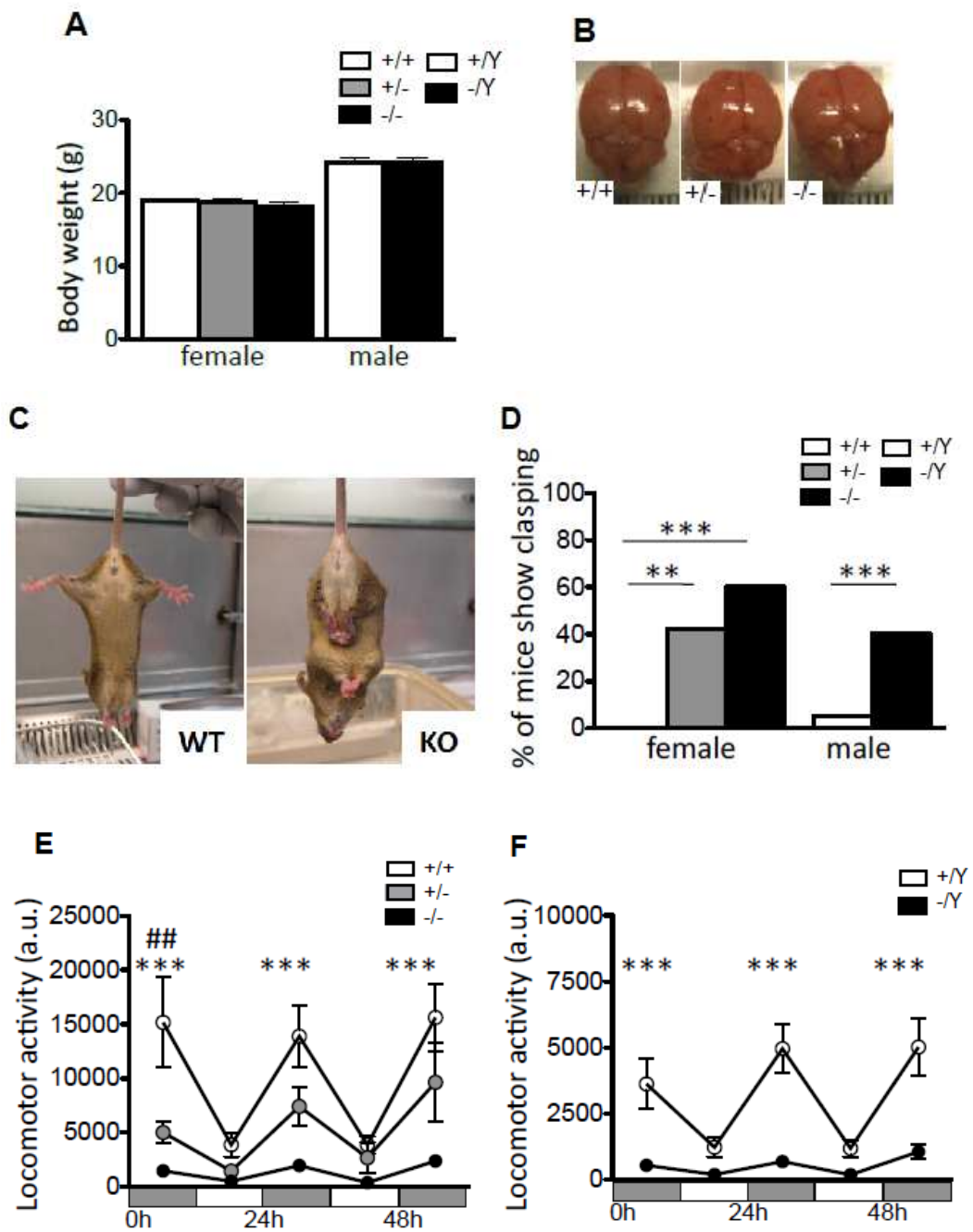
Figure 19 **Behavioral impairments in the Cdkl5 knockout mice.**

(A) Histogram showing body weight (expressed in grams) of 6 weeks old wild-type an Cdkl5 KO mice. No differences in body weight was observed in heterozygous (+/-) and homozygous (-/-) female Cdkl5 KO mice, as well as hemizyous (-/Y) male KO mice compared to sex-matched wild-type littermates.

(B) Representative images of dissected brains from wild-type (+/+), heterozygous (+/-) and homozygous (-/-) female Cdkl5 KO mice. No differences in brain size and brain weight were observed in female Cdkl5 KO mice compared to wild-type littermates.

(C-D) Percentage of mice showing hind-limb clasping was significantly increased in adult female and male Cdkl5 KO mice (+/+, n = 28; +/-, n = 38; -/-, n = 32; +/Y, n = 55; -/Y, n =42). Data are expressed as mean±SE,**P<0.01, ***P<0.001; two-tailed t-test.

(E-F) Home cage activity was significantly decreased in adult female (E) and male (F) Cdkl5 KO mice. Data are expressed as mean±SE,***P<0.001; two-tailed t-test;

Although early onset seizures are one of the prominent features of the CDKL5 disorder, we surprisingly found no evidence for spontaneous seizures during videotaped observations of adult Cdkl5 KO mice either in the home cage or following transfer to a novel cage (data not shown). Electroencephalographic (EEG) recordings from implanted surface electrodes in freely behaving animals did not reveal spontaneous epileptiform activity in hemizygous (-/Y) male Cdkl5 KO mice (Fig. 20A,B left panel).

Pharmacological induction of seizures with kainic acid was monitored by surface EEG. Low dose kainic acid did not induce overt seizures, but caused occasional epileptiform activity patterns in both hemizygous (-/Y) Cdkl5 male KO mice and wild-type (+/Y) littermates (data not shown). At the higher dose, kainic acid induced overt seizures, as evidenced by periods of sudden immobility and in some cases tonic clonic convulsions in both hemizygous (-/Y) Cdkl5 KO and wild-type (+/Y) littermate mice. Correspondingly, prominent epileptiform activity bursts were observed in the EEG of both genotypes (Fig. 20A,B right pannel). Cdkl5 KO mice did not differ from wild-type littermates in latency to epileptiform activity bursts suggesting similar susceptibility to the drug (Fig. 20C). However,

the mean duration of high-amplitude bursts was longer and the frequency lower in Cdkl5 KO mice compared to wild-type littermates (Fig. 20D,E). Power spectrum analysis revealed a significant dose-dependent increase in low frequency EEG power in wild-type, but not in hemizygous (-/Y) Cdkl5 male KO mice treated with kainic acid when compared to baseline (Fig. 20F,G).
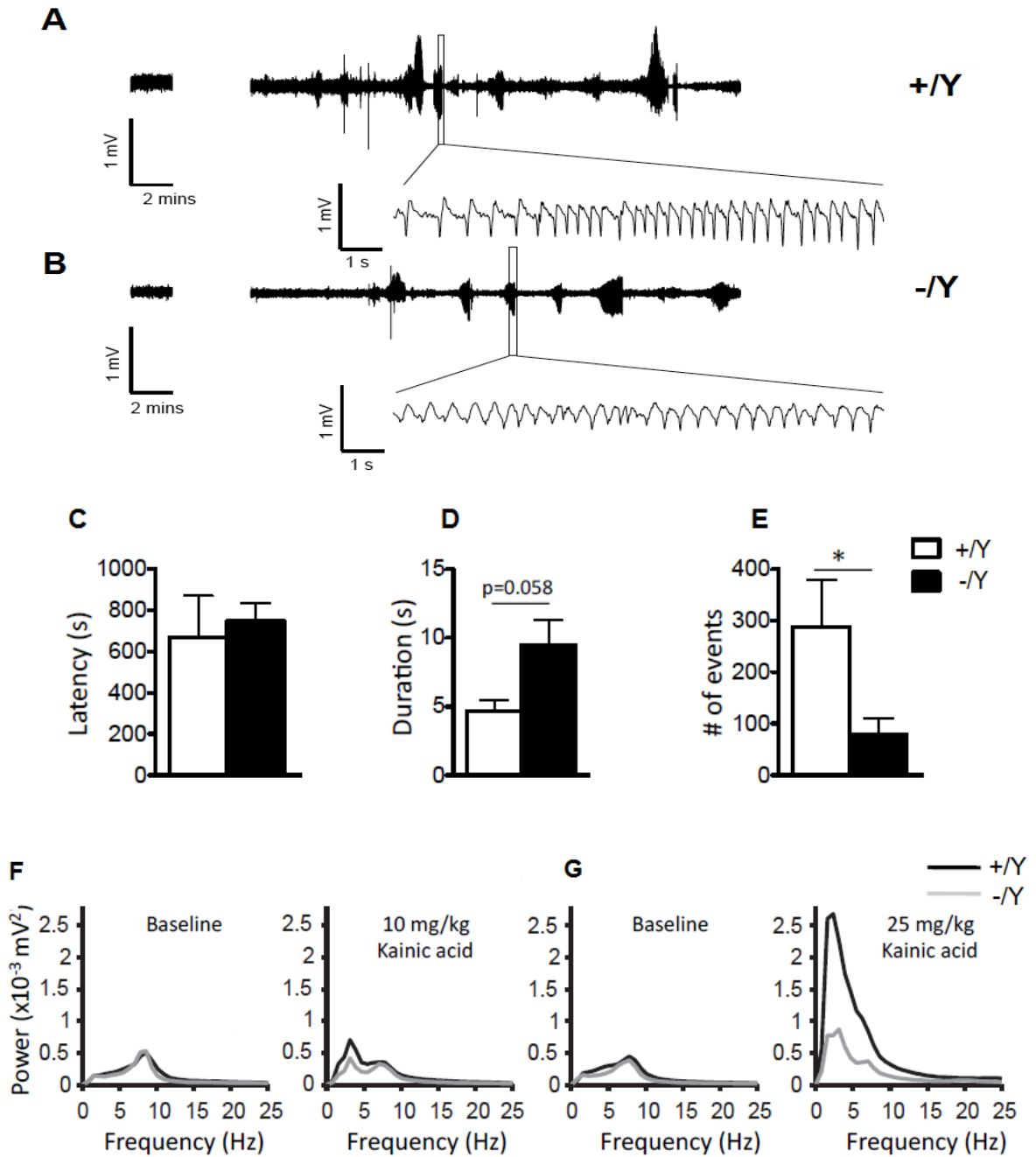
*Figure 20 **Altered seizure response in Cdkl5 knockout mice.***

(A-B) Representative electroencephalogram (EEG) traces recorded from surface electrodes placed over the somatosensory cortex in freely moving male wild-type (+/Y) and Cdkl5 KO (-/Y) mice. (Left) Baseline EEG before drug treatment. (Right) EEG taken during 2 hour post-injection period following treatment with high dose (25 mg/kg, i.p.) kainic acid. (expanded trace) Detail of epileptiform event showing low frequency, high amplitude activity.

(C-E) Latency (C) to the first epileptiform event did not differ between wild-type (+/Y) and Cdkl5 KO (-/Y) male mice, but (D) mean duration of events was longer (p=0.058) and (E) mean frequency was lower in hemizygous (-/Y) male Cdkl5 KO mice (+/Y: n = 4, -/Y: n= 5). Data are expressed as mean±SE, *P<0.05; two-tailed t-test.

(F-G) Average EEG power spectra of (left) baseline and (right) post-injection periods for (F) low dose (10 mg/kg, i.p.) and (G) high dose (25 mg/kg, i.p.) kainic acid treatment revealed a significant, dose-dependent increased in low frequency EEG power in wild-type, but not Cdkl5 KO mice.

In order to examine hippocampal-dependent learning and memory in Cdkl5 KO mice, we evaluated hippocampus-dependent spatial working memory by using the Y-maze paradigm. We found that while wild-type mice entered more frequently into the novel, previously unvisited arm of the maze (Fig. 21A), Cdkl5 KO mice showed no preference toward the novel arm and entered randomly into the different arms approximately with the same frequency (Fig. 21A). This difference was not due to a reduced motility, as shown by the distance travelled by both mice (Fig. 21B), suggesting that **Cdkl5 KO mice have deficits in spatial working memory**.

To sum up **we demonstrated that Cdkl5 KO mice show hind-limb clasping, hypoactivity, deficits in spatial working memory and abnormal EEG responses to convulsants,** features that may model the stereotypic hand

movements, hypotonia, cognitive disabilities and seizures, respectively, reported in the human condition.
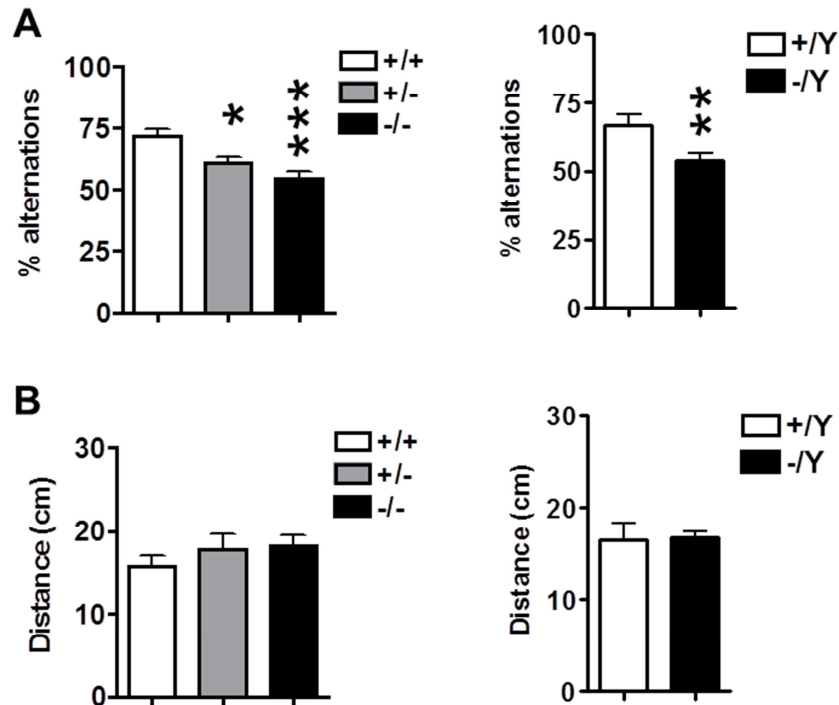
Figure 21 **Working memory test in Cdkl5 knockout mice.**

(A) Cdkl5 KO female and male mice were tested in a single trial Y maze task, to measure arm alternation. The percentage of spontaneous alternations is defined as (total alternations/total arm entries-2) x 100.

(B) Motor activity during testing is shown as the distance during the task.

All data are presented as mean ± SEM. Statistical analysis: female, two-way ANOVA and Duncan's test after ANOVA, *p < 0.05 ***p < 0.001; male, Student's t test, **p<0.01.

4.5. Loss of Cdkl5 increases proliferation rate in the hippocampal dentate gyrus

In order to establish whether lack of Cdkl5 affects cell proliferation in the hippocampal dentate gyrus (DG), wild-type and Cdkl5 KO mice aged 45 days (P45) were injected for 5 consecutive days with BrdU and sacrificed 24 hours after the last BrdU injection.

Observation of images from wild-type (+/+) and homozygous (-/-) female Cdkl5 KO mice clearly show that mutant mice had more BrdU positive cells than wild-type littermates (Fig. 22A). A quantitative analysis revealed that the number of BrdU positive cells was significantly higher in both homozygous female (-/-) and hemizygous male (-/Y) Cdkl5 KO mice (+20% and +23%, respectively) compared to wild-type littermates (Fig. 22B). The number of BrdU positive cells in heterozygous female (+/-) Cdkl5 KO mice showed a slight but not significant increase in comparison with wild-type females (Fig. 22B), which may be consistent with a mosaic of knockout and wild-type cells as a result of X-inactivation (Goto and Monk 1998). Similar results were obtained with immunohistochemistry for Ki-67, an endogenous marker of actively proliferating cells (Fig. 22C).

The increased proliferative ability of neuronal precursor cells in Cdkl5 KO mice suggest that CDKL5 exerts a negative role on cell proliferation, similar to those observed *in vitro*.
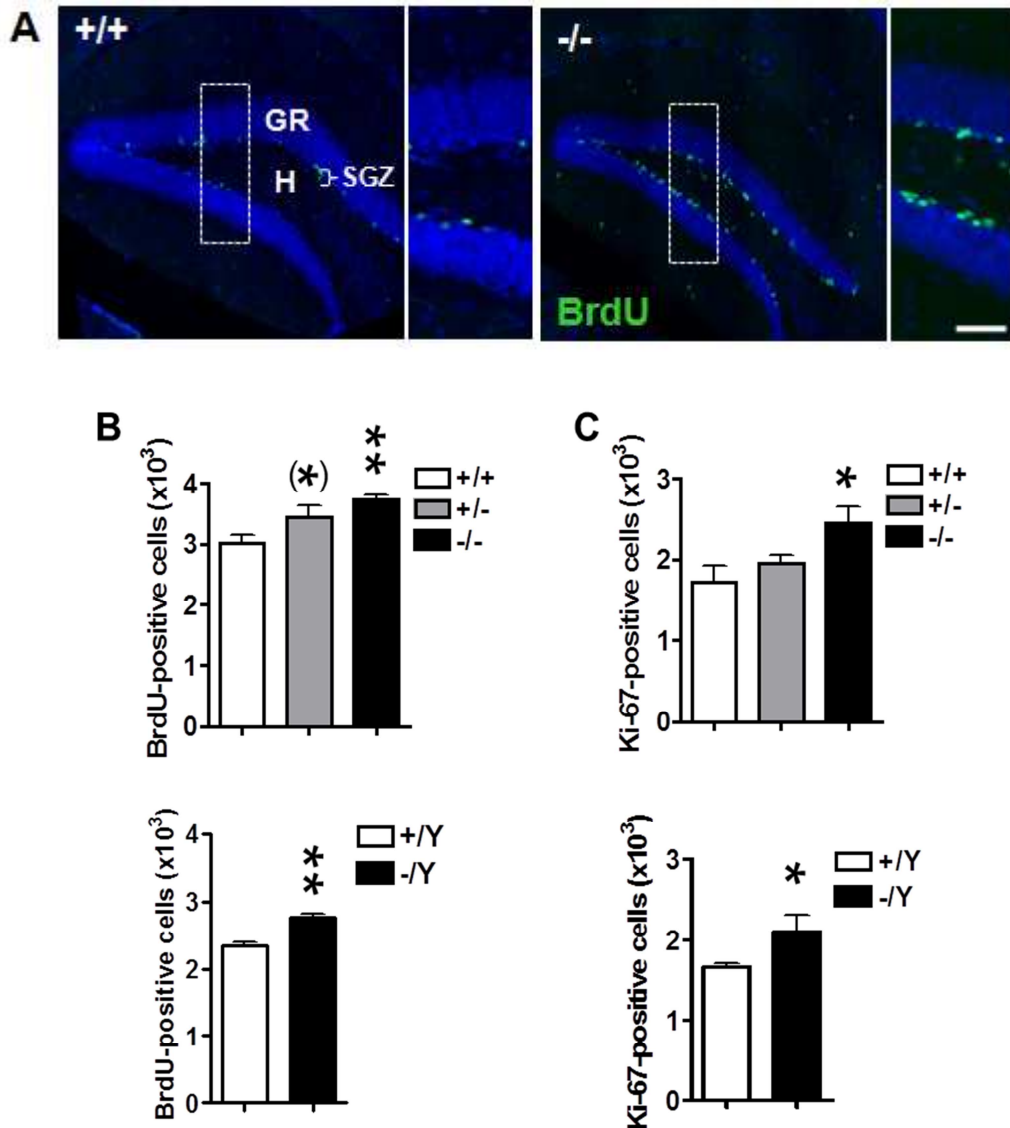
*Figure 22 **Precursor proliferation in the dentate gyrus of Cdkl5 knockout mice.***

(A) Examples of sections processed for fluorescent immunostaining for BrdU from the DG of wild-type (+/+) and homozygous (-/-) female Cdkl5 KO mice. These animals were injected for 5 consecutive days with BrdU and sacrificed 24 hours after the last BrdU injection on P45. Calibrations = 200 μm (lower magnification) and 80 μm (higher magnification). Abbreviations: DG, dentate gyrus; SGZ, subgranular zone; GR, granule cell layer; H, hilus.

(B-C) Number of BrdU-positive cells (B) and Ki67-postivie cells (C) in the whole DG (GR+H) of homozygous (-/-), heterozygous (+/-) and wild-type (+/+) female Cdkl5 KO mice (upper histogram) and hemizygous (-/Y) and

4.6. Loss of Cdkl5 reduces the survival of newborn cells in the hippocampal dentate gyrus

In order to evaluate the survival of the newborn cells, we counted the number of BrdU positive cells present in the hippocampal dentate gyrus (DG) 30 days after BrdU administration, in mice aged 75 days (P75). Most of the surviving cells were located in the granule cell layer (GR), the final destination of new granule neurons. We found that both female (-/-) and male (-/Y) Cdkl5 KO mice had the same number of BrdU-labeled cells as wild-type littermates (Fig. 23A). This suggests that the surplus of cells born at P45 in the mutant mice was offset by a reduction in the survival rate. The ratio between the number of BrdU positive cells present in the DG at one month (Fig. 23A) and 24 hours (Fig. 22B) after the last BrdU injection provides an estimate of the net survival rate. We found that the surviving cells were 50% of the cells born at P45 in wild-type mice and 39 ± 1.2 % and 43 ± 1.9%, respectively, in female (-/-) (p< 0.01 two-tailed t-test) and male (-/Y) Cdkl5 KO mice (p< 0.01 two-tailed t-test). A significant difference in the survival rate was also found in the heterozygous (+/-) female Cdkl5 KO mice compared to wild-type littermates (45 ± 1.7 %; p<0.01 two-tailed t-test).

In the attempt to examine whether lack of Cdkl5 triggers apoptotic cell death we evaluated the number of apoptotic cells in the DG by counting the number of cells that expressed cleaved caspase-3 (Fig. 23B). Most of the apoptotic cells were in the innermost portion of the GR. We observed an increase of cell death in both homozygous female (-/-) and hemizygous male (-/Y) Cdkl5

KO mice (+40% and +32%, respectively; Fig. 23B) vs. wild-type littermates and a less pronounced but significant increase also in heterozygous (+/-) females (+14%; Fig. 23B).
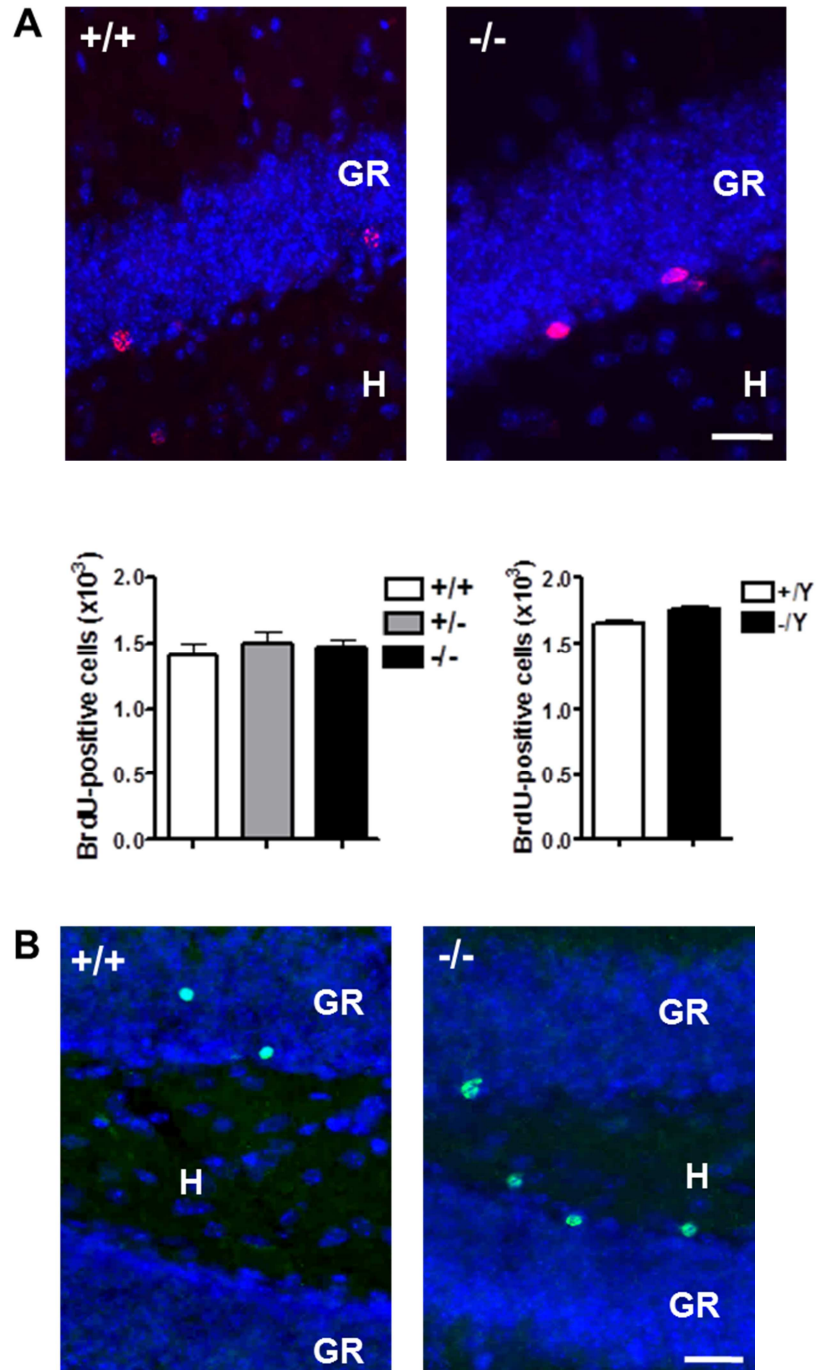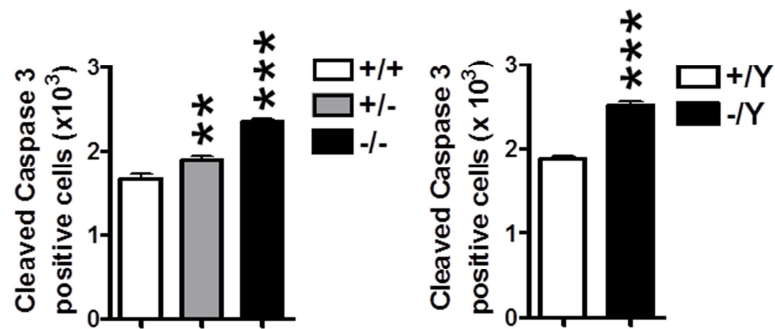
Figure 23 **Survival of precursors in the dentate gyrus of Cdkl5 knockout mice.**

(A) Examples of sections processed for fluorescent immunostaining for BrdU from the DG of wild-type (+/+) and homozygous (-/-) female Cdkl5 KO mice. These animals were injected for five consecutive days with BrdU and sacrificed after one month after the last BrdU injection on P75. Calibrations = 50 μm.

Number of BrdU-positive cells in the whole DG (GR+H) of homozygous (-/-), heterozygous (+/-) and wild-type (+/+) female Cdkl5 KO mice (left histogram) and hemizygous (-/Y) and wild-type (+/Y) male mice (right histogram).

(B) Examples of sections processed for fluorescent immunostaining for cleaved caspase-3 from the DG of wild type (+/+) and homozygous (-/-) female Cdkl5 KO mice. Calibrations = 40 μm.

Number of cleaved caspase-3-positive cells in the whole DG (GR+H) of animals as in A.

Values in (A-B) represent totals for one DG (mean ± SD). **p < 0.01; ***p < 0.001 (Duncan's test after ANOVA). Abbreviations: DG, dentate gyrus; GR, granule cell layer; H, hilus.

This evidence suggests that lack of Cdkl5 decreases the survival rate of newborn cells in Cdkl5 KO mice.

4.7. Loss of Cdkl5 specifically decreases survival of postmitotic neurons in the hippocampal dentate gyrus

In order to examine the phenotype of the surviving cells 30 days after BrdU administration we performed an immunofluorescent double-labeling for BrdU and either a neuronal marker (NeuN) or an astrocytic marker (GFAP) on wild-type and Cdkl5 mutant mice. Both female (-/-) and male (-/Y) Cdkl5 KO mice had fewer (-20% and -30%, respectively) new neurons (NeuN/BrdU positive cells; Fig. 24A,B) in comparison with wild-type littermates, while the number of new astrocytes (GFAP/BrdU positive cells; Fig. 24A,B) was similar in both genotypes. Consequently a larger number of cells with an undetermined phenotype was present in female (-/-) and male (-/Y) Cdkl5 KO mice (+190% and +300%, respectively; neither; Fig. 24A,B). A similar effect was also found in heterozygous (+/-) female Cdkl5 KO mice compared to wild-type littermates (Fig. 24A).
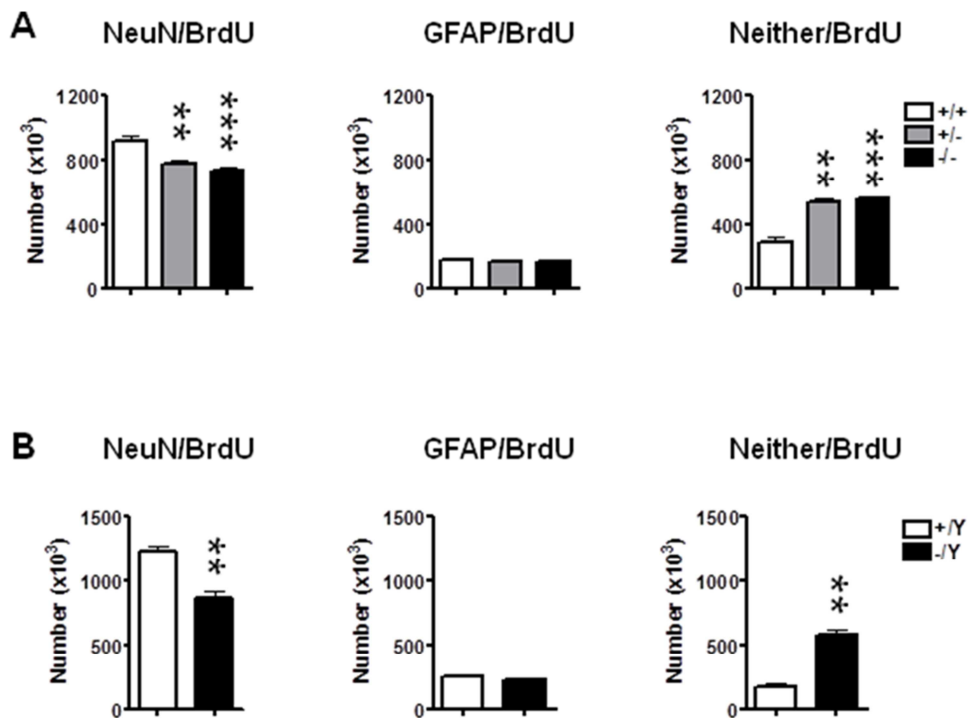
*Figure 24 **Phenotype of the surviving cells in the dentate gyrus of Cdkl5 knockout mice.***

(A,B) Absolute number of surviving cells with neuronal phenotype (NeuN/BrdU), astrocytic phenotype (GFAP/BrdU) and undetermined phenotype (Neither/BrdU) in the DG (GR+H) of homozygous (-/-), heterozygous (+/-) and wild-type (+/+) female Cdkl5 KO mice (A) and hemizygous (-/Y) and wild-type (+/Y) male Cdkl5 KO mice (B). These animals were injected for five consecutive days with BrdU and sacrificed after one month after the last BrdU injection on P75.

Values represent totals for one DG (mean ± SD). **p < 0.01; ***p < 0.001 (Duncan's test after ANOVA).

These data show that the lack of Cdkl5 dampens the formation of new granule neuron without affecting astrogliogenesis.

The hippocampal dentate gyrus (DG) is formed over a long time period that begins during gestation and continues in the postnatal period. It contains a neurogenic niche, the subgranular zone (SGZ), which is inhabited by a heterogonous population of cells and cellular elements, which play an important role in neurogenesis. In the course of adult hippocampal neurogenesis, new cells within the SGZ of the DG go through a series of stages associated with proliferative activity, from stem cell (type 1) over intermediate progenitor stages (type 2/3) to postmitotic maturation (Fig. 25A). Doublecortin (DCX), a microtubule associated protein, is widely expressed by the actively dividing type 2b and type 3 progenitor cells and also by immature granule neurons (Fig. 25A). As shown in Fig. 25A,B, these cell types can be distinguished based on their morphology: while type 2b/3 cells are orientated parallel to the SGZ (Fig. 25A,B; asterisk), immature granule neurons have a vertical orientation and extend long apical processes into the granule cell layer (GR) (Fig. 25A,B; arrows). Based on these features, we determined whether loss of Cdkl5 specifically affects a

particular stage of granule cell formation. We found that Cdkl5 KO mice had more 2b/3 type cells in comparison with wild-type littermates but a reduced number of immature neurons (Fig. 25C). These data indicate that the lack of Cdkl5 affects in an opposite manner type 2b/3 cells (mitotic cells) and differentiating (postmitotic) neurons. This is consistent with the increased number of undifferentiated cells (neither) and the reduced number of cells differentiated into neurons (BrdU/NeuN positive cells) found in Cdkl5 KO mice (see Fig. 24A,B).

In order to establish whether the reduced number of immature neurons in Cdkl5 KO mice was due to an increase in cell death we evaluated the number of cells that were positive for both DCX and cleaved caspase-3. We found that hemizygous male (-/Y) Cdkl5 KO mice showed a notably higher number of DCX/ cleaved caspase-3 positive immature neurons in comparison to wild-type littermates (+/Y) (Fig. 25D,E), with no difference in the number of DCX/caspase-3 positive 2b/3 type cells (Fig. 25D,E). Similar results were obtained also in the female Cdkl5 KO mice (data not shown).
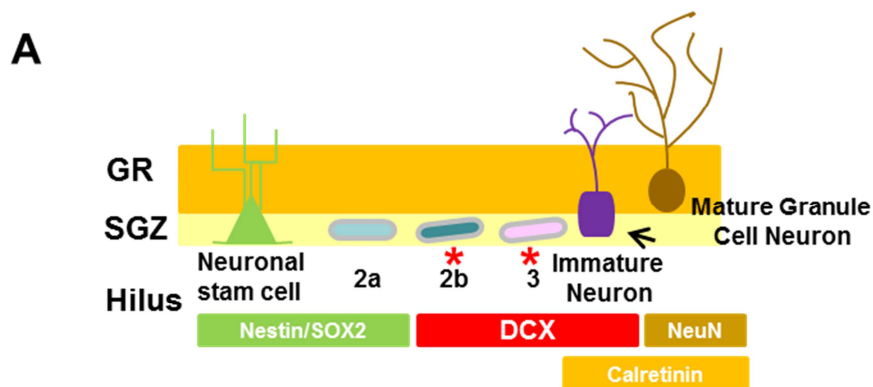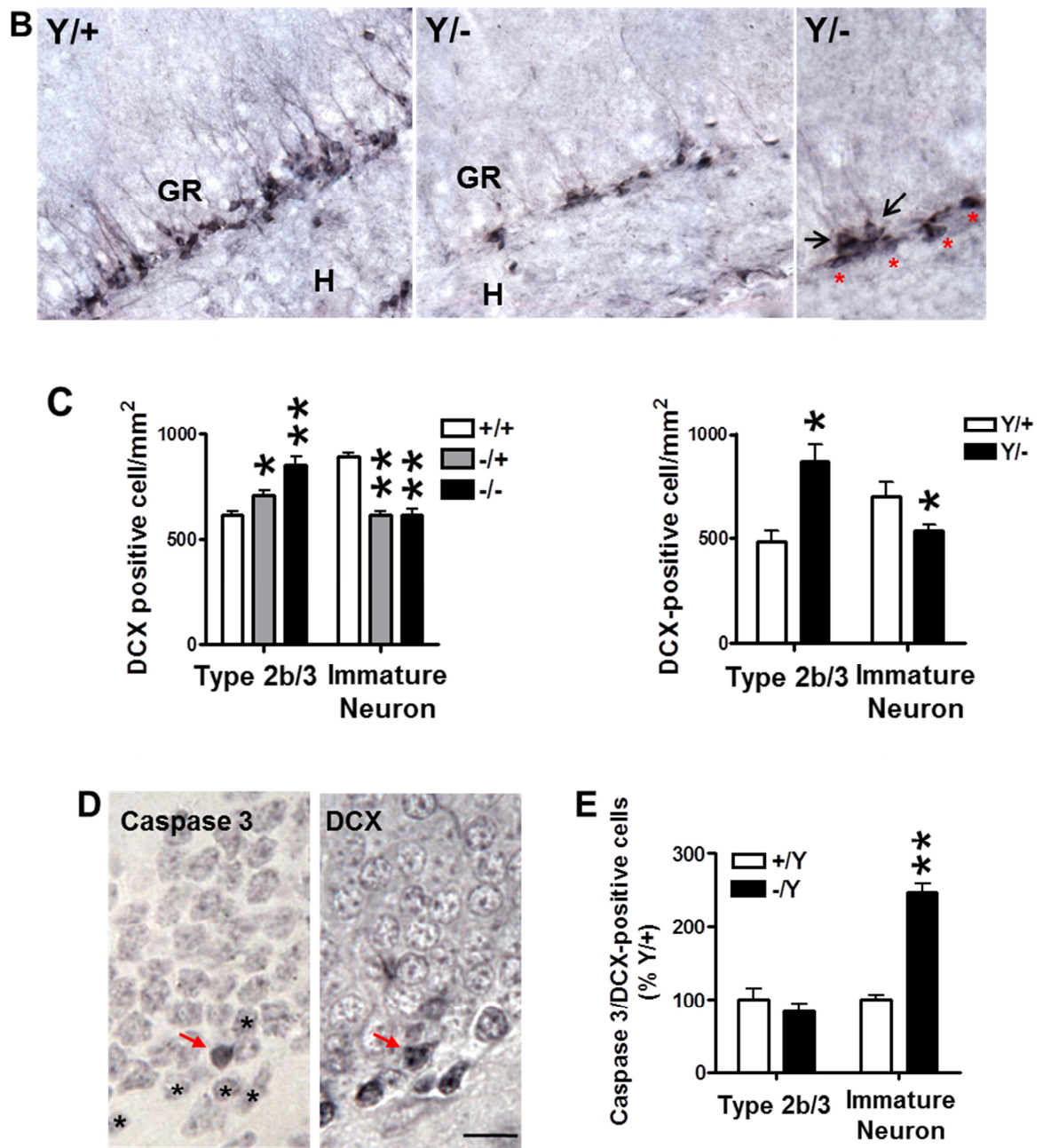
Figure 25 **Survival of post-mitotic neurons in the dentate gyrus of Cdkl5 knockout mice.**

(A) Schematic representation of adult hippocamapal neurogenesis. The subgranular zone (SGZ) of the dentate gyrus (DG) is inhabited by a heterogonous population of cells which go through a series of stages associated with proliferative activity: from stem cell (type 1 cells, expressing Nestin and SOX2) over intermediate progenitor stages (type 2a/b and type 3) to postmitotic maturation. Doublecortin (DCX), a microtubule associated

protein, is widely expressed by the actively dividing type 2b and type 3 intermediate progenitor cells and also by immature granule neurons and these two cell types can be distinguished based on their morphology: while type 2b/3 cells are orientated parallel to the SGZ (red asterisks), immature granule neurons have a vertical orientation and extend long apical processes into the granule cell layer (GR).

(B) Examples of sections processed for DCX immunostaining from the DG of wild-type (+/Y) and hemizygous male (-/Y) Cdkl5 KO mice. The high magnification photomicrograph show immature DCX-positive neurons (vertical orientation with apical processes; black arrows) in the innermost portion of the GR and type 2b/3 DCX-positive granule cells (orientated parallel to the GR; red asterisks) in the SGZ. Calibrations = 60 μm (lower magnification) and 15 μm (higher magnification).

(C) Number of DCX-positive cells in the whole DG (GR+H), divided in immature neurons and type 2b/3 cells, of homozygous (-/-), heterozygous (-/+) and wild-type (+/+) female Cdkl5 KO mice (left histogram) and hemizygous (-/Y) and wild-type (+/Y) male Cdkl5 KO mice (right histogram).

(D) Examples of ultra-thin sections processed for immunostaining for cleaved caspase-3 and DCX from the DG of wild-type male (+/Y) mice. Computer-based image overlay of two serial ultra-thin sections allow to identify DCX-positive cells (black asterisks)/cleaved caspase-3-positive cells (red arrow). Calibrations = 15 μm.

(E) Number of cleaved caspase-3/DCX-positive cells in the whole DG (GR+H), divided in immature neurons and type 2b/3 cells, of hemizygous (-/Y) and wild-type (+/Y) male Cdkl5 KO mice. Data are expressed as fold difference in comparison to wild-type mice.

Values in (B-E) represent totals for one DG (mean ± SD). $^*p < 0.05$; $^{**}p < 0.01$ (Duncan's test after ANOVA).

This evidence suggests that **the reduced number of new neurons in Cdkl5 KO mice** (see Fig. 24A and Fig. 25C) **is due to an increase in cell death that specifically affects early postmitotic neurons.**

4.8. Loss of Cdkl5 results in reduced net number of granule cells in the dentate gyrus

To establish the impact of the reduction in the number of newly formed granule neurons in Cdkl5 KO mice on overall granule cell number, we stereologically evaluated total granule cell number in mice aged 45 (Fig. 26) and 75 days (data not shown). We found no difference between Cdkl5 KO and wild-type mice in the volume of the granule cell layer (data not shown), but a reduced granule cell density (Fig. 26B) and reduced number of granule cells (Fig. 26C) in Cdkl5 KO mice compared to wild-type littermates. The reduction in cell number was -12% ,–8% and -10%, respectively, in homozygous female (-/-), heterozygous female (+/-) and hemizyogous male (-/Y) Cdkl5 KO mice compared to their wild-type littermates (Fig. 26C).

Consistent with the higher apoptotic cell death in Cdkl5 KO mice estimated by cleaved caspase-3 immunostaining (Fig. 23B), we noted a higher number of pyknotic nuclei in the innermost granule cell layer in the Cdkl5 mutant mice, indicating a larger number of dying cells (Fig. 26A, yellow arrowheads).
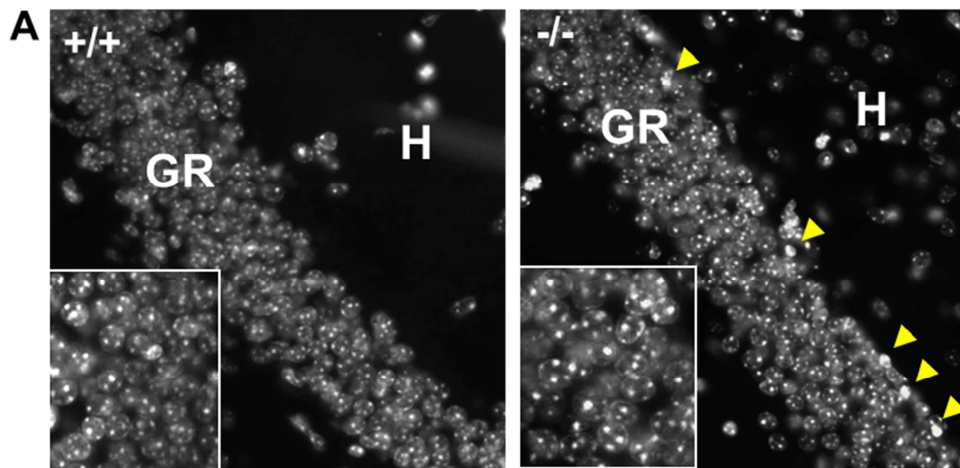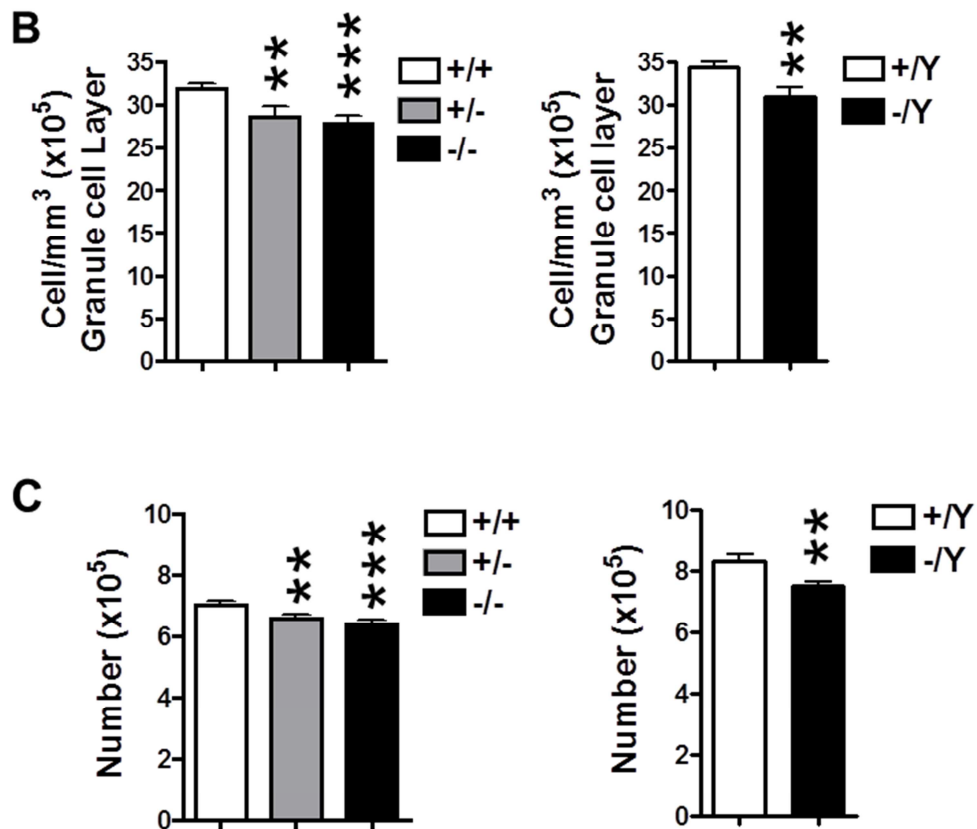
Figure 26 **Net number of granule cells in the dentate gyrus of Cdkl5 knockout mice.**

(A) Examples of sections processed for Hoechst immunostaining from the DG of wild-type (+/+) and homozygous (-/-) female Cdkl5 KO mice.

(B-C) Density of granule cells (B) and total number of granule cells (C) in P45 homozygous (-/-), heterozygous (+/-) and wild-type (+/+) female Cdkl5 KO mice (left histogram) and hemizygous (-/Y) and wild-type (+/Y) male Cdkl5 KO mice (right histogram).

Values refer to one DG (mean ± SD). **p < 0.01; ***p < 0.001 (Duncan's test after ANOVA).

4.9. Loss of Cdkl5 results in reduced dendrite tree and synaptic contacts of newborn granule cells

To establish the effect of loss of Cdkl5 on dendritic development of newborn granule cells, we examined the dendritic morphology of DCX-positive cells. Dendritic morphology of newborn granule cells can be analyzed with immunohistochemistry for DCX, taking advantage of the expression of this protein in the cytoplasm of immature neurons during the period of neurite elongation (from one to four weeks after neuron birth). Fig. 25B clearly shows that in Cdkl5 KO mice DCX-positive immature neurons had fewer processes than in their wild-type counterparts. Quantification of the dendritic size of DCX-positive cells showed that homozygous female (-/-) and hemizygous male (-/Y) Cdkl5 mutant mice had a shorter dendritic length (-44% and -34% respectively; Fig. 27A) and a reduced number of segments (-46% and -36% respectively; Fig. 27B) than wild-type littermates. The decrease in the dendritic length and in the number of segments in heterozygous (+/-) female Cdkl5 KO mice (-41% and -45% respectively; Fig. 27A,B) was very similar to that found in homozygous female (-/-) mutant mice .

To dissect the effects of loss of Cdkl5 on details of the dendritic architecture we examined each dendritic order separately. A striking difference between wild-type and Cdkl5 KO mice was the absence of branches of higher order in the mutant mice. While wild-type (+/+) female mice had up to 9 orders of branches, homozygous (-/-) and heterozygous (+/-) female Cdkl5 KO mice completely lacked branches of orders 7 and 8-9 (Fig. 27C, arrows). Analysis of the branch length of individual orders showed reduced branch length of orders 4-6 in female Cdkl5 KO mice (Fig. 27C). In contrast, analyzing the length of the branches of orders 1-3 we found no difference between wild-type and mutant mice (Fig. 27C). Similar results were also obtained in hemizygous male (-/Y)

Cdkl5 mutant mice compared to wild-type littermates (absence of branches of higher order 8-10 and reduced branch length of order 7 (Fig. 27C). Analysis of the number of branches showed that homozygous (-/-) and heterozygous (+/-) female Cdkl5 KO mice had a similar number of branches of order 1 -4 as wild-type mice, fewer branches of orders 5-6 and, as noted above, no branches of higher orders. In the male mutant mice (-/Y), there was a progressive worsening in branch number from order 5 and no branches of orders 8-10 (Fig. 27D).

Taken together these data indicate that in Cdkl5 KO mice the dendritic tree of the newborn granule cells is hypotrophic and that this effect is mainly due to a reduction in the number of branches of intermediate order and a lack of branches of higher order.
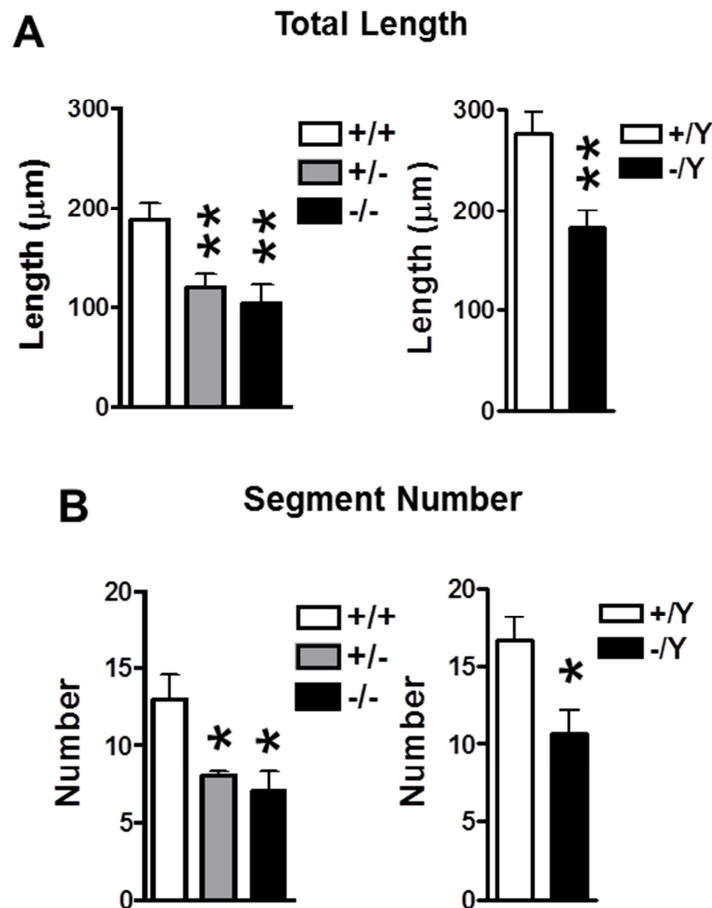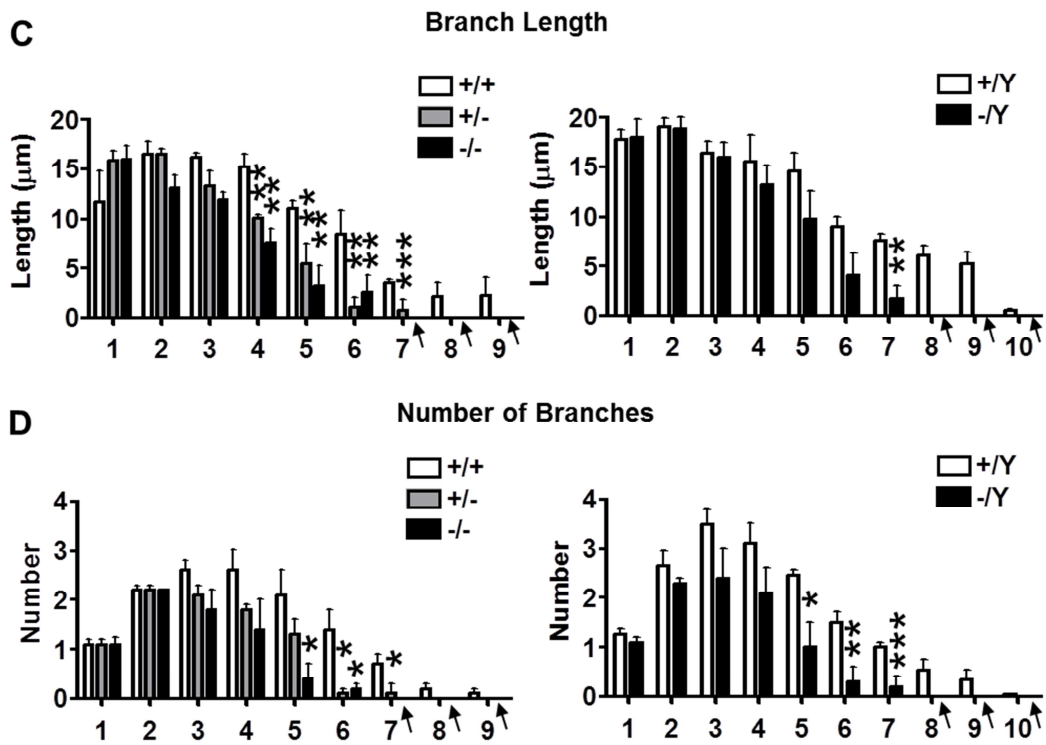
*Figure 27 **Dendritic architecture of newborn granule cells of Cdkl5 knockout mice.***

(A,B) Mean total dendritic length (A) and mean number of dendritic segments (B) in homozygous (-/-), heterozygous (-/+) and wild-type (+/+) female Cdkl5 KO mice (left histogram) and hemizygous (-/Y) and wild-type (+/Y) male Cdkl5 KO mice (right histogram).

(C,D) Quantification of the mean length (C) and mean number (D) of branches of the different orders in animals as in A. The arrows indicate the absence of branches in Cdkl5 KO mice.

Values represent as mean ± SD. *p < 0.05; **p < 0.01; ***p < 0.001 (Duncan's test after ANOVA).

It is likely that a reduction in connectivity is the counterpart of the severe dendritic hypotrophy that characterizes the newborn granule cells of Cdkl5 KO mice. Synaptophysin (SYN; also known as p38) is a synaptic vesicle glycoprotein, that is a specific marker of presynaptic terminals. Quantitative analysis showed that in Cdkl5 KO mice the optical density of SYN was significantly lower than in wild-type littermates in the outer (O), middle (M) and inner (I) molecular layer (Fig. 28A,B), suggesting that **Cdkl5 mutant mice had fewer synaptic contacts in the dentate gyrus**.
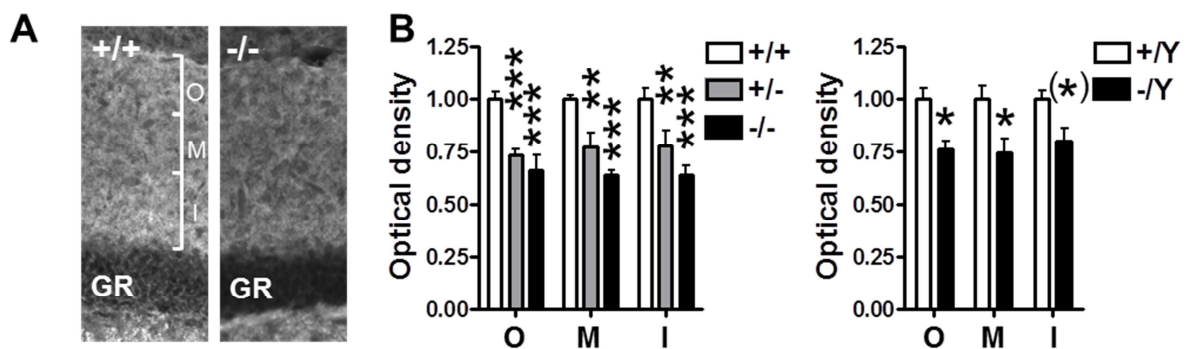
*Figure 28 **Synaptic contacts in the dentate gyrus of Cdkl5 knockout mice.***

(A) Images of sections processed for synaptophysin immunofluorescence from the DG of wild-type (+/+) and homozygous (-/-) female Cdkl5 KO mice. Calibration: 50 μm.

(B) Optical density of synaptophysin immunoreactivity in the inner (I), middle (M) and outer (O) third of the molecular layer of homozygous (-/-), heterozygous (+/-) and wild-type (+/+) female Cdkl5 KO mice (left histogram) and hemizygous (-/Y) male Cdkl5 KO mice and wild-type (+/Y) littermates (right histogram).

Data are given as fold difference vs. inner molecular layer of wild-type mice. Values represent as mean ± SD. *p < 0.05; **p < 0.01; ***p < 0.001 (Duncan's test after ANOVA).

4.10. Loss of Cdkl5 increases proliferation rate and decreases survival of precursor cells in the subventricular zone

Neurogenesis persists in the postnatal and adult brain in two distinct brain regions, the subventricular zone (SVZ) and the hippocampal dentate gyrus (DG).

In order to establish if the increased proliferation of precursor cells shown in the DG of Cdkl5 KO mice (see Fig. 22) was also present in the SVZ we evaluated proliferation in this area by Ki-67 immunohistochemistry on P45 mice. SVZ proliferating precursor cells are located in the lateral wall of the ventricle, at the corner formed by the lateral wall and the dorsal roof of the ventricle and at the lower corner of the ventricle (Fig. 29A). Qualitative observation of images from Cdkl5 KO and wild-type mice clearly showed that Cdkl5 mutant mice had more Ki-67 positive cells (Fig. 29A) compared to wild-type littermates. Quantification of the number of Ki-67 positive cells in the SVZ showed that homozygous female (-/-) and hemizygous male (+/Y) Cdkl5 KO mice had more Ki-67 positive cells (+30% and +20%, respectively; Fig. 29A) vs. wild-type littermates. A less pronounced but significant disparity in the proliferation rate was also found in heterozygous female (+/-) Cdkl5 KO mice (+14%; Fig. 29A).

In order to establish whether the greater proliferation in the SVZ of Cdkl5 KO mice was accompanied by a higher apoptotic cell death, similar to those observed in the DG (see Fig. 23B). we performed immunohistochemistry for cleaved caspase-3 also in this area. We found that Cdkl5 KO mice had more apoptotic cells in this area compared to wild-type littermates (Fig. 29B), similar as those observed in the DG. More caspase-3 positive cells were present in the SVZ of both homozygous female (-/-) and hemizygous male (+/Y) Cdkl5 KO mice (+21%; Fig. 29B) and in heterozygous female (+/-) Cdkl5 KO mice (+15%; Fig. 29B).
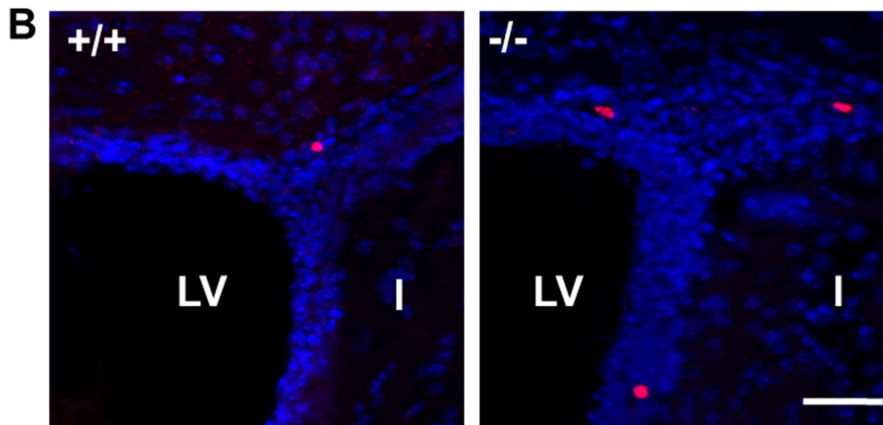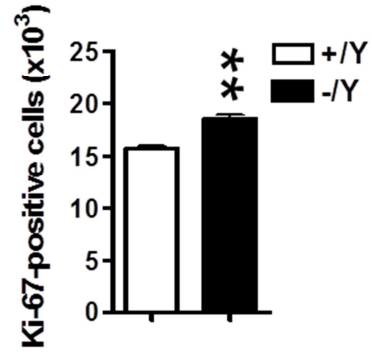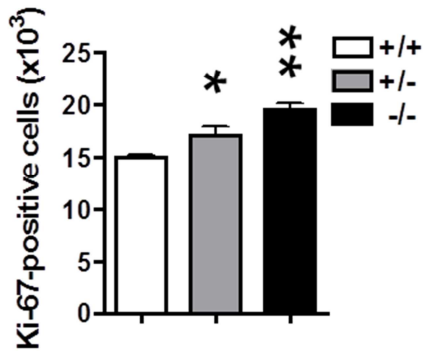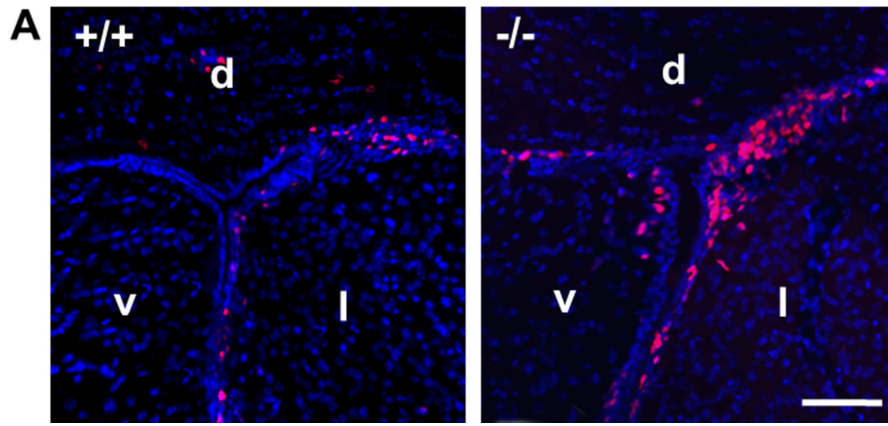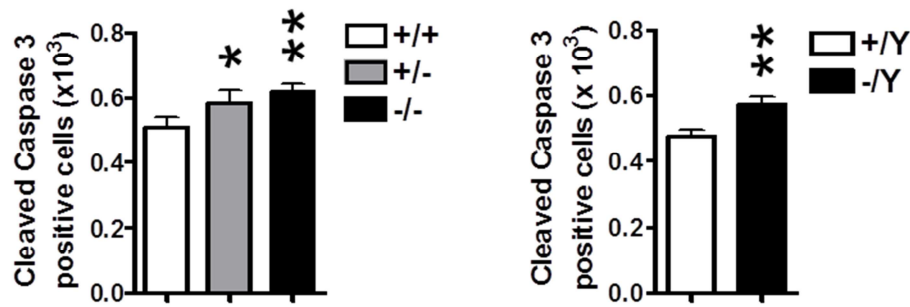
*Figure 29 **Precursor proliferation and survival in the subventricular zone of Cdkl5 knockout mice.***

(A) Examples of sections processed for fluorescent immunostaining for Ki-67 from the SVZ of wild-type (+/+) and homozygous female (-/-) Cdkl5 KO mice aged P45. Calibrations = 200 μm.

Number of Ki-67 positive cells in the SVZ of homozygous (-/-), heterozygous (+/-) and wild-type (+/+) female Cdkl5 KO mice (left histogram) and hemizygous (-/Y) and wild-type (+/Y) male Cdkl5 KO mice (right histogram).

(B) Examples of sections processed for fluorescent immunostaining for cleaved caspase-3 from the SVZ of wild-type (+/+) and homozygous female (-/-) Cdkl5 KO mice aged P45. Calibrations = 200 μm.

Number of cleaved caspase-3 positive cells in the SVZ of animals as in A.

*Values represent totals for one hemisphere (mean ± SD). *p < 0.05; **p < 0.01 (Duncan's test after ANOVA). Abbreviations: d, dorsal; l, lateral; LV, lateral ventricle; m, medial; SVZ, subventricular zone.*

Taken together, our findings of increased proliferation and cell death in the DG and SVZ of Cdkl5 KO mice suggest that these developmental alterations are generalized defects of neuronal precursor cells in Cdkl5 KO mice.

4.11. Alterations in Akt/GSK3-β pathway underlie developmental defects in Cdkl5 knockout mice

Glycogen synthase kinase-3 (GSK3-β) is a ubiquitously active serine/threonine kinase which is inhibited upon phosphorylation at Ser9 by activated protein kinase B (PKB/Akt). Dephosphorylated GSK3-β is a crucial inhibitory regulator of many neuronal functions, including neurite outgrowth, synapse formation, neurogenesis and survival of newly generated neurons (Cole 2012). The Akt/GSK3-β pathway exerts its functions by modulating the activity of a wide range of substrates (Cole 2012). An outline of key elements of this pathway is reported in Fig. 30.
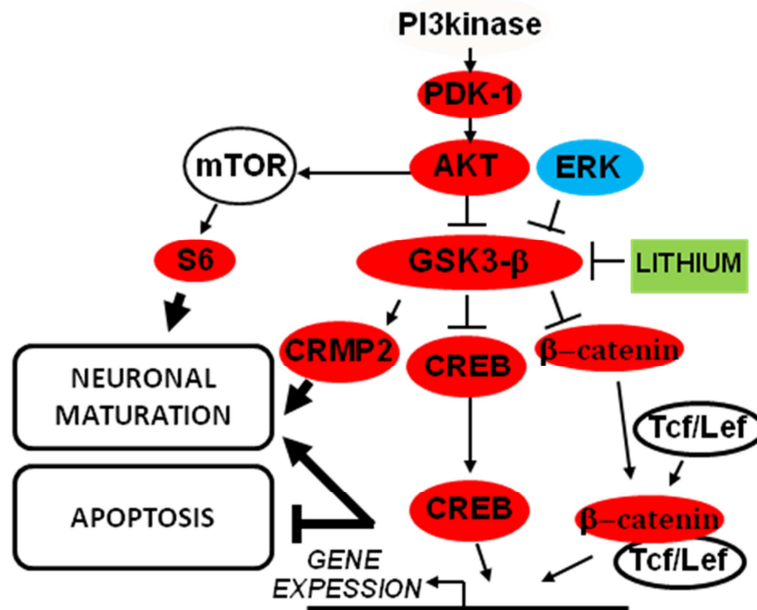
*Figure 30 **Diagram of Akt/GSK3-β signaling cascade**.*

The proteins emphasized in red showed significantly altered phosphorylation or expression whereas proteins emphasized in blue did not show significantly alteration in Cdkl5 KO mice in comparison to wild-type littermates. Lithium, an inhibitor of GSK3-β, is green colored.

In the current study we were interested to establish whether the Akt/GSK3-β pathway is deregulated in Cdkl5 KO mice. In order to address this issue we performed western blot analysis on hippocampal extracts from Cdkl5 KO and wild-type mice aged P19. We found a deregulation in several substrates of this pathway (Fig 30A, 31A,B).

Evaluation of the phosphorylation levels of the Akt/GSK3-β pathway showed lower phosphorylation levels of: i) PDK1 (PDK1 stands at the head of the Akt/GSK-3 β pathway by phosphorylating Akt), ii) Akt, at its two critical residues namely Thr308 and Ser473, iii) GSK3-β at Ser9 (its inhibitory site) and iv) CREB at Ser133 in Cdkl5 KO mice compared to wild-type littermates (Fig. 31A,B). While CREB phosphorylation and consequent DNA binding is inhibited by activated (dephosphorylated) GSK3-β (Grimes and Jope 2001), CRMP2 phosphorylation and activity are positively modulated by GSK3β (Yoshimura et al. 2005). In contrast, GSK3-β controls the amount of β-catenin by negatively regulating β-catenin protein stability (Wada 2009). In line with an increased activity of GSK3-β, we found higher phosphorylation levels of CRMP2 at Thr514 and lower levels of β-catenin (Fig. 31A,B) in Cdkl5 KO mice. No differences were found the phosphorylation levels of ERK (Fig. 31A,B), suggesting a specific alteration of the Akt/GSK3-β pathway in the absence of Cdkl5.
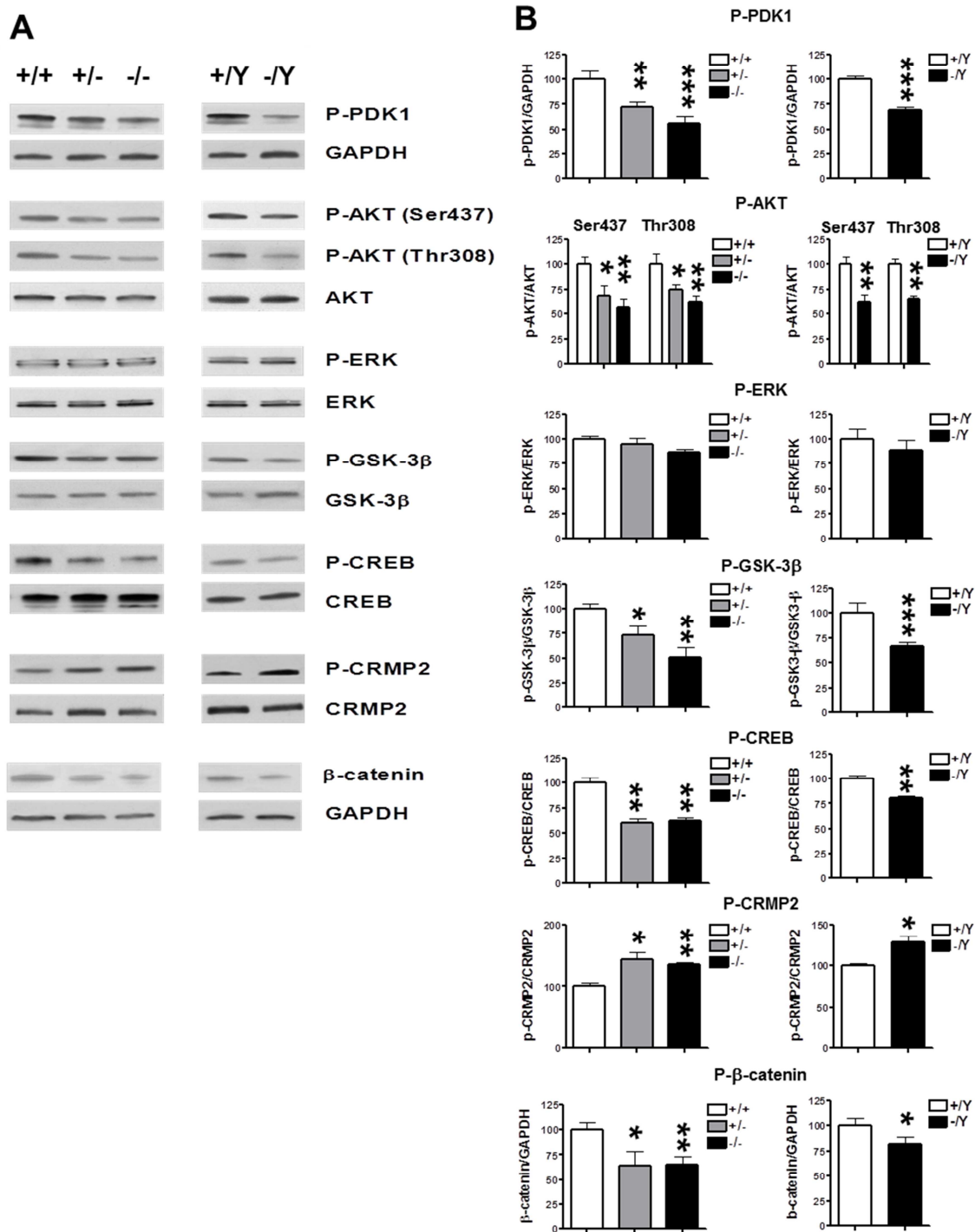
*Figure 31 **Akt/GSK3- β pathway immunoreactivity in the hippocampus of Cdkl5 knockout mice.***

This evidence suggests that alteration of the Akt/GSK3-β pathway may underlie the developmental defects due to loss of Cdkl5.

To clear this issue, we exploited cultures of neuronal precursor cells (NPCs) from Cdkl5 KO mice. We first sought to establish whether cultures of NPCs exhibit the same defects observed *in vivo*. Neurospheres derived from the SVZ of homozygous (-/-) Cdkl5 KO females exhibited a higher proliferation rate vs. the wild-type counterparts (+15%; Fig. 32A). No difference in apoptotic cell death was observed between wild-type and Cdkl5 knockout neurospheres, as estimated by cleaved caspase-3 immunostaining (Fig. 32A) and pyknotic appearance of the nuclei of dying cells (data not shown). This confirms that loss of Cdkl5 does not induce an increase in cell death during the stage of proliferation of NPCs.

To determine the effect of loss of Cdkl5 on cell death in post-mitotic NPCs, we evaluated the number of cleaved caspase-3 positive cells after 1 day in differentiating culture conditions. We found that differentiating NPCs from Cdkl5 KO mice had a notably higher number of caspase-3 positive cells (Fig. 32B), confirming that loss of Cdkl5 is accompanied by an increase in cell death during the stage of differentiation.

Evaluation of the number of new neurons (β-tubulin III-positive cells) and new astrocytes (GFAP-positive cells) after 7 days of differentiation, showed that in differentiated Cdkl5 knockout NPCs the number of neurons was remarkably smaller compared to wild-type NPCs (-82% Fig. 32C), while there was no difference in the number of astrocytes (Fig. 32C). This confirms that loss of Cdkl5 specifically decreases the survival of postmitotic neurons. Assessment of neurite outgrowth in β-tubulin III-positive cells revealed that neurons generated from Cdkl5 knockout NPCs were less differentiated compared to wild-type neurons (-40%; Fig. 32C). These results confirm that post-mitotic NPCs from Cdkl5 KO mice have an intrinsic defect, not only in cell survival, but also in neuronal maturation.

Evaluation of the Akt/GSK3-β pathway activation in cultures of Cdkl5 KO NPCs showed lower levels of phosphorylated Akt and GSK3-β (Fig. 32D).
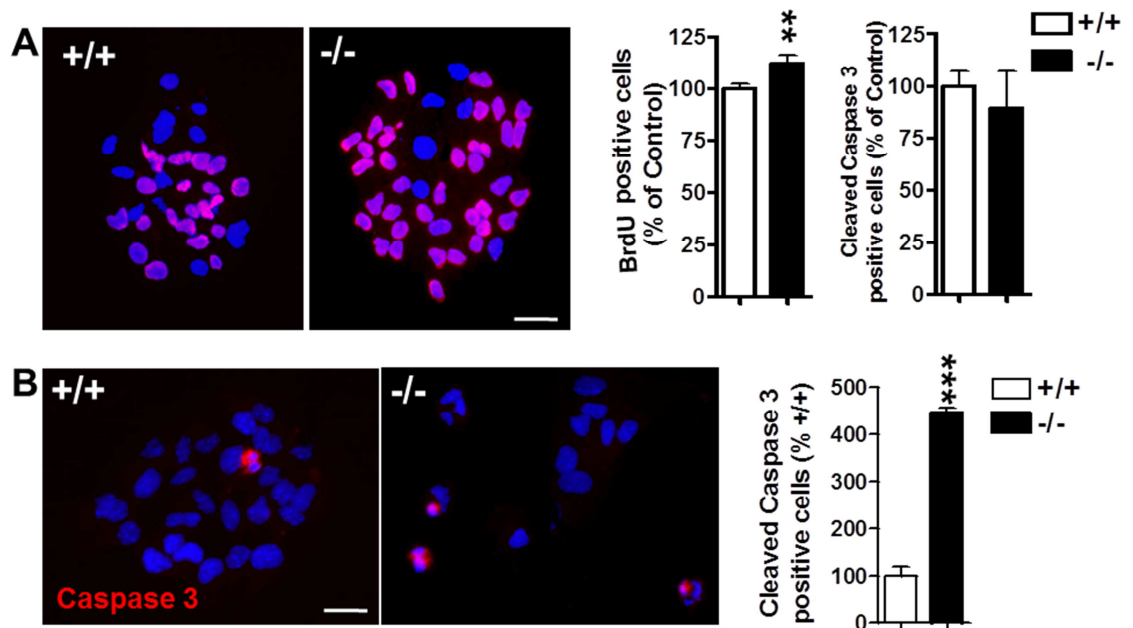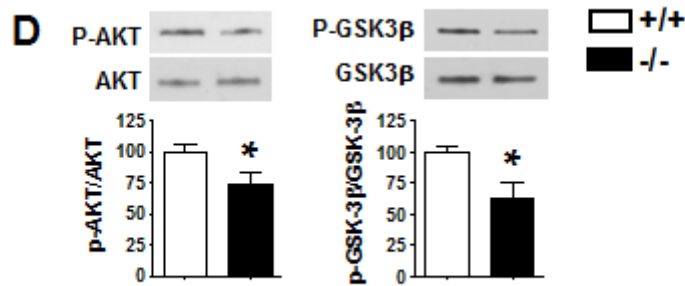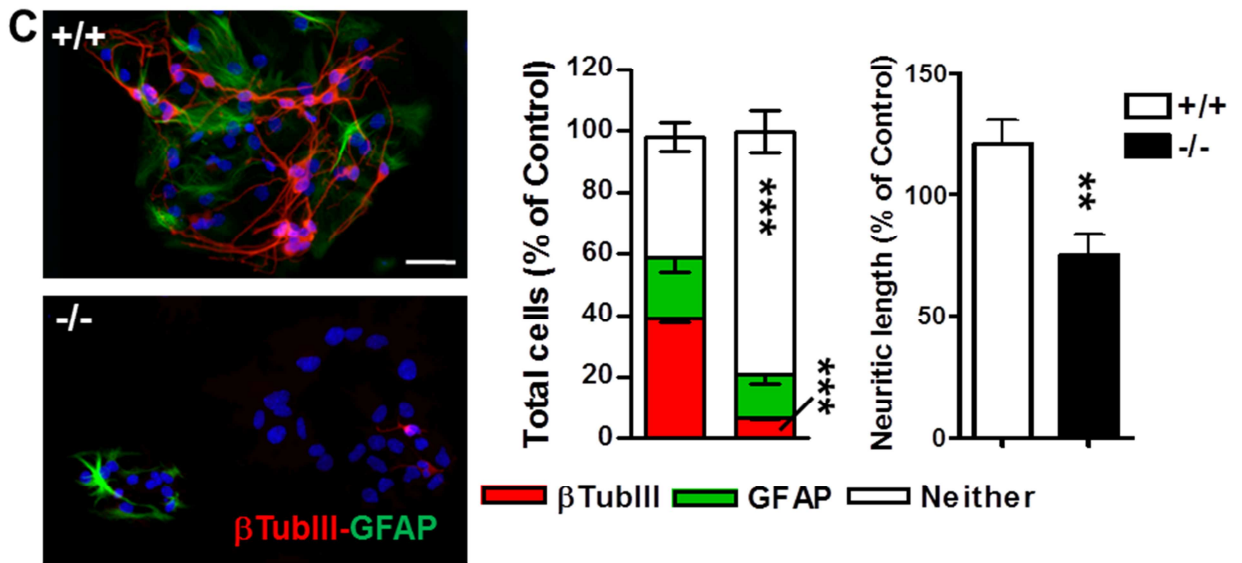
*Figure 32 **NPCs from Cdkl5 knockout mice show similar defects as those observed in vivo.***

(A) Cell proliferation and apoptotic cell death in proliferating neurospheres from wild-type and Cdkl5 KO mice. Images of BrdU-positive cells (red) in neurospheres from female wild-type (+/+) and homozygous (-/-) Cdkl5 KO mice. Cell nuclei were stained using Hoechst dye (blue). Scale bar: 40μm.

Percentage of BrdU-positive cells (left histogram) and cleaved caspase-3-positive cells (right histogram) in neurospheres from female wild-type (+/+) and homozygous (-/-) Cdkl5 KO mice.

(B) Apoptotic cell death in differentiating NPCs from wild-type and and Cdkl5 KO mice. Images of cleaved-caspse-3-positive cells (red) of NPCs from female wild-type (+/+) and homozygous (-/-) Cdkl5 KO mice after 1 day of differentiation. Cell nuclei were stained using Hoechst dye (blue). Scale bar: 20 μm.

Percentage of cleaved caspase-3-positive cells in differentiate NPCs from female wild-type (+/+) and homozygous (-/-) Cdkl5 KO mice.

(C) Phenotype and neuronal morphology of differentiated NPCs from wild-type and Cdkl5 KO mice. Representative double-fluorescence images of NPCs from female wild-type (+/+) and homozygous (-/-) Cdkl5 KO mice after 6 days of differentiation. Cells with neuronal phenotype are immunopositive for β-tubulin III (red) and cells with astrocytic phenotype are immunopositive for GFAP (green). Cell nuclei were stained using Hoechst dye (blue).

Stacked column charts represent the percentages of β-tubulin III-positive cells, GFAP-positive cells and cells with undetermined phenotype (Neither) of the total cell population after 6 days of in vitro differentiation.

Quantification of neurite outgrowth of differentiated neurons in female wild-type (+/+) and homozygous (-/-) Cdkl5 KO mice.

(D) Western blot quantification of P-Akt (Ser437) and P-GSK3-β (Ser9) expression, normalized to respective total protein levels in differentiated NPCs from wild-type and Cdkl5 KO mice. Data are given as fold difference vs. wild-type mice.

Values in (A-D) represent in mean ± SD. *p < 0.05; **p < 0.01; ***p < 0.001 (two-tailed t-test).

In order to obtain evidence that the neurodevelopmental defects observed in Cdkl5 KO mice and Cdkl5 knockout NPCs were due to loss of Cdkl5, we re-expressed Cdkl5 in cultures of NPCs. We found that adenvirus-mediated expression of Cdkl5 in NPCs from Cdkl5 KO mice (Fig. 33B) restored cell proliferation (Fig. 33A), neuronal survival and maturation (Fig. 33C,D). Importantly, we also found a parallel restoration of the phosphorylation levels of Akt and GSK3-β (Fig. 33E), confirming the hypothesized link between CDKL5 and the Akt/GSK3-β pathway.

We next treated Cdkl5 knockout NPCs with lithium, a well-known inhibitor of GSK3-β activity (Fig. 30). We found that, in NPCs from Cdkl5 KO mice, the lithium-induced increase in the GSK3-β phosphorylation (Fig. 33E) was accompanied by complete restoration of neuronal survival, number of new neurons and neuronal maturation (Fig. 33C,D).
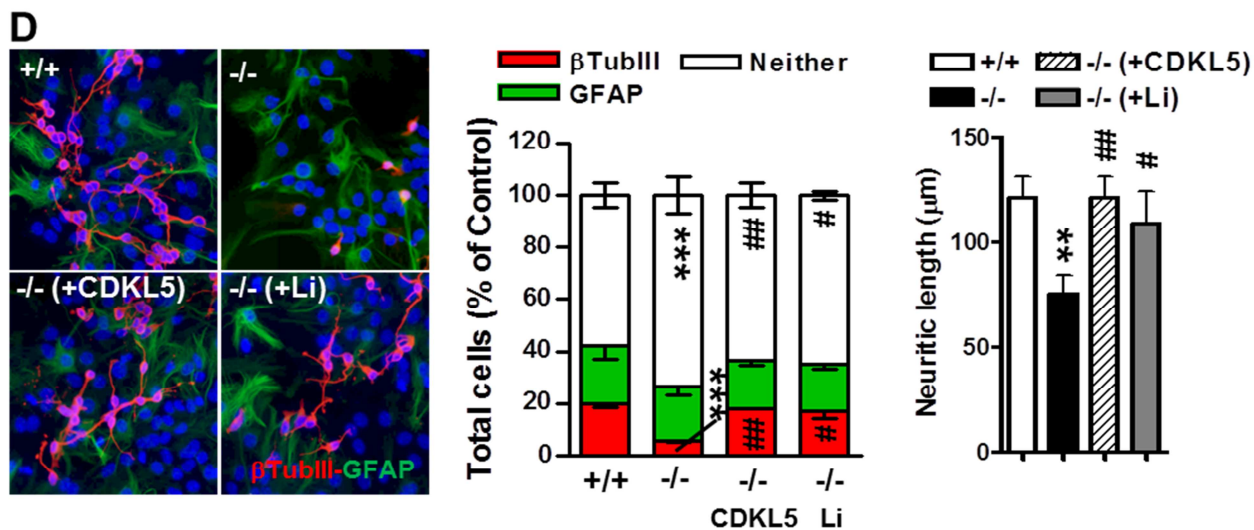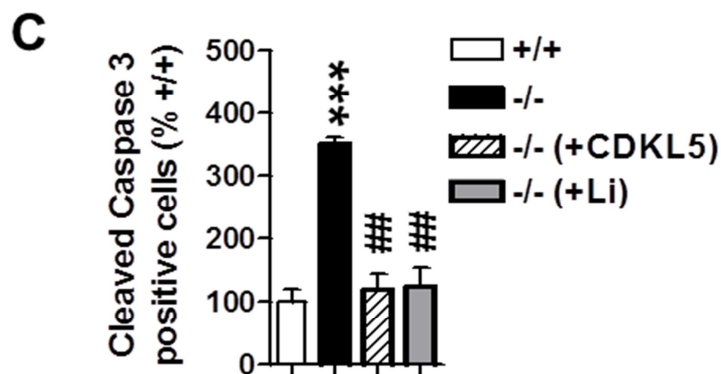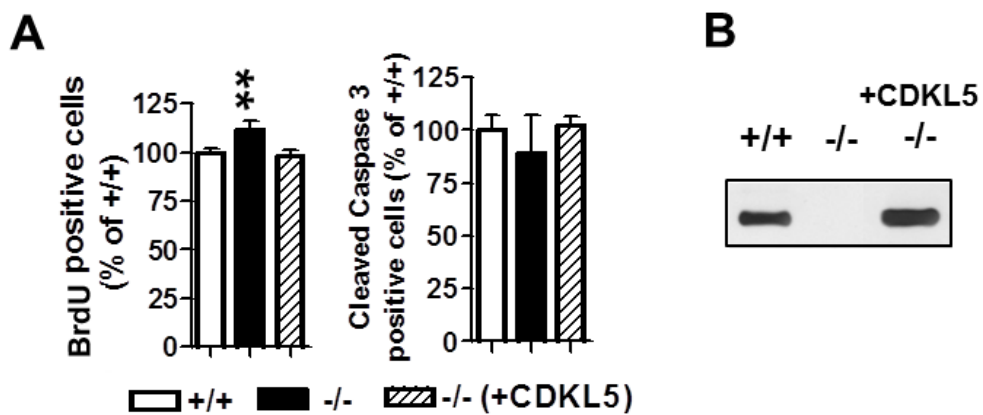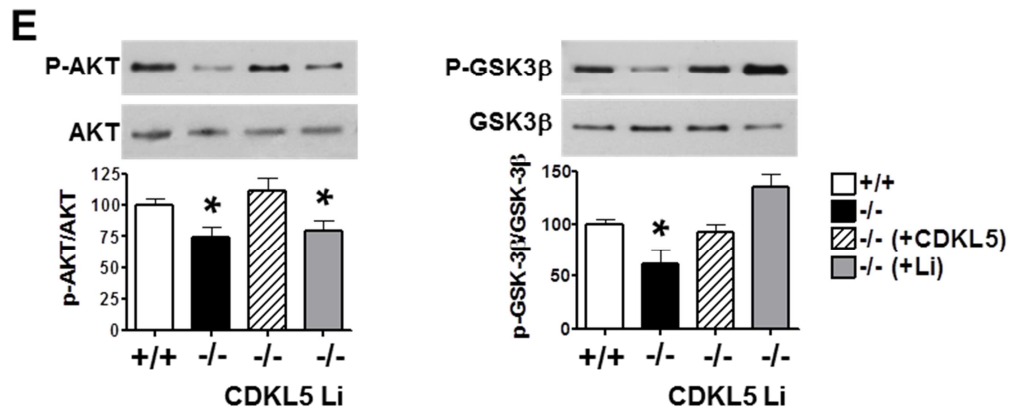
*Figure 33 **Akt/GSK3- β pathway immunoreactivity in NPCs from Cdkl5 knockout mice.***

(A) Percentage of BrdU-positive cells (left histogram) and cleaved caspase-3 positive cells (right histogram) from untreated female wild-type (+/+) and homozygous (-/-) Cdkl5 KO mice and in neurospheres from homozygous (-/-) Cdkl5 KO mice infected with CDKL5 adenovirus particles (MOI: 100) for 72 h starting from DIV1.

(B) Representative example of a western blot showing Cdkl5 expression in neurospheres as in (A).

(C) Percentage of cleaved caspase-3 positive cells from differentiating NPCs from female wild-type (+/+) and homozygous (-/-) Cdkl5 KO mice. Cdkl5 knockout NPCs (-/-) were infected with CDKL5 adenovirus particles (MOI: 100) or treated with Lithium (4 mM) throughout the entire differentiation period.

(D) Representative double-fluorescence images of NPCs as in (C) after 6 days of differentiation. Cells with neuronal phenotype are immunopositive for β-tubulin III (red) and cells with astrocytic phenotype are immunopositive for GFAP (green). Cell nuclei were stained using Hoechst dye (blue). NPC cultures were treated as in (C).

Stacked column charts represent the percentages of β-tubulin III-positive cells, GFAP-positive cells and cells with undetermined phenotype (Neither) of the total cell population after 6 days of in vitro differentiation.

Quantification of neurite outgrowth of differentiated neurons in female wild-type (+/+) and homozygous (-/-) Cdkl5 KO mice treated as in (C).

(E) Western blot quantification of P-Akt (Ser437) and P-GSK3-β (Ser9) expression normalized to respective total protein levels in differentiated NPCs from wild-type and Cdkl5 KO mice treated as in (C). Data are given as fold difference vs. wild-type mice.

Values represent mean ± SE. *p < 0.05; **p < 0.01; ***p<0.001 as compared to the wild-type condition; #P<0.05, ##P<0.01 as compared to untreated Cdkl5 KO samples (Duncan's test after ANOVA).

These data suggest that alteration of the Akt/GSK3-β signaling, due to loss of CDKL5 expression, may be responsible for the developmental alterations observed in Cdkl5 KO mice.

5. DISCUSSION

In the last few years CDKL5 has been associated with early-onset epileptic encephalopathies characterized by the manifestation of intractable epileptic seizures within the first weeks of life, severe developmental delay and RTT-like features. The association of CDKL5 and neurodevelopmental disorders and its high expression levels in the maturing brain (Rusconi et al. 2008; Chen et al. 2010) underscore the important of this kinase for proper brain development. In spite of the clear importance of CDKL5 for the central nervous system, the biological functions of this kinase were largely unknown.

Here we show for the first time that CDKL5 affects both proliferation and differentiation of neural cells. In particular in this study, using of a newly created Cdkl5 KO mouse model, we report the role of Cdkl5 during postnatal neurogenesis. Precursor cell proliferation and survival are two forces that control the generation of the correct neuron number. Lack of Cdkl5 leads to increased proliferation of neuronal precursor cells. The final neuronal output, however, was reduced due to the greater apoptosis of post-mitotic cells. Moreover, lack of Cdkl5 led to decreased neuronal maturation.

Our hypothesis from these results is that CDKL5 is a critical factor controlling the balance between progenitor self-renewal, survival and maturation during postnatal neurogenesis.

5.1. CDKL5 induces differentiation and inhibits proliferation of the SH-SY5Y neuroblastoma cell line

To establish the role of CDKL5 on neuronal maturation, we used human neuroblastoma cell lines as a neuronal model system. We first provide evidence that in the SH-SY5Y neuroblastoma cell line there is a direct correlation between neurite elongation and CDKL5 expression. This evidence is consistent with recent studies showing that Cdkl5 regulates neurite growth and dendritic arborization of cortical rat neurons (Chen et al. 2010) and strengthen the role of CDKL5 during development as a pro-differentiating gene.

Neuronal differentiation and proliferation are two closely linked processes during brain development. Neuronal differentiation requires the progenitor cells to exit the cell cycle and the processes of proliferation and differentiation intersect at the regulation of cell cycle regulatory proteins. Proliferation promotes positive regulation of cell cycle proteins (e.g. cyclins and cyclin-dependent kinases (Cdk)), whereas differentiation results in inhibition of these cell cycle proteins (Ohnuma et al. 2001). We found that in the SH-SY5Y cell line induction of CDKL5 expression caused a strong inhibition of cell proliferation with no increase in apoptotic cell death. Inhibition of cell proliferation was due to a block of cell cycle progression in the $G_0/_1$ phase, supporting the view that CDKL5 can function as an anti-proliferative gene.

Our findings show that CDKL5 affects both neurite growth and cell proliferation, suggesting that CDKL5 may not only modulate dendritic maturation, as shown by Chen et al. (Chen et al. 2010), but also cell proliferation in the developing brain and underline the important role of CDKL5 during correct brain development. The fact that CDKL5 plays a role in the control both of neuronal proliferation and differentiation is consistent with the appearance of neurological symptoms during the early period of brain maturation in patients with mutations of *CDKL5*.

5.2. Cdkl5 knockout mice recapitulate several core features of the CDKL5 disorder

Behavioral characterizations of constitutive **Cdkl5 KO mice** show that they recapitulate several features that mimic the clinical features described in CDKL5 patients and **are a useful tool to investigate phenotypic and functional aspects of Cdkl5 loss.** In particular Cdkl5 KO mice showed hind-limb clasping and hypoactivity, features that may model the stereotypic hand movements and hypotonia, respectively, reported in the human condition.

Although early-onset seizures are a key feature of CDKL5 disorder, we failed to detect any spontaneous seizure or epileptiform EEG activity under baseline conditions in Cdkl5 mutant mice. Moreover, following pharmacological induction of seizures with kainic acid no evidence emerged for increased susceptibility for seizures or epileptiform activity in Cdkl5 KO mice, although we found an increased duration and reduced frequency of epileptiform events as well as reduced EEG power in response to the high dose of kainic acid. These results are in line with those observed by Wang and colleagues in a different Cdkl5 KO mouse model recently created (Wang et al. 2012). Wang et al. describe several behavioral abnormalities including autistic-like behavior deficits, such as impaired motor control and decreased anxiety in their Cdkl5 KO mouse model, but also in this mouse model spontaneous seizure or epileptiform activity are absent (Wang et al. 2012). At the moment it remains unclear whether the lack of spontaneous seizures observed in both Cdkl5 KO mice is the result of differences in the function of the mouse and human protein, in its interactors, or the presence of genetic modifiers.

We found that **loss of Cdkl5 results in impaired hippocampus-dependent learning and memory**, consistently with the cognitive deficits that characterize CDKL5 patients. Memory loss and subsequent cognitive impairment might occur through diminished neurogenic capacity within the principal brain

areas involved in memory and learning, such as the hippocampus. Results from several laboratories suggest that postnatal hippocampal neurogenesis is functional and participates in learning and memory consolidation (van Praag et al. 2002). In mammals, increased neurogenesis is mediated by environmental factors such as exercise (van Praag et al. 2005) or stimuli-enriched environments (Tashiro et al. 2007) that concomitantly improve learning and memory capacities. In the adult human hippocampus, both structural and functional changes have been demonstrated in individuals exposed to intensive spatial learning (Maguire et al. 1997). Inhibition of neurogenesis is known to impair learning and memory (Shors et al. 2001) and increased neurogenesis improves LTP of synaptic transmission (van Praag et al. 1999).

Our finding that loss of Cdkl5 impaired hippocampal neurogenesis could underlie hippocampal-dependent memory performance alterations that characterized Cdkl5 mutant mice.

5.3. Cdkl5 has an important role in postnatal development of the hippocampal dentate gyrus

In rodents, the hippocampal dentate gyrus produces its neurons mainly postnatally (Altman and Bayer 1990) and this makes the hippocampus an ideal structure in order to examine the role of CDKL5 on fundamental neurodevelopmental processes such as neurogenesis and dendritic development. Adult hippocampal neurogenesis is a constitutive but highly regulated process that occurs in a neurogenic niche, the subgranular zone (SGZ) of the dentate gyrus (DG). Type 1 neural stem cells (NSCs), characterized by nestin and Sox2/BLBP expression, exhibit morphology typical of radial glia and divide asymmetrically to self-renew and give rise to daughter cells, termed intermediate progenitor cells (IPCs), a type of transit amplifying cell (Kempermann et al. 2004). Undifferentiated IPCs (type 2a and type 2b) divide rapidly to produce neuronal

committed IPCs (type 3) and are responsive to stimuli that affect neuron production in the DG (Encinas et al. 2006). Type 3 IPCs generate immature neurons that within 1 month during which network connections are established and the selection for long-term survival occurs, integrate into the granule layer (GR) as mature granule cells (Kempermann et al. 2004) (see Fig.14 introduction, see Fig 25A results). The majority of these immature neurons are subject to a selection process, during which they are either recruited into function or eliminated (Biebl et al. 2000).

We demonstrated here that Cdkl5 knockdown leads to an increase in proliferation of IPCs of the DG. This result is in line with the anti-proliferative role observed also in human neuroblastoma cell line and support the view that CDKL5 can function as an inhibitor of progenitor cell proliferation.

Interestingly we report an increased number of dead cells in the Cdkl5 deleted DG. Using double-labeling with apoptotic marker and immature neuronal marker we found that Cdkl5 expression specifically influence immature granule cells survival. These findings suggest that CDKL5 may be required for postmitotic neuron survival, and may elucidate the role of the higher expression of CDKL5 in postmitotic/differentiating neurons seen *in vitro*.

Based on these results, we assume that **CDKL5 might influence exit of the cell cycle of IPCs and survival of post-mitotic neurons by prompting immature neurons to differentiate and recruiting into function neurons**. Consistently with increased cell death of post-mitotic granular neurons, Cdkl5 KO mice were characterized by hypocellularity in the dentate gyrus.

Phenotypic analysis of the BrdU-labeled cell population in the dentate gyrus at 4 weeks after labeling revealed that loss Cdkl5 did not affect astogliogenesis. It is reasonable to suppose **that loss of Cdkl5 suppresses**

neuronal but not glial survival/differentiation. This is in agreement with the predominant expression of CDKL5 in neurons (Rusconi et al. 2008).

Dendritic arborization is significantly reduced in cortical pyramidal neurons from both RTT patients (Armstrong et al. 1999; Belichenko et al. 2008; Belichenko et al. 2009) as well as Mecp2 KO mice (Kishi and Macklis 2005; Stuss et al. 2012). Actually it is not known if similar deficits exist also in the brains of subjects carrying *CDKL5* mutations. In order to establish the effect of loss of Cdkl5 on dendritic development of newborn granule cells, we examined the dendritic morphology of immunohistochemistry for DCX and found that Cdkl5 KO mice show a significant reduces in dendritic length. Our detailed analysis of the dendritic arborization of new generated granule neurons of Cdkl5 KO mice clearly shows that dendritic complexity was significantly reduced, mainly due to absence of dendritic arbors of higher order. Dendritic pathology is also a possible substrate for cognitive disability in different conditions. In RTT, the pathogenesis of dendritic abnormalities is distinctive and appears to correlate with the cognitive profile. Likewise individuals with CDKL5 disorder show impairment in long-term memory, a function that requires the participation of the hippocampal region. It would be reasonable to hypothesize that **the hypocellularity and the dendritic hypotrophy observed in hippocampal dentate gyrus of the Cdkl5 KO mice could lead to memory loss and thereby to cognitive impairment, in CDKL5-related disease patients.**

Most CDKL5 patients are females who are heterozygous for CDKL5 deficiency due to random X-chromosome inactivation (XCI). Mammalian female cells randomly inactivate one of the two X chromosomes in somatic cells, and the genes on the inactive X chromosome (with a few exceptions) are not expressed. XCI occurs before the completion of gastrulation during early embryonic development and is believed to be irreversible (Plath et al. 2002). Skewed XCI can occur when there is preferential inactivation of the maternal or paternal X chromosome and has been linked to both autism (Talebizadeh et al. 2005) and X-

chromosome-linked mental retardation (Plenge et al. 2002). Thus, to understand the etiology of CDKL5-linked disease, determining the characteristics of the heterozygous female Cdkl5 KO mice that reproduce the human CDKL5 deficiency is critical. We found that loss of Cdkl5 in heterozygous female mice elicited decreased survival and aberrant dendritic phenotype of newly generated granule cells rather similar to homozygous female mice, suggesting that even mosaic depletion of Cdkl5 in 50% of the cells in the brain is sufficient to affect neuronal survival/differentiation in a more global manner.
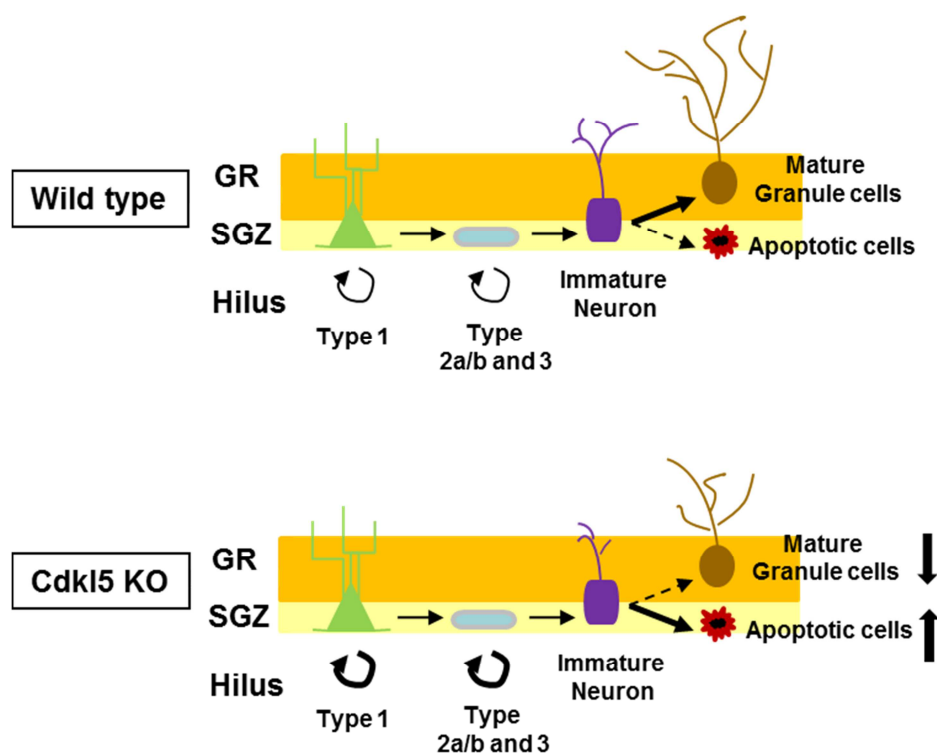
Figure 34 **Hypothetical model of CDKL5 function in postnatal hippocampus development.**

Top: In normal dentate gyrus (DG) primary progenitor cells (type 1) and intermediate progenitor cells (IPCs, type 2a/b and type 3 cells) keep proliferating, maintaining normal progenitor pool. During postmitotic and neuronal differentiation stage, some immature neurons are destined to die, while neurons mature to integrate into a functional neural circuit survived.

Bottom: Inactivation of Cdkl5 leads to a hypocellularity and dendritic hypotrophy of granule cells in hippocampal dentate gyrus (DG). The

numbers of Type 1 and IPCs in theDG were increased, due to the increased proliferation rate of these cells. The final neuronal output, however, was reduced, due to increase apoptosis of immature neurons, probably due to a reduce dendrite development and complexity.

5.4. Cdkl5 acts as a pro-survival and pro–differentiative gene by modulating Akt/GSK3-β signaling

In order to identify a molecular pathway that could underlie the defective neurogenesis in Cdkl5 KO mice, we analyzed the Akt/GSK3-β signaling. Glycogen synthase kinase-3 (GSK3-β) is a ubiquitously active serine/threonine kinase which is inhibited upon phosphorylation at Ser9 by activated protein kinase B (PKB/Akt). Dephosphorylated GSK3-β is a crucial inhibitory regulator of many neuronal functions, including neurite outgrowth, synapse formation, neurogenesis and survival of newly generated neurons (Cole 2012). We found a deregulation in several substrates of the Akt/GSK3-β pathway in Cdkl5 KO mice, suggesting a specific alteration of the Akt/GSK3-β pathway in the absence of Cdkl5 that may underlie the developmental defects observed.

Akt/GSK3-β signaling regulates diverse developmental events in the brain, including neurogenesis, survival and differentiation. Several studies suggest that Akt/GSK3-β signalling plays a role in the death/survival of neural precursors or immature neurons. For example, the activation of GSK3-β promotes apoptotic signaling in cultured neural precursor cells (NPCs) derived from embryonic mouse brains (Eom et al. 2007). GSK3-β also regulates the maturation and neurite outgrowth in neurons. Neuronal overexpression of a constitutively active GSK3-β causes a delayed postnatal maturation and differentiation of neurons in the mouse brain (Spittaels et al. 2000; Spittaels et al. 2002).

The results presented in this study suggest that loss of Cdkl5 impairs neural precursor survival and maturation within the DG of the hippocampus,

probably by disrupting the Akt/GSK3-β signaling pathway of neuroblasts. Given that Akt/GSK3-β signaling is a known regulator of cell proliferation, survival, and neural differentiation (Luo 2012), one consequence of reduced Akt/GSK3-β activity in the absence of Cdkl5 is the disruption of neuronal development. We found that re-expression of CDKL5 in NPCs from Cdkl5 KO mice recovers Akt/GSK3-β signaling in parallel to NPCs proliferation/survival and differentiation. Similarly, lithium treatments that increase the inhibitory phosphorylation of GSK3-β, leading to GSK3-β suppression, result in a fully recover of neuronal precursor survival and maturation. **These results support the view that CDKL5 can function as a pro-survival and -differentiative gene by modulating the Akt/GSK3-β signaling.**

Although these signaling changes may be indirect effects of Cdkl5 loss-of-function, these data suggest that CDKL5 plays a critical role in coordinating multiple signaling cascades downstream to Akt. Together, these data suggest a mechanism by which CDKL5 regulates Akt mediated cellular development, thus implicating the Akt pathways as a potential therapeutic target for treatment of patients with CDKL5-related disorders.

6.CONCLUSIONS

Taken together, our data suggest that CDKL5 modulates the intricate balance between precursor proliferation, survival and differentiation by contributing to the proper execution of differentiation program. A possible mechanism of action of CDKL5 on postnatal development in the DG is illustrated (Fig. 34). We suggest that loss of Cdkl5 impairs neurogenic capacity within the hippocampal DG, disrupting the Akt/GSK3-β signaling pathway of neuroblasts. Since it has been proposed that these regions are involved in memory retrieval (Moser and Moser 1998; Greicius et al. 2003), it would be reasonable to hypothesize that the mechanisms described could lead to memory loss and thereby to cognitive impairment, in CDKL5-related disease patients.

7.REFERENCES

Adler D. A., Quaderi N. A., Brown S. D., Chapman V. M., Moore J., Tate P. and Disteche C. M. (1995) The X-linked methylated DNA binding protein, Mecp2, is subject to X inactivation in the mouse. Mammalian genome : official journal of the International Mammalian Genome Society 6, 491-492.

Altman J. and Bayer S. A. (1990) Prolonged sojourn of developing pyramidal cells in the intermediate zone of the hippocampus and their settling in the stratum pyramidale. The Journal of comparative neurology 301, 343-364.

Alvarez-Buylla A. (1997) Mechanism of migration of olfactory bulb interneurons. Seminars in cell & developmental biology 8, 207-213.

Amir R. E., Van den Veyver I. B., Wan M., Tran C. Q., Francke U. and Zoghbi H. Y. (1999) Rett syndrome is caused by mutations in X-linked MECP2, encoding methyl-CpG-binding protein 2. Nature genetics 23, 185-188.

Ariani F., Hayek G., Rondinella D., Artuso R., Mencarelli M. A., Spanhol-Rosseto A., Pollazzon M., Buoni S., Spiga O., Ricciardi S., Meloni I., Longo I., Mari F., Broccoli V., Zappella M. and Renieri A. (2008) FOXG1 is responsible for the congenital variant of Rett syndrome. American journal of human genetics 83, 89-93.

Armstrong D., Dunn J. K., Antalffy B. and Trivedi R. (1995) Selective dendritic alterations in the cortex of Rett syndrome. Journal of neuropathology and experimental neurology 54, 195-201.

Armstrong D. D. (2002) Neuropathology of Rett syndrome. Mental retardation and developmental disabilities research reviews 8, 72-76.

Armstrong D. D. (2005) Neuropathology of Rett syndrome. Journal of child neurology 20, 747-753.

Armstrong D. D., Dunn J. K., Schultz R. J., Herbert D. A., Glaze D. G. and Motil K. J. (1999) Organ growth in Rett syndrome: a postmortem examination analysis. Pediatr Neurol 20, 125-129.

Asaka Y., Jugloff D. G., Zhang L., Eubanks J. H. and Fitzsimonds R. M. (2006) Hippocampal synaptic plasticity is impaired in the Mecp2-null mouse model of Rett syndrome. Neurobiology of disease 21, 217-227.

Bahi-Buisson N., Villeneuve N., Caietta E., Jacquette A., Maurey H., Matthijs G., Van Esch H., Delahaye A., Moncla A., Milh M., Zufferey F., Diebold B. and Bienvenu T. (2012) Recurrent mutations in the CDKL5 gene: genotype-phenotype relationships. Am J Med Genet A 158A, 1612-1619.

Bahi-Buisson N., Nectoux J., Rosas-Vargas H., Milh M., Boddaert N., Girard B., Cances C., Ville D., Afenjar A., Rio M., Heron D., N'Guyen Morel M. A., Arzimanoglou A., Philippe C., Jonveaux P., Chelly J. and Bienvenu T. (2008) Key clinical features to identify girls with CDKL5 mutations. Brain 131, 2647-2661.

Belichenko N. P., Belichenko P. V. and Mobley W. C. (2009) Evidence for both neuronal cell autonomous and nonautonomous effects of methyl-CpG-binding

protein 2 in the cerebral cortex of female mice with Mecp2 mutation. Neurobiology of disease 34, 71-77.

Belichenko N. P., Belichenko P. V., Li H. H., Mobley W. C. and Francke U. (2008) Comparative study of brain morphology in Mecp2 mutant mouse models of Rett syndrome. The Journal of comparative neurology 508, 184-195.

Belichenko P. V., Kleschevnikov A. M., Salehi A., Epstein C. J. and Mobley W. C. (2007) Synaptic and cognitive abnormalities in mouse models of Down syndrome: exploring genotype-phenotype relationships. The Journal of comparative neurology 504, 329-345.

Belichenko P. V., Masliah E., Kleschevnikov A. M., Villar A. J., Epstein C. J., Salehi A. and Mobley W. C. (2004) Synaptic structural abnormalities in the Ts65Dn mouse model of Down Syndrome. The Journal of comparative neurology 480, 281-298.

Bertani I., Rusconi L., Bolognese F., Forlani G., Conca B., De Monte L., Badaracco G., Landsberger N. and Kilstrup-Nielsen C. (2006) Functional consequences of mutations in CDKL5, an X-linked gene involved in infantile spasms and mental retardation. The Journal of biological chemistry 281, 32048-32056.

Bianchi P., Ciani E., Guidi S., Trazzi S., Felice D., Grossi G., Fernandez M., Giuliani A., Calza L. and Bartesaghi R. (2010) Early pharmacotherapy restores neurogenesis and cognitive performance in the Ts65Dn mouse model for Down syndrome. The Journal of neuroscience : the official journal of the Society for Neuroscience 30, 8769-8779.

Biebl M., Cooper C. M., Winkler J. and Kuhn H. G. (2000) Analysis of neurogenesis and programmed cell death reveals a self-renewing capacity in the adult rat brain. Neuroscience letters 291, 17-20.

Bienvenu T. and Chelly J. (2006) Molecular genetics of Rett syndrome: when DNA methylation goes unrecognized. Nature reviews. Genetics 7, 415-426.

Borg I., Freude K., Kubart S., Hoffmann K., Menzel C., Laccone F., Firth H., Ferguson-Smith M. A., Tommerup N., Ropers H. H., Sargan D. and Kalscheuer V. M. (2005) Disruption of Netrin G1 by a balanced chromosome translocation in a girl with Rett syndrome. European journal of human genetics : EJHG 13, 921-927.

Brankack J., Kukushka V. I., Vyssotski A. L. and Draguhn A. (2010) EEG gamma frequency and sleep-wake scoring in mice: comparing two types of supervised classifiers. Brain research 1322, 59-71.

Brazel C. Y., Romanko M. J., Rothstein R. P. and Levison S. W. (2003) Roles of the mammalian subventricular zone in brain development. Progress in neurobiology 69, 49-69.

Buschdorf J. P. and Stratling W. H. (2004) A WW domain binding region in methyl-CpG-binding protein MeCP2: impact on Rett syndrome. Journal of molecular medicine 82, 135-143.

Cameron H. A. and McKay R. D. (2001) Adult neurogenesis produces a large pool of new granule cells in the dentate gyrus. The Journal of comparative neurology 435, 406-417.

Carouge D., Host L., Aunis D., Zwiller J. and Anglard P. (2010) CDKL5 is a brain MeCP2 target gene regulated by DNA methylation. Neurobiology of disease 38, 414-424.

Casanova M. F., Buxhoeveden D., Switala A. and Roy E. (2003) Rett syndrome as a minicolumnopathy. Clinical neuropathology 22, 163-168.

Chandler S. P., Guschin D., Landsberger N. and Wolffe A. P. (1999) The methyl-CpG binding transcriptional repressor MeCP2 stably associates with nucleosomal DNA. Biochemistry 38, 7008-7018.

Chao H. T., Zoghbi H. Y. and Rosenmund C. (2007) MeCP2 controls excitatory synaptic strength by regulating glutamatergic synapse number. Neuron 56, 58-65.

Chapleau C. A., Calfa G. D., Lane M. C., Albertson A. J., Larimore J. L., Kudo S., Armstrong D. L., Percy A. K. and Pozzo-Miller L. (2009) Dendritic spine pathologies in hippocampal pyramidal neurons from Rett syndrome brain and after expression of Rett-associated MECP2 mutations. Neurobiology of disease 35, 219-233.

Charman T., Neilson T. C., Mash V., Archer H., Gardiner M. T., Knudsen G. P., McDonnell A., Perry J., Whatley S. D., Bunyan D. J., Ravn K., Mount R. H., Hastings R. P., Hulten M., Orstavik K. H., Reilly S., Cass H., Clarke A., Kerr A. M. and Bailey M. E. (2005) Dimensional phenotypic analysis and functional categorisation of mutations reveal novel genotype-phenotype associations in Rett syndrome. European journal of human genetics : EJHG 13, 1121-1130.

Chen Q., Zhu Y. C., Yu J., Miao S., Zheng J., Xu L., Zhou Y., Li D., Zhang C., Tao J. and Xiong Z. Q. (2010) CDKL5, a protein associated with rett syndrome, regulates neuronal morphogenesis via Rac1 signaling. The Journal of neuroscience : the official journal of the Society for Neuroscience 30, 12777-12786.

Chen R. Z., Akbarian S., Tudor M. and Jaenisch R. (2001) Deficiency of methyl-CpG binding protein-2 in CNS neurons results in a Rett-like phenotype in mice. Nature genetics 27, 327-331.

Chen W. G., Chang Q., Lin Y., Meissner A., West A. E., Griffith E. C., Jaenisch R. and Greenberg M. E. (2003) Derepression of BDNF transcription involves calcium-dependent phosphorylation of MeCP2. Science 302, 885-889.

Ciani E., Severi S., Contestabile A., Bartesaghi R. and Contestabile A. (2004) Nitric oxide negatively regulates proliferation and promotes neuronal differentiation through N-Myc downregulation. J Cell Sci 117, 4727-4737.

Cohen D. R., Matarazzo V., Palmer A. M., Tu Y., Jeon O. H., Pevsner J. and Ronnett G. V. (2003) Expression of MeCP2 in olfactory receptor neurons is developmentally regulated and occurs before synaptogenesis. Molecular and cellular neurosciences 22, 417-429.

Colantuoni C., Jeon O. H., Hyder K., Chenchik A., Khimani A. H., Narayanan V., Hoffman E. P., Kaufmann W. E., Naidu S. and Pevsner J. (2001) Gene expression profiling in postmortem Rett Syndrome brain: differential gene expression and patient classification. Neurobiology of disease 8, 847-865.

Cole A. R. (2012) GSK3 as a Sensor Determining Cell Fate in the Brain. Front Mol Neurosci 5, 4.

Collins A. L., Levenson J. M., Vilaythong A. P., Richman R., Armstrong D. L., Noebels J. L., David Sweatt J. and Zoghbi H. Y. (2004) Mild overexpression of MeCP2 causes a progressive neurological disorder in mice. Human molecular genetics 13, 2679-2689.

Contestabile A., Fila T., Cappellini A., Bartesaghi R. and Ciani E. (2009) Widespread impairment of cell proliferation in the neonate Ts65Dn mouse, a model for Down syndrome. Cell Prolif 42, 171-181.

Contestabile A., Fila T., Ceccarelli C., Bonasoni P., Bonapace L., Santini D., Bartesaghi R. and Ciani E. (2007) Cell cycle alteration and decreased cell proliferation in the hippocampal dentate gyrus and in the neocortical germinal matrix of fetuses with Down syndrome and in Ts65Dn mice. Hippocampus 17, 665-678.

Croll S. D., Suri C., Compton D. L., Simmons M. V., Yancopoulos G. D., Lindsay R. M., Wiegand S. J., Rudge J. S. and Scharfman H. E. (1999) Brain-derived neurotrophic factor transgenic mice exhibit passive avoidance deficits, increased seizure severity and in vitro hyperexcitability in the hippocampus and entorhinal cortex. Neuroscience 93, 1491-1506.

Curtis M. A., Eriksson P. S. and Faull R. L. (2007) Progenitor cells and adult neurogenesis in neurodegenerative diseases and injuries of the basal ganglia. Clinical and experimental pharmacology & physiology 34, 528-532.

D'Esposito M., Quaderi N. A., Ciccodicola A., Bruni P., Esposito T., D'Urso M. and Brown S. D. (1996) Isolation, physical mapping, and northern analysis of the X-linked human gene encoding methyl CpG-binding protein, MECP2. Mammalian genome : official journal of the International Mammalian Genome Society 7, 533-535.

Dani V. S., Chang Q., Maffei A., Turrigiano G. G., Jaenisch R. and Nelson S. B. (2005) Reduced cortical activity due to a shift in the balance between excitation and inhibition in a mouse model of Rett syndrome. Proceedings of the National Academy of Sciences of the United States of America 102, 12560-12565.

Encinas J. M., Vaahtokari A. and Enikolopov G. (2006) Fluoxetine targets early progenitor cells in the adult brain. Proceedings of the National Academy of Sciences of the United States of America 103, 8233-8238.

Eom T. Y., Roth K. A. and Jope R. S. (2007) Neural precursor cells are protected from apoptosis induced by trophic factor withdrawal or genotoxic stress by inhibitors of glycogen synthase kinase 3. The Journal of biological chemistry 282, 22856-22864.

Evans J. C., Archer H. L., Colley J. P., Ravn K., Nielsen J. B., Kerr A., Williams E., Christodoulou J., Gecz J., Jardine P. E., Wright M. J., Pilz D. T., Lazarou L., Cooper D. N., Sampson J. R., Butler R., Whatley S. D. and Clarke A. J. (2005) Early onset seizures and Rett-like features associated with mutations in CDKL5. European journal of human genetics : EJHG 13, 1113-1120.

Farley F. W., Soriano P., Steffen L. S. and Dymecki S. M. (2000) Widespread recombinase expression using FLPeR (flipper) mice. Genesis 28, 106-110.

Fehr S., Wilson M., Downs J., Williams S., Murgia A., Sartori S., Vecchi M., Ho G., Polli R., Psoni S., Bao X., de Klerk N., Leonard H. and Christodoulou J. (2013)

The CDKL5 disorder is an independent clinical entity associated with early-onset encephalopathy. European journal of human genetics : EJHG 21, 266-273.

Fichou Y., Nectoux J., Bahi-Buisson N., Chelly J. and Bienvenu T. (2011) An isoform of the severe encephalopathy-related CDKL5 gene, including a novel exon with extremely high sequence conservation, is specifically expressed in brain. J Hum Genet 56, 52-57.

Freilinger M., Bebbington A., Lanator I., De Klerk N., Dunkler D., Seidl R., Leonard H. and Ronen G. M. (2010) Survival with Rett syndrome: comparing Rett's original sample with data from the Australian Rett Syndrome Database. Developmental medicine and child neurology 52, 962-965.

Gemelli T., Berton O., Nelson E. D., Perrotti L. I., Jaenisch R. and Monteggia L. M. (2006) Postnatal loss of methyl-CpG binding protein 2 in the forebrain is sufficient to mediate behavioral aspects of Rett syndrome in mice. Biological psychiatry 59, 468-476.

Georgel P. T. (2007) Role of chromatin/epigenetic modifications on DNA accessibility. Drug news & perspectives 20, 549-556.

Goto T. and Monk M. (1998) Regulation of X-chromosome inactivation in development in mice and humans. Microbiol Mol Biol Rev 62, 362-378.

Greicius M. D., Krasnow B., Boyett-Anderson J. M., Eliez S., Schatzberg A. F., Reiss A. L. and Menon V. (2003) Regional analysis of hippocampal activation during memory encoding and retrieval: fMRI study. Hippocampus 13, 164-174.

Grimes C. A. and Jope R. S. (2001) CREB DNA binding activity is inhibited by glycogen synthase kinase-3 beta and facilitated by lithium. J Neurochem 78, 1219-1232.

Guy J., Hendrich B., Holmes M., Martin J. E. and Bird A. (2001) A mouse Mecp2-null mutation causes neurological symptoms that mimic Rett syndrome. Nature genetics 27, 322-326.

Hagberg B., Aicardi J., Dias K. and Ramos O. (1983) A progressive syndrome of autism, dementia, ataxia, and loss of purposeful hand use in girls: Rett's syndrome: report of 35 cases. Annals of neurology 14, 471-479.

Hagberg B., Hanefeld F., Percy A. and Skjeldal O. (2002) An update on clinically applicable diagnostic criteria in Rett syndrome. Comments to Rett Syndrome Clinical Criteria Consensus Panel Satellite to European Paediatric Neurology Society Meeting, Baden Baden, Germany, 11 September 2001. European journal of paediatric neurology : EJPN : official journal of the European Paediatric Neurology Society 6, 293-297.

Hammer S., Dorrani N., Dragich J., Kudo S. and Schanen C. (2002) The phenotypic consequences of MECP2 mutations extend beyond Rett syndrome. Mental retardation and developmental disabilities research reviews 8, 94-98.

Hanefeld F. (1985) The clinical pattern of the Rett syndrome. Brain & development 7, 320-325.

Haydar T. F., Wang F., Schwartz M. L. and Rakic P. (2000) Differential modulation of proliferation in the neocortical ventricular and subventricular zones. The Journal of neuroscience : the official journal of the Society for Neuroscience 20, 5764-5774.

Horike S., Cai S., Miyano M., Cheng J. F. and Kohwi-Shigematsu T. (2005) Loss of silent-chromatin looping and impaired imprinting of DLX5 in Rett syndrome. Nature genetics 37, 31-40.

Intusoma U., Hayeeduereh F., Plong-On O., Sripo T., Vasiknanonte P., Janjindamai S., Lusawat A., Thammongkol S., Visudtibhan A. and Limprasert P. (2011) Mutation screening of the CDKL5 gene in cryptogenic infantile intractable epilepsy and review of clinical sensitivity. European journal of paediatric neurology : EJPN : official journal of the European Paediatric Neurology Society 15, 432-438.

Jones P. L., Veenstra G. J., Wade P. A., Vermaak D., Kass S. U., Landsberger N., Strouboulis J. and Wolffe A. P. (1998) Methylated DNA and MeCP2 recruit histone deacetylase to repress transcription. Nature genetics 19, 187-191.

Jordan C., Li H. H., Kwan H. C. and Francke U. (2007) Cerebellar gene expression profiles of mouse models for Rett syndrome reveal novel MeCP2 targets. BMC medical genetics 8, 36.

Julu P. O., Kerr A. M., Apartopoulos F., Al-Rawas S., Engerstrom I. W., Engerstrom L., Jamal G. A. and Hansen S. (2001) Characterisation of breathing and associated central autonomic dysfunction in the Rett disorder. Archives of disease in childhood 85, 29-37.

Jung B. P., Jugloff D. G., Zhang G., Logan R., Brown S. and Eubanks J. H. (2003) The expression of methyl CpG binding factor MeCP2 correlates with cellular differentiation in the developing rat brain and in cultured cells. Journal of neurobiology 55, 86-96.

Kalscheuer V. M., Tao J., Donnelly A., Hollway G., Schwinger E., Kubart S., Menzel C., Hoeltzenbein M., Tommerup N., Eyre H., Harbord M., Haan E., Sutherland G. R., Ropers H. H. and Gecz J. (2003) Disruption of the serine/threonine kinase 9 gene causes severe X-linked infantile spasms and mental retardation. American journal of human genetics 72, 1401-1411.

Kameshita I., Sekiguchi M., Hamasaki D., Sugiyama Y., Hatano N., Suetake I., Tajima S. and Sueyoshi N. (2008) Cyclin-dependent kinase-like 5 binds and phosphorylates DNA methyltransferase 1. Biochem Biophys Res Commun 377, 1162-1167.

Kaufmann W. E. and Moser H. W. (2000) Dendritic anomalies in disorders associated with mental retardation. Cerebral cortex 10, 981-991.

Kaufmann W. E., Johnston M. V. and Blue M. E. (2005) MeCP2 expression and function during brain development: implications for Rett syndrome's pathogenesis and clinical evolution. Brain & development 27 Suppl 1, S77-S87.

Kempermann G., Jessberger S., Steiner B. and Kronenberg G. (2004) Milestones of neuronal development in the adult hippocampus. Trends Neurosci 27, 447-452.

Kerr A. M. (1992) A review of the respiratory disorder in the Rett syndrome. Brain & development 14 Suppl, S43-45.

Kilstrup-Nielsen C., Rusconi L., La Montanara P., Ciceri D., Bergo A., Bedogni F. and Landsberger N. (2012) What we know and would like to know about CDKL5 and its involvement in epileptic encephalopathy. Neural Plast 2012, 728267.

Kishi N. and Macklis J. D. (2005) Dissecting MECP2 function in the central nervous system. Journal of child neurology 20, 753-759.

Klose R. J., Sarraf S. A., Schmiedeberg L., McDermott S. M., Stancheva I. and Bird A. P. (2005) DNA binding selectivity of MeCP2 due to a requirement for A/T sequences adjacent to methyl-CpG. Molecular cell 19, 667-678.

Kokura K., Kaul S. C., Wadhwa R., Nomura T., Khan M. M., Shinagawa T., Yasukawa T., Colmenares C. and Ishii S. (2001) The Ski protein family is required for MeCP2-mediated transcriptional repression. The Journal of biological chemistry 276, 34115-34121.

Kriaucionis S. and Bird A. (2004) The major form of MeCP2 has a novel N-terminus generated by alternative splicing. Nucleic acids research 32, 1818-1823.

Kuhn H. G., Dickinson-Anson H. and Gage F. H. (1996) Neurogenesis in the dentate gyrus of the adult rat: age-related decrease of neuronal progenitor proliferation. The Journal of neuroscience : the official journal of the Society for Neuroscience 16, 2027-2033.

Kurt M. A., Davies D. C., Kidd M., Dierssen M. and Florez J. (2000) Synaptic deficit in the temporal cortex of partial trisomy 16 (Ts65Dn) mice. Brain research 858, 191-197.

Lewis J. D., Meehan R. R., Henzel W. J., Maurer-Fogy I., Jeppesen P., Klein F. and Bird A. (1992) Purification, sequence, and cellular localization of a novel chromosomal protein that binds to methylated DNA. Cell 69, 905-914.

Lie D. C., Song H., Colamarino S. A., Ming G. L. and Gage F. H. (2004) Neurogenesis in the adult brain: new strategies for central nervous system diseases. Annual review of pharmacology and toxicology 44, 399-421.

Lin C., Franco B. and Rosner M. R. (2005) CDKL5/Stk9 kinase inactivation is associated with neuronal developmental disorders. Human molecular genetics 14, 3775-3786.

Lois C., Garcia-Verdugo J. M. and Alvarez-Buylla A. (1996) Chain migration of neuronal precursors. Science 271, 978-981.

Lowry O. H., Rosebrough N. J., Farr A. L. and Randall R. J. (1951) Protein measurement with the Folin phenol reagent. The Journal of biological chemistry 193, 265-275.

Luikenhuis S., Giacometti E., Beard C. F. and Jaenisch R. (2004) Expression of MeCP2 in postmitotic neurons rescues Rett syndrome in mice. Proceedings of the National Academy of Sciences of the United States of America 101, 6033-6038.

Luo J. (2012) The role of GSK3beta in the development of the central nervous system. Front. Biol. 7, 212 – 220.

Maguire E. A., Frackowiak R. S. and Frith C. D. (1997) Recalling routes around london: activation of the right hippocampus in taxi drivers. The Journal of neuroscience : the official journal of the Society for Neuroscience 17, 7103-7110.

Makedonski K., Abuhatzira L., Kaufman Y., Razin A. and Shemer R. (2005) MeCP2 deficiency in Rett syndrome causes epigenetic aberrations at the PWS/AS imprinting center that affects UBE3A expression. Human molecular genetics 14, 1049-1058.

Mari F., Azimonti S., Bertani I., Bolognese F., Colombo E., Caselli R., Scala E., Longo I., Grosso S., Pescucci C., Ariani F., Hayek G., Balestri P., Bergo A., Badaracco G., Zappella M., Broccoli V., Renieri A., Kilstrup-Nielsen C. and Landsberger N. (2005) CDKL5 belongs to the same molecular pathway of MeCP2

and it is responsible for the early-onset seizure variant of Rett syndrome. Human molecular genetics 14, 1935-1946.

Martinowich K., Hattori D., Wu H., Fouse S., He F., Hu Y., Fan G. and Sun Y. E. (2003) DNA methylation-related chromatin remodeling in activity-dependent BDNF gene regulation. Science 302, 890-893.

Masiulis I., Yun S. and Eisch A. J. (2011) The interesting interplay between interneurons and adult hippocampal neurogenesis. Molecular neurobiology 44, 287-302.

Matarazzo V. and Ronnett G. V. (2004) Temporal and regional differences in the olfactory proteome as a consequence of MeCP2 deficiency. Proceedings of the National Academy of Sciences of the United States of America 101, 7763-7768.

Melino G., Thiele C. J., Knight R. A. and Piacentini M. (1997) Retinoids and the control of growth/death decisions in human neuroblastoma cell lines. J Neurooncol 31, 65-83.

Mnatzakanian G. N., Lohi H., Munteanu I., Alfred S. E., Yamada T., MacLeod P. J., Jones J. R., Scherer S. W., Schanen N. C., Friez M. J., Vincent J. B. and Minassian B. A. (2004) A previously unidentified MECP2 open reading frame defines a new protein isoform relevant to Rett syndrome. Nature genetics 36, 339-341.

Montini E., Andolfi G., Caruso A., Buchner G., Walpole S. M., Mariani M., Consalez G., Trump D., Ballabio A. and Franco B. (1998) Identification and characterization of a novel serine-threonine kinase gene from the Xp22 region. Genomics 51, 427-433.

Moser M. B. and Moser E. I. (1998) Distributed encoding and retrieval of spatial memory in the hippocampus. The Journal of neuroscience : the official journal of the Society for Neuroscience 18, 7535-7542.

Nan X., Campoy F. J. and Bird A. (1997) MeCP2 is a transcriptional repressor with abundant binding sites in genomic chromatin. Cell 88, 471-481.

Nan X., Ng H. H., Johnson C. A., Laherty C. D., Turner B. M., Eisenman R. N. and Bird A. (1998) Transcriptional repression by the methyl-CpG-binding protein MeCP2 involves a histone deacetylase complex. Nature 393, 386-389.

Nelson E. D., Kavalali E. T. and Monteggia L. M. (2006) MeCP2-dependent transcriptional repression regulates excitatory neurotransmission. Current biology : CB 16, 710-716.

Neul J. L., Fang P., Barrish J., Lane J., Caeg E. B., Smith E. O., Zoghbi H., Percy A. and Glaze D. G. (2008) Specific mutations in methyl-CpG-binding protein 2 confer different severity in Rett syndrome. Neurology 70, 1313-1321.

Neul J. L., Kaufmann W. E., Glaze D. G., Christodoulou J., Clarke A. J., Bahi-Buisson N., Leonard H., Bailey M. E., Schanen N. C., Zappella M., Renieri A., Huppke P., Percy A. K. and RettSearch C. (2010) Rett syndrome: revised diagnostic criteria and nomenclature. Annals of neurology 68, 944-950.

Nuber U. A., Kriaucionis S., Roloff T. C., Guy J., Selfridge J., Steinhoff C., Schulz R., Lipkowitz B., Ropers H. H., Holmes M. C. and Bird A. (2005) Up-regulation of glucocorticoid-regulated genes in a mouse model of Rett syndrome. Human molecular genetics 14, 2247-2256.

Ohnuma S., Philpott A. and Harris W. A. (2001) Cell cycle and cell fate in the nervous system. Curr Opin Neurobiol 11, 66-73.

Palmer A., Qayumi J. and Ronnett G. (2008) MeCP2 mutation causes distinguishable phases of acute and chronic defects in synaptogenesis and maintenance, respectively. Molecular and cellular neurosciences 37, 794-807.

Plath K., Mlynarczyk-Evans S., Nusinow D. A. and Panning B. (2002) Xist RNA and the mechanism of X chromosome inactivation. Annu Rev Genet 36, 233-278.

Plenge R. M., Stevenson R. A., Lubs H. A., Schwartz C. E. and Willard H. F. (2002) Skewed X-chromosome inactivation is a common feature of X-linked mental retardation disorders. American journal of human genetics 71, 168-173.

Quaderi N. A., Meehan R. R., Tate P. H., Cross S. H., Bird A. P., Chatterjee A., Herman G. E. and Brown S. D. (1994) Genetic and physical mapping of a gene encoding a methyl CpG binding protein, Mecp2, to the mouse X chromosome. Genomics 22, 648-651.

Rademacher N., Hambrock M., Fischer U., Moser B., Ceulemans B., Lieb W., Boor R., Stefanova I., Gillessen-Kaesbach G., Runge C., Korenke G. C., Spranger S., Laccone F., Tzschach A. and Kalscheuer V. M. (2011) Identification of a novel CDKL5 exon and pathogenic mutations in patients with severe mental retardation, early-onset seizures and Rett-like features. Neurogenetics 12, 165-167.

Rett A. (1966) [On a unusual brain atrophy syndrome in hyperammonemia in childhood]. Wiener medizinische Wochenschrift 116, 723-726.

Ricciardi S., Kilstrup-Nielsen C., Bienvenu T., Jacquette A., Landsberger N. and Broccoli V. (2009) CDKL5 influences RNA splicing activity by its association to the nuclear speckle molecular machinery. Human molecular genetics 18, 4590-4602.

Ricciardi S., Ungaro F., Hambrock M., Rademacher N., Stefanelli G., Brambilla D., Sessa A., Magagnotti C., Bachi A., Giarda E., Verpelli C., Kilstrup-Nielsen C., Sala C., Kalscheuer V. M. and Broccoli V. (2012) CDKL5 ensures excitatory synapse stability by reinforcing NGL-1-PSD95 interaction in the postsynaptic compartment and is impaired in patient iPSC-derived neurons. Nat Cell Biol 14, 911-923.

Rogers D. C., Jones D. N., Nelson P. R., Jones C. M., Quilter C. A., Robinson T. L. and Hagan J. J. (1999) Use of SHIRPA and discriminant analysis to characterise marked differences in the behavioural phenotype of six inbred mouse strains. Behavioural brain research 105, 207-217.

Rosas-Vargas H., Bahi-Buisson N., Philippe C., Nectoux J., Girard B., N'Guyen Morel M. A., Gitiaux C., Lazaro L., Odent S., Jonveaux P., Chelly J. and Bienvenu T. (2008) Impairment of CDKL5 nuclear localisation as a cause for severe infantile encephalopathy. J Med Genet 45, 172-178.

Rusconi L., Kilstrup-Nielsen C. and Landsberger N. (2011) Extrasynaptic N-methyl-D-aspartate (NMDA) receptor stimulation induces cytoplasmic translocation of the CDKL5 kinase and its proteasomal degradation. The Journal of biological chemistry 286, 36550-36558.

Rusconi L., Salvatoni L., Giudici L., Bertani I., Kilstrup-Nielsen C., Broccoli V. and Landsberger N. (2008) CDKL5 expression is modulated during neuronal

development and its subcellular distribution is tightly regulated by the C-terminal tail. The Journal of biological chemistry 283, 30101-30111.

Samaco R. C. and Neul J. L. (2011) Complexities of Rett syndrome and MeCP2. The Journal of neuroscience : the official journal of the Society for Neuroscience 31, 7951-7959.

Samaco R. C., Hogart A. and LaSalle J. M. (2005) Epigenetic overlap in autism-spectrum neurodevelopmental disorders: MECP2 deficiency causes reduced expression of UBE3A and GABRB3. Human molecular genetics 14, 483-492.

Sekiguchi M., Katayama S., Hatano N., Shigeri Y., Sueyoshi N. and Kameshita I. (2013) Identification of amphiphysin 1 as an endogenous substrate for CDKL5, a protein kinase associated with X-linked neurodevelopmental disorder. Arch Biochem Biophys.

Shahbazian M., Young J., Yuva-Paylor L., Spencer C., Antalffy B., Noebels J., Armstrong D., Paylor R. and Zoghbi H. (2002a) Mice with truncated MeCP2 recapitulate many Rett syndrome features and display hyperacetylation of histone H3. Neuron 35, 243-254.

Shahbazian M. D., Antalffy B., Armstrong D. L. and Zoghbi H. Y. (2002b) Insight into Rett syndrome: MeCP2 levels display tissue- and cell-specific differences and correlate with neuronal maturation. Human molecular genetics 11, 115-124.

Shors T. J., Miesegaes G., Beylin A., Zhao M., Rydel T. and Gould E. (2001) Neurogenesis in the adult is involved in the formation of trace memories. Nature 410, 372-376.

Singh J. and Kaur G. (2007) Transcriptional regulation of polysialylated neural cell adhesion molecule expression by NMDA receptor activation in retinoic acid-differentiated SH-SY5Y neuroblastoma cultures. Brain research 1154, 8-21.

Skene P. J., Illingworth R. S., Webb S., Kerr A. R., James K. D., Turner D. J., Andrews R. and Bird A. P. (2010) Neuronal MeCP2 is expressed at near histone-octamer levels and globally alters the chromatin state. Molecular cell 37, 457-468.

Smeets E. E., Pelc K. and Dan B. (2012) Rett Syndrome. Molecular syndromology 2, 113-127.

Smrt R. D., Eaves-Egenes J., Barkho B. Z., Santistevan N. J., Zhao C., Aimone J. B., Gage F. H. and Zhao X. (2007) Mecp2 deficiency leads to delayed maturation and altered gene expression in hippocampal neurons. Neurobiology of disease 27, 77-89.

Spittaels K., Van den Haute C., Van Dorpe J., Geerts H., Mercken M., Bruynseels K., Lasrado R., Vandezande K., Laenen I., Boon T., Van Lint J., Vandenheede J., Moechars D., Loos R. and Van Leuven F. (2000) Glycogen synthase kinase-3beta phosphorylates protein tau and rescues the axonopathy in the central nervous system of human four-repeat tau transgenic mice. The Journal of biological chemistry 275, 41340-41349.

Spittaels K., Van den Haute C., Van Dorpe J., Terwel D., Vandezande K., Lasrado R., Bruynseels K., Irizarry M., Verhoye M., Van Lint J., Vandenheede J. R., Ashton D., Mercken M., Loos R., Hyman B., Van der Linden A., Geerts H. and Van Leuven F. (2002) Neonatal neuronal overexpression of glycogen synthase kinase-3 beta reduces brain size in transgenic mice. Neuroscience 113, 797-808.

Stancheva I., Collins A. L., Van den Veyver I. B., Zoghbi H. and Meehan R. R. (2003) A mutant form of MeCP2 protein associated with human Rett syndrome cannot be displaced from methylated DNA by notch in Xenopus embryos. Molecular cell 12, 425-435.

Steffenburg U., Hagberg G. and Hagberg B. (2001) Epilepsy in a representative series of Rett syndrome. Acta paediatrica 90, 34-39.

Stuss D. P., Boyd J. D., Levin D. B. and Delaney K. R. (2012) MeCP2 mutation results in compartment-specific reductions in dendritic branching and spine density in layer 5 motor cortical neurons of YFP-H mice. PLoS One 7, e31896.

Talebizadeh Z., Bittel D. C., Veatch O. J., Kibiryeva N. and Butler M. G. (2005) Brief report: non-random X chromosome inactivation in females with autism. J Autism Dev Disord 35, 675-681.

Tang S. H., Silva F. J., Tsark W. M. and Mann J. R. (2002) A Cre/loxP-deleter transgenic line in mouse strain 129S1/SvImJ. Genesis 32, 199-202.

Tao J., Van Esch H., Hagedorn-Greiwe M., Hoffmann K., Moser B., Raynaud M., Sperner J., Fryns J. P., Schwinger E., Gecz J., Ropers H. H. and Kalscheuer V. M. (2004) Mutations in the X-linked cyclin-dependent kinase-like 5 (CDKL5/STK9) gene are associated with severe neurodevelopmental retardation. American journal of human genetics 75, 1149-1154.

Tashiro A., Makino H. and Gage F. H. (2007) Experience-specific functional modification of the dentate gyrus through adult neurogenesis: a critical period during an immature stage. The Journal of neuroscience : the official journal of the Society for Neuroscience 27, 3252-3259.

Traynor J., Agarwal P., Lazzeroni L. and Francke U. (2002) Gene expression patterns vary in clonal cell cultures from Rett syndrome females with eight different MECP2 mutations. BMC medical genetics 3, 12.

Trazzi S., Mitrugno V. M., Valli E., Fuchs C., Rizzi S., Guidi S., Perini G., Bartesaghi R. and Ciani E. (2011) APP-dependent up-regulation of Ptch1 underlies proliferation impairment of neural precursors in Down syndrome. Human molecular genetics 20, 1560-1573.

Tudor M., Akbarian S., Chen R. Z. and Jaenisch R. (2002) Transcriptional profiling of a mouse model for Rett syndrome reveals subtle transcriptional changes in the brain. Proceedings of the National Academy of Sciences of the United States of America 99, 15536-15541.

van Praag H., Christie B. R., Sejnowski T. J. and Gage F. H. (1999) Running enhances neurogenesis, learning, and long-term potentiation in mice. Proceedings of the National Academy of Sciences of the United States of America 96, 13427-13431.

van Praag H., Shubert T., Zhao C. and Gage F. H. (2005) Exercise enhances learning and hippocampal neurogenesis in aged mice. The Journal of neuroscience : the official journal of the Society for Neuroscience 25, 8680-8685.

van Praag H., Schinder A. F., Christie B. R., Toni N., Palmer T. D. and Gage F. H. (2002) Functional neurogenesis in the adult hippocampus. Nature 415, 1030-1034.

Wada A. (2009) Lithium and neuropsychiatric therapeutics: neuroplasticity via glycogen synthase kinase-3beta, beta-catenin, and neurotrophin cascades. J Pharmacol Sci 110, 14-28.

Wang I. T., Allen M., Goffin D., Zhu X., Fairless A. H., Brodkin E. S., Siegel S. J., Marsh E. D., Blendy J. A. and Zhou Z. (2012) Loss of CDKL5 disrupts kinome profile and event-related potentials leading to autistic-like phenotypes in mice. Proceedings of the National Academy of Sciences of the United States of America 109, 21516-21521.

Weaving L. S., Ellaway C. J., Gecz J. and Christodoulou J. (2005) Rett syndrome: clinical review and genetic update. J Med Genet 42, 1-7.

Weaving L. S., Christodoulou J., Williamson S. L., Friend K. L., McKenzie O. L., Archer H., Evans J., Clarke A., Pelka G. J., Tam P. P., Watson C., Lahooti H., Ellaway C. J., Bennetts B., Leonard H. and Gecz J. (2004) Mutations of CDKL5 cause a severe neurodevelopmental disorder with infantile spasms and mental retardation. American journal of human genetics 75, 1079-1093.

Williamson S. L., Giudici L., Kilstrup-Nielsen C., Gold W., Pelka G. J., Tam P. P., Grimm A., Prodi D., Landsberger N. and Christodoulou J. (2011) A novel transcript of cyclin-dependent kinase-like 5 (CDKL5) has an alternative C-terminus and is the predominant transcript in brain. Hum Genet 131, 187-200.

Witt-Engerstrom I. and Hagberg B. (1990) The Rett syndrome: gross motor disability and neural impairment in adults. Brain & development 12, 23-26.

Yoshimura T., Kawano Y., Arimura N., Kawabata S., Kikuchi A. and Kaibuchi K. (2005) GSK-3beta regulates phosphorylation of CRMP-2 and neuronal polarity. Cell 120, 137-149.

Young J. I., Hong E. P., Castle J. C., Crespo-Barreto J., Bowman A. B., Rose M. F., Kang D., Richman R., Johnson J. M., Berget S. and Zoghbi H. Y. (2005) Regulation of RNA splicing by the methylation-dependent transcriptional repressor methyl-CpG binding protein 2. Proceedings of the National Academy of Sciences of the United States of America 102, 17551-17558.

Zhao N., Zhong C., Wang Y., Zhao Y., Gong N., Zhou G., Xu T. and Hong Z. (2008) Impaired hippocampal neurogenesis is involved in cognitive dysfunction induced by thiamine deficiency at early pre-pathological lesion stage. Neurobiology of disease 29, 176-185.

Zhou Z., Hong E. J., Cohen S., Zhao W. N., Ho H. Y., Schmidt L., Chen W. G., Lin Y., Savner E., Griffith E. C., Hu L., Steen J. A., Weitz C. J. and Greenberg M. E. (2006) Brain-specific phosphorylation of MeCP2 regulates activity-dependent Bdnf transcription, dendritic growth, and spine maturation. Neuron 52, 255-269.

Zhu Y. C., Li D., Wang L., Lu B., Zheng J., Zhao S. L., Zeng R. and Xiong Z. Q. (2013) Palmitoylation-dependent CDKL5-PSD-95 interaction regulates synaptic targeting of CDKL5 and dendritic spine development. Proceedings of the National Academy of Sciences of the United States of America.

http://syndromepictures.com/rett-syndrome-pictures

http://www.hindawi.com/journals/np/2012/415825/fig2

ACKNOWLEDGMENTS

Apart of the efforts of myself, the success of any project depends largely on the encouragement and guidelines of many others. I would take this opportunity to express my gratitude to the people who have been instrumental in the successful completion of my PhD.

First and foremost, I would like to thank my supervisor Dr. Elisabetta Ciani for the valuable guidance and advice. She patiently provided the vision, encouragement and advice necessary for me to proceed through the doctoral program and complete my dissertation. The joy and enthusiasm she has for her research was contagious and motivational for me, even during tough times in the PhD pursuit.

Beside I would like to express my deepest gratitude to Prof. Renata Bartesaghi, the head of the laboratory I spent the last years. Without her knowledge and assistance this study would not have been successful.

A special thank goes also to all the members of my laboratory, which have contributed immensely to my personal and professional maturation over this years. I would like to especially thank Stefania, Marianna and Rocchina. Their friendship and assistance during these years has meant more to me than I could ever express.

I would thank also Dr. Cornelius Gross and Prof. Laura Calzà and their group members. The creation of the KO model and the behavioral experiments discussed in this dissertation would not have been possible without their contribution.

I gratefully acknowledge also to the "CDKL5 Assocciazione di volontariato onlus" and the "International foundation for CDKL5 research" for their funding sources that made my PhD work possible. I really hope that my work could contribute to

understand this devastating disorder and hopefully be a first step in order to find a therapy for their children.

A special thank and hug goes to my friends, my friends from my hometown and my friends from Bologna. The last three years weren't easy all the time, and their support was essential for me. Special thanks go to Manu, Mari, Pahli, Michi and Chiara, for all the moments spend together, all the tiers cried together and all the smiles had together.

A special thanks goes to my loving, supportive, encouraging, and patient boyfriend Saverio whose faithful support especially during the final stages of this PhD was amazing.

Lastly, I would like to thank my mom, my little brother Alex, my grandma and my uncles for all their love and encouragement. I owe them everything and wish I could show them just how much I love and appreciate them.

Finally, I would like to dedicate this work to my grandpa, who left us too soon. I hope that this work makes you proud of me.